



Lawrence Berkeley Laboratory

UNIVERSITY OF CALIFORNIA

Materials & Molecular Research Division

MICROSTRUCTURE DEVELOPMENT AND INTERFACE
STUDIES IN THICK FILM CONDUCTOR SYSTEMS

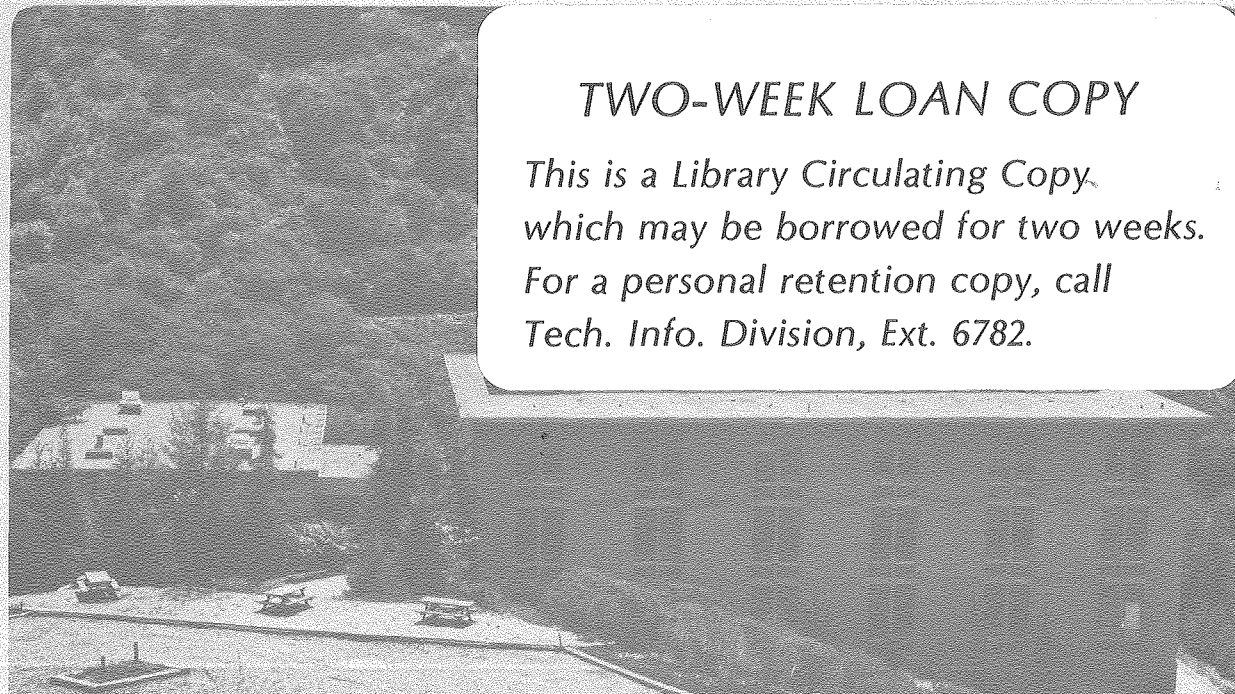
V. K. Nagesh
(Ph.D. thesis)

December 1979

RECEIVED
LAWRENCE
BERKELEY LABORATORY

APR 11 1980

LIBRARY AND
DOCUMENTS SECTION



TWO-WEEK LOAN COPY

*This is a Library Circulating Copy
which may be borrowed for two weeks.
For a personal retention copy, call
Tech. Info. Division, Ext. 6782.*

LBL 9274 C.2

DISCLAIMER

This document was prepared as an account of work sponsored by the United States Government. While this document is believed to contain correct information, neither the United States Government nor any agency thereof, nor the Regents of the University of California, nor any of their employees, makes any warranty, express or implied, or assumes any legal responsibility for the accuracy, completeness, or usefulness of any information, apparatus, product, or process disclosed, or represents that its use would not infringe privately owned rights. Reference herein to any specific commercial product, process, or service by its trade name, trademark, manufacturer, or otherwise, does not necessarily constitute or imply its endorsement, recommendation, or favoring by the United States Government or any agency thereof, or the Regents of the University of California. The views and opinions of authors expressed herein do not necessarily state or reflect those of the United States Government or any agency thereof or the Regents of the University of California.

MICROSTRUCTURE DEVELOPMENT AND
INTERFACE STUDIES IN THICK FILM CONDUCTOR SYSTEMS

V. K. Nagesh

Degree: Doctor of Philosophy
in Engineering

Major Department: Materials
Science and Mineral Engineering


Chairman, Thesis Committee

ABSTRACT

A new thick film conductor system which used acid treated (.01N HCl) lead borosilicate glass particles with chemically coated metal (silver) film was developed. Using only 40 wt% metal (silver), sheet resistivities as low as 45 milliohms/sq were obtained in this system. Detailed study of the microstructure development was done. Effect of the acid treatment of the glass particles prior to the metal coating was analyzed. X-ray photoelectron spectra studies showed preferential leaching of lead and boron from the surface of the glass. Good bonding between silver film and the glass was attributed to the oxidation of silver (to form Ag^+) in the presence of oxygen and H^+ ions on the glass surface (from acid treatment) and subsequent diffusion of Ag^+ into the glass to form a continuous chemical interface. A model to predict sheet resistivities of the new thick film conductors was developed.

Studies were extended to the nickel-silver conductor system. By using silver coated nickel particles, air fireable thick film conductors which use a minimum amount of precious metal were obtained. With 25 w/o Ag, sheet resistivities of 15 milliohms/sq were obtained.

In Part II, sessile drop measurements of (i) lead borosilicate glass on silver, gold and platinum (at 700°C), and (ii) silver on nickel (at 970°C) were conducted in controlled atmospheres. Wetting and good adherence of glass on silver, gold and platinum were observed in the presence of oxygen. This was attributed to the driving force provided by the dissolution of the metal surface oxide layer into glass at the interface. Good bonding observed between glass and silver in vacuum conditions were suggested to be due to a redox reaction between lead oxide and silver. Under the conditions of the experiment, lead (Pb(g)) evaporated away from the site of the reaction keeping the partial pressure of Pb at the interface low enough for the redox reaction to continue. Carbon adsorption by platinum caused the contact angle of glass to increase from 58° to 73° in vacuum conditions. The decrease in the surface energy (γ_{SV}) of platinum due to carbon adsorption was calculated to be ~43 ergs/cm².

Silver wetted nickel in helium atmosphere (contact angle 9.5°). In air atmosphere, however, a contact angle of 90° was obtained. This rare phenomenon was analyzed on the basis of thermodynamics of wetting and spreading.

MICROSTRUCTURE DEVELOPMENT AND
INTERFACE STUDIES IN THICK FILM CONDUCTOR SYSTEMS
contents

| | |
|---|-----|
| Abstract | iii |
| PART I. THICK FILM SYSTEMS. | 1 |
| Introduction | 1 |
| (A) General. | 1 |
| (B) Literature Review. | 3 |
| (C) Objectives | 6 |
| Experimental Details | 9 |
| (A) Processing | 9 |
| 1. Glass Preparation. | 9 |
| 2. Precious Metal Coating | 10 |
| 3. Thick Film Formulation and Firing. | 11 |
| (B) Characterization | 12 |
| 1. Electrical Resistivity Measurements. | 12 |
| 2. Microstructural Analysis | 13 |
| 3. Measurements Related to Surfaces | 15 |
| Results and Discussion | 17 |
| (A) Materials. | 17 |
| (B) Glass-Alumina Interface. | 20 |
| (C) Surface Activation | 21 |
| (D) Precious Metal Coating on Glass. | 24 |
| (E) Reaction Mechanisms. | 26 |
| (F) Firing Effects | 30 |

| | |
|--|-----|
| (G) Dependence of Sheet Resistivity on Metal Content and Matrix Particle Size | 33 |
| (H) Nickel-Silver System | 38 |
| SUMMARY AND CONCLUSIONS. | 40a |
| Tables | 41 |
| Figures. | 57 |
| References | 89 |
| PART II. WETTING STUDIES. | 91 |
| Introduction | 91 |
| Experimental Details | 95 |
| Results and Discussion | 98 |
| (A) Lead Borosilicate Glass and Precious Metals. | 98 |
| (B) Silver on Nickel | 109 |
| Appendix | 116 |
| Summary and Conclusions. | 119 |
| Tables | 121 |
| Figures. | 125 |
| References | 137 |
| Acknowledgment | 139 |

MICROSTRUCTURE DEVELOPMENT AND
INTERFACE STUDIES IN THICK FILM CONDUCTOR SYSTEMS

V. K. Nagesh

Materials and Molecular Research Division, Lawrence Berkeley Laboratory
and Department of Materials Science and Mineral
Engineering, University of California,
Berkeley, California

ABSTRACT

A new thick film conductor system which used acid treated (.01N HCl) lead borosilicate glass particles with chemically coated metal (silver) film was developed. Using only 40 wt % metal (silver), sheet resistivities as low as 45 milliohms/sq were obtained in this system. Detailed study of the microstructure development was done. Effect of the acid treatment of the glass particles prior to the metal coating was analyzed. X-ray photoelectron spectra studies showed preferential leaching of lead and boron from the surface of the glass. Good bonding between silver film and the glass was attributed to the oxidation of silver (to form Ag^+) in the presence of oxygen and H^+ ions on the glass surface (from acid treatment) and subsequent diffusion of Ag^+ into the glass to form a continuous chemical interface. A model to predict sheet resistivities of the new thick film conductors was developed.

Studies were extended to the nickel-silver conductor system. By using silver coated nickel particles, air fireable thick film conductors which use a minimum amount of precious metal were obtained. With 25 w/o Ag, sheet resistivities of 15 milliohms/sq were obtained.

In Part II, sessile drop measurements of (i) lead borosilicate glass on silver, gold and platinum (at 700°C), and (ii) silver on nickel (at 970°C) were conducted in controlled atmospheres. Wetting and good

adherence of glass on silver, gold and platinum were observed in the presence of oxygen. This was attributed to the driving force provided by the dissolution of the metal surface oxide layer into glass at the interface. Good bonding observed between glass and silver in vacuum conditions were suggested to be due to a redox reaction between lead oxide and silver. Under the conditions of the experiment, lead (Pb(g)) evaporated away from the site of the reaction keeping the partial pressure of Pb at the interface low enough for the redox reaction to continue. Carbon adsorption by platinum caused the contact angle of glass to increase from 58° to 73° in vacuum conditions. The decrease in the surface energy (γ_{SV}) of platinum due to carbon adsorption was calculated to be $\sim 43 \text{ ergs/cm}^2$.

Silver wetted nickel in helium atmosphere (contact angle 9.5°). In air atmosphere, however, a contact angle of 90° was obtained. This rare phenomenon was analyzed on the basis of thermodynamics of wetting and spreading.

PART I
THICK FILM SYSTEMS

I. INTRODUCTION

(A) General

The internal structure in ceramic materials is very important in determining the final properties and usefulness of the materials. A noteworthy feature of these internal structures, termed microstructures, is the arrangement of the different phases, grains and the associated boundaries. The properties - electrical, mechanical and thermal, depend not only on the composition of the material but also on the distribution and orientation of the phases. It is useful to differentiate between the intrinsic properties of the material (phases) and properties which depend on the microstructure. The intrinsic properties are determined by the structural parameters on an atomic level (such as the type of atomic bonding, crystal structure, etc.) and are best studied in single crystals of the respective materials. In most of the polycrystalline materials, however, important properties for engineering applications are produced by one or more microstructural parameters.

In electronic ceramics the importance of developing proper microstructure by controlled processing is well recognized. Quite extensive microstructure/property relationship studies have been done in dielectric, ferroelectric, magnetic and optical ceramic materials.^{1,2}

However, literature is lacking in such a detailed study in the field of thick film technology, which is one of the very important aspects of modern electronics. Hybrid microelectronics, which is a combination of monolithic and thick film technologies, uses thick film components like capacitors, resistors and conductors quite extensively.^{3,4} High power

T.V. circuits, microwave devices, pocket calculators, computer circuits are some of the areas where hybrid circuits find wide applications.^{5,6,7} Flexibility of the properties, tight electrical tolerances, good power dissipation capabilities, stability and reliability are quite well obtained in these hybrid circuits. Also, thick film circuits are very economical compared to thin film circuits.^{8,9} Thin films are essentially of a thickness ranging from a few thousand Å to a few microns and are normally vacuum evaporated, sputtered or chemically deposited.

Conventional thick film conductors are essentially composite films of glass and noble metals on ceramic substrates with the thicknesses ranging from ~15-50µm. The method of formulation is as indicated in the flow chart (Fig. 1). Conventionally, conducting thick films are obtained by applying a mixture of glass and metal particles in an organic vehicle onto a substrate and subsequently firing in an air atmosphere. The glass usually is a low softening glass with a composition giving an expansion coefficient less than that of the substrate (usually 96 w/o Al₂O₃). This glass is powdered to a micron size* and mixed with micron size* metallic powder (70-90 w/o), and the mixture is suspended in an organic vehicle. The organic vehicle consists of a resin binder, solvent and additives to give a suitable viscosity.¹⁰ The liquid ratio is usually about 75 w/o depending on the viscosity of the thixotropic paste. The liquid/solid mixture is screen printed onto an alumina substrate, dried and then fired at a specific temperature for a specific time to give a conducting thick film. The amount of precious metals used in these films is as high as 80 to 90 w/o. Sheet resistivity data of several conventional thick film conductors are given in Table 1.^{11,12}

*1 to 10 microns.

Even though a considerable amount of development work has been done, very little research to obtain a basic understanding of the development of microstructure and processing is reported. Studies are mostly limited to achieving a certain property and not much attention is paid to the basic mechanisms involved in the processing. In the development of thick film systems the major emphasis has been mainly to develop useful materials on an empirical basis and on the measurement of properties necessary for design purposes. A brief review of the basic research done in the field of thick films follows.

B) Literature Review

The mechanism of conduction has been studied in thick film resistor systems (RuO_2 crystal, Ru resinate Pd-Ag system) under the application of high electromagnetic stress by Polinski.¹³ It is believed that interfacial energies between glass and the conductive phase cause the glass particles to sinter together and allow the conductive phases to form a channel. The resistance would then depend on the amount of discontinuity of this channel. Increase of electromagnetic stress is found to increase the conductivity.

Sintering studies have been conducted in the silver-palladium-glass system by Cole.¹⁴ These have led to certain important conclusions. Selective solution and reprecipitation is found to be the reason for the necessity of close control of both peak furnace temperature and time of firing. Heating rates and particle size are also found to be very important in determining the final properties of the film. Knowledge of intrinsic properties of the glass have been thought to be important because changes in silver and palladium solubility and changes in contact

angles will have profound affects on the film properties.

The interrelationships of surface oxidation and solderabilities on silver-palladium thick film conductors and the variations of conductivity characteristics with the metal content have been studied by Kubota and Shimura.¹⁵ With the increase of the palladium content silver migration rates are found to increase whereas the cohesive strength of the solder joints are found to decrease.

Adhesion, phase morphology, and bondability of reactively bonded and frit bonded gold and silver thick film conductors as a function of firing conditions and material types have been studied by Hitch.¹⁶ From SEM studies of the interfaces of the binding phases in the reactively bonded silver and gold inks, he concluded that the main force of adhesion between the metal and the substrate was due to chemical bonding rather than mechanical interlocking. He did not, however, discuss the affect of the glass phase in his 96 w/o alumina substrates.

Detailed studies on material properties and conduction mechanisms in thick film resistors have been carried out by Vest and coworkers.¹⁷ The system studied is ruthenium dioxide and lead borosilicate glass on alumina substrates. Dependence of sheet resistance and temperature coefficient of resistance of the resistors on the material properties have been investigated and a model is developed to reproduce the blending curve over six orders of magnitude in sheet resistance as well as account for any observed temperature coefficient of resistance in thick film resistors.

Recent developments in the bonding performances of gold thick film conductors have been analyzed by Horowitz, et al.¹⁸ The different types

of thick film conductors discussed are (a) glass bonded - where glass acts as the adhesive medium between the substrate and the metal, (b) oxide bonded - where the binder is a crystalline material (usually containing copper oxide as the chief component) and (c) mixed bonded - which contains both glass and crystalline binders. Description of new compositions optimized for specialized wire bonding applications is given. Addition of palladium to the gold conductor is found to increase the aluminum wire bonding performance. This has been explained as due to the formation of a stable Pd/Al/Au phase(s) in the region between the gold conductor and Al/Au intermetallic phases.

The limitations of reactively bonded commercial thick film gold conductors (which are found to contain Cu and Cd) has been studied by Coleman and Gurnett.¹⁹ Under most circumstances, the adhesion strengths of reactively bonded and mixed bonded conductors to the alumina substrate are found to be better than those of glass bonded conductors. With the presence of copper improved aged results have been obtained. However, the disadvantage is the disability of firing at higher temperatures. Moreover, there is a certain uncertainty about the presence of copper oxide at the top surface of the conductor.

Adhesion mechanisms of thick film conductors have been studied by Kim, et al.²⁰ A method for quantitative measurements of adhesion strength has been described. Silver-palladium conductors with lead-borosilicate glass flux and alumina (94-96%) substrates were used in the study. They could not detect any reaction between glass and substrate or between glass and metal with EDAX (energy dispersive analysis of x-rays) at magnifications of 3000X in the SEM. Also, reasons for

deterioration of adhesion strengths on ageing were not clear. Considering the strong bonding they obtained and insufficient accuracy of EDAX for quantitative measurements at the interfaces (which may as well be a few 100 Å thick), the glass-metal and the glass-alumina interfacial bonds are most probably chemical in nature. However, more detailed study is needed for a proper understanding of these interfaces.

C) Objectives

The development and study of the microstructure of the thick film conductor systems is very important. Studying the development of microstructure and property relations would give an insight of the processes at the microlevel and a knowledge of how to develop new systems with more reliable properties and, if possible, more economically. It is indeed also necessary to study the interactions between the coexisting phases in these thick film composite systems. Another major objective of interest is the fundamental understanding of the development of interfaces and bonding of the components involved in the making of the thick film - glass/metal, metal/metal, glass/ Al_2O_3 (substrate), and of the reactions associated with them.

Conventionally, the purpose of the glass is to provide good bonding between the substrate and the metallic film. The microstructure of the fired system should have metallic particles in contact with one another and the glass phase should be interspersed, the major portion of it going in between the metal layer and the substrate. Schematically this is shown in Fig. 2. It is desirable to obtain the same degree of conductivity with a reduced metal content by development of a proper microstructure. If glass or base metal matrix particles coated with a precious metal

like silver with uniform thickness and sufficient bonding are used, it would be possible to get a microstructure necessary for a conducting film (Fig. 3). This procedure would reduce the metal content to a large extent and the glass phase would become the major phase in the composite system.

With this perspective, a new process involving an acid treatment of the glass particles and subsequently coating them with silver was invented for making a thick film conductor.²¹ Conductors were obtained with an Ag metal content as low as 20 w/o. The identification of the acid treatment process as a crucial step in this process was the center point in the earlier study (M.S. project).²² However, additional detailed characterization of each of the steps in this new process, and scientific understanding of the development of microstructure and glass-metal bonding in these films are crucial to derive maximum benefit from the developed process as well as to further our knowledge in the applicability of this process to other thick film systems. It is also important to obtain a mathematical formulation for the sheet resistivity of the new thick film in terms of the system variables for an ideal microstructure. (Sheet resistivity is one of the very important properties whose values are used to differentiate resistors-conductors.) Such an approach will help us understand the relation between the microstructural features (variables) and the final film property. It was the main objective in the initial part of this study. The lead borosilicate glass/silver metal system was used as the model system. Applicability of the new process to glass/silver/gold composites was also studied.

In the latter part of this program, the nickel/silver/glass system for conducting films was studied. The choice of the metal for the thick

film conductors is usually determined by the conductivity cost, type of firing atmosphere, bondability and solderability, temperature coefficient of resistance, etc. Noble metals provide good conductivity and oxidation resistance, but the cost per unit volume is quite high compared to the base metals (Table 2).²³ Base metals, while offering the cost advantages, suffer from the lack of oxidation resistance and sometimes difficulty in bonding to other metals. Almost always, base metal films have to be fired in neutral or inert atmospheres. The new system conceived to solve these problems is the silver/nickel/glass composite system. The philosophical approach was to obtain a microstructure similar to that obtained with glass/silver thick films, nickel being the matrix and a little glass providing reactive bonding of the film to the alumina substrate. Objectives were to obtain such films by air firing, and to understand the nickel-silver interface relations and the microstructure development.

II. EXPERIMENTAL DETAILS

A. Processing

The flow diagram for the new process to make a conducting thick film is given in Fig. 4. The intended microstructure has a glass (lead borosilicate) matrix formed by coating the glass particles with a conducting phase (Ag, Ag-Au) which maintains electrical continuity. This procedure forms a conductor with much lesser volume content of the precious metal. The flow diagram for the nickel-silver thick film conductors is given in Fig. 5. The basic philosophy of the intended microstructure remained the same. In this case, Ni particles are the matrix particles and coating them with silver metal provides the electrical conductivity and protection of the nickel from oxidation during firing.

1. Glass Preparation

The glass system used in this study was lead borosilicate. The starting materials for making the glass were chemical reagent grade (H_3BO_3) boric acid, lead oxide (PbO) and silica flour (SiO_2), all 99.8% pure.

Different compositions were melted at $1000^\circ C$, cast in graphite molds and annealed at $400^\circ C$ for 15 min. Rectangular specimens $1'' \times 0.2'' \times 0.2''$, were cut from these bulk specimens. Thermal expansion coefficients were measured for the different compositions using a dilatometer. The particular composition for the thick film study (70 w/o PbO, 10 w/o SiO_2 , 20 w/o B_2O_3) was selected to provide of a thermal expansion coefficient to match that of the 96% alumina substrate.* Bulk specimens

*From WESGO, Belmont CA.

used for the silver resinate solution spreading studies were obtained from Corning Glass Works and were annealed at 400°C for 15 mins.

The glass was powdered using alumina balls in an organic lined mill with isopropyl alcohol as the liquid medium. After milling, the glass particles were size separated and suitable particle size fractions were selected by using the Fisher subsieve sizer.

Surface activation involved treating the glass particles with dilute hydrochloric acid (0.01N) for 0.75 to 5 minutes. The weight loss characteristics were obtained by treating known amounts of glass particles (20-44 μ m). An optimum etching time of 45 secs which corresponded to 2.8% weight loss was used (Fig. 6). This loss corresponded to ~0.25 μ m depth etching from the surface assuming spherical particles with an average diameter of 30 μ m.

2. Precious Metal Coating

Precious metal coatings were applied using the silver and gold metal resinates* over the surface treated glass particles. Thermogravimetric analysis of silver resinate indicated that the decomposition temperature was 210°C; and of gold resinate, close to 500°C. For the glass/silver thick film system, surface activated glass particles were treated with silver resinate solution which was decomposed at 250°C in an oven with a constant flow of air. Better uniformity of coating was obtained with slow decomposition. For a coating of silver-gold, the resinate solutions were mixed to give a suitable composition, mixed with

*Manufactured by WESGO, California:

Silver Resinate - 15 w/o in xylene, and
Gold Resinate - 8 w/o in xylene.

glass particles and then decomposed.

For nickel-silver thick film conductors, spherical nickel particles were obtained from Linde Company (Union Carbide) and were size separated. Particles in the size range of 20-30 μ m were treated with proper amounts of silver resinate solution to give the required nickel to silver ratio. Decomposition was done using two different methods. In the first method the mixture of silver resinate and nickel was placed in a furnace which was maintained at a temperature of 250°C. The decomposition of the organic resinate was sudden and resulted in agglomerates which were quite strongly bonded. In the second method the mixture was kept in an oven which was slowly heated from room temperature to 250°C with constant stirring and flow of air. Ni particles were coated with silver more uniformly than in the first method. The particles (glass as well as nickel) thus coated with the precious metal or metals were ready for thick film formulation and firing.

3. Thick Film Formulation and Firing

Precious metal coated glass particles were well mixed with the organic vehicle* to form a thixotropic paste. The solid to liquid ratio was approximately 80 to 20 w/o for a paste which was screen printable. The films were screen printed manually onto alumina substrates to get a specific pattern using a 200 mesh silk screen (stainless steel) and a squeegee. The thickness could be varied by varying the distance between the silk screen and the substrate for a given viscosity of the paste. Due to the large number of variables in the process, it was intended to

* Manufactured by Drakenfield colors, oil 14.

keep the thickness of the fired film constant at 1 mil. This objective was attained by having a constant separation between the screen and the substrate and by using the same solid to liquid ratio for a given system.

The substrates used were 96% alumina pieces of dimension 1" X 1" X .030". After printing, the films were dried for 15 mins and fired in air. The temperature increase was 16°C/min to the different firing temperatures and held constant for different times. The furnace used was based on an alumina tube (2" dia) wound with Pt-40Rh wire. After soaking, the films were fast cooled in air. Firing temperatures from 500 to 1000°C and times from 0 to 45 min were used. For silver-gold/glass composite films different firing rates were also used. For firing in an N₂ atmosphere, an alumina tube furnace (Pt-40%Rh resistant wire heating) with capabilities of vacuum or constant N₂ flow was used. Details of this furnace are given elsewhere.²³ The vacuum furnaces used for sessile drop measurements are described in the second part of the thesis.

B. Characterization

1. Electrical Resistivity Measurements

The electrical sheet resistivity was measured using a four point probe method. The circuit diagram is shown in Fig. 7. The voltage drop across the specimen was determined at currents from 4.53 to 15mA. Typical data (Fig. 8) indicate a linear variation of current with voltage. The voltage (in μV), at a current 4.53 mA is numerically equal to the sheet resistivity in $\text{m}\Omega/\square$. For thick films it is customary to define a quantity called "sheet resistivity,"²⁴ R_s , which is equal to ρ/d , where ρ

is the resistivity and d is the thickness of the film. As the film is essentially 2-dimensional, R_s can be considered to be a material property. Sheet resistivity is conveniently measured using the four point probe method, wherein four contacts are made to the film and current is injected and taken out through the end contacts. Voltage drop is measured between the two middle contacts. The sheet resistance is proportional to the ratio of the voltage, V to the current, I . That is,

$$R_s = C(V/I)$$

where C is a constant of proportionality that depends on the configuration, position and orientation of the probes and on shape and size of the sample. For an infinite film $C = \frac{\pi}{\ln 2} = 4.5324$. If the ratio of the length of the film to the distance between the probes ~ 100 , then C would be equal to 4.53 and when the ratio is of the order of 10, C would be 4.36. Hence, when the current is made equal to 4.53 A, the measured volts would directly give the sheet resistance in ohms per square.

2. Microstructural Analysis

Optical and scanning electron microscopy were used for microstructural observations. Standard techniques of specimen preparation for microscopy were followed. With transmission optical microscopy better phase contrast was obtained for the glass/metal thick film composites. However, for observing the metal coated particles, the glass surface, the nickel-silver interface and the nickel-silver thick films scanning electron microscopy was the better technique. For non-conducting films and glass specimens, a gold coating (thickness 200\AA) was sputtered on to the surface to avoid charging effects. The scanning

microscope used was an AMR Model 1000. For elemental analysis of the different phases, an EDAX unit (energy dispersive analysis of x-rays) attached with the SEM, and an electron microprobe analyzer were used.

Secondary electrons generated by scanning of the specimens surface by an electron beam (100-150 \AA diameter) are used to generate the images in the SEM. The signal generated varies gradually as the local surface slope varies and the image generated reflects the topography of the specimen. The characteristic x-rays generated in the sample are used to obtain elemental analysis of the region of the sample being hit by the electrons. The electron microprobe analyzer uses this method with wavelength dispersive diffracting spectrometers to measure, identify and count x-rays. The advent of the SEM with its much lower electron beam currents in order to achieve smaller beams for high resolution images and rough samples (which do not lie in the focusing circle of a wavelength dispersive spectrometer) has led to the development of the energy dispersive x-ray analyzer.²⁵ This unit has an Li doped Si solid state detector which measures x-ray energy directly when the incoming x-rays produce a shower of photoelectrons whose number depends on the energy of the incoming x-rays. Lithium atoms fill up the imperfections in silicon to prevent any loss of photoelectrons due to trapping. Even though this method is quick and convenient (even for poorly prepared specimen surfaces), for quantitative measurements (of the amount of each element present) the microprobe analyzer is the more accurate instrument.

For looking at the thick film-alumina substrate interface, there was considerable difficulty in the preparation of the specimen. Transoptic powder was used for mounting the sectioned specimens and then they were

finely polished (using $.3\mu\text{m Al}_2\text{O}_3$).

An in situ hot stage facility in the scanning microscope* was used to observe the microstructure in these thick films during firing. Even though the firing atmosphere in the microscope (vacuum 1 to 3×10^{-5} torr) is different from the actual firing atmosphere (air atmosphere), these hot stage scanning studies were helpful in understanding the microstructure development along with the optical micrographs of the thick films fired at different temperatures. The specimens for the hot stage were prepared in the following manner: Silver coated glass particles were mixed with an organic vehicle to give a thixotropic paste which was then brushed onto a circular substrate (cut from 96% alumina) of diameter $\sim 2\text{mm}$, specially prepared for the hot stage. Then, it was dried and heat treated at 450°C to drive off all the organics and was ready for observation.

3. Measurements Related to Surfaces

a. X-ray photoelectron spectroscopy: For surface studies, the XPS technique was used. In addition to being a surface elemental analysis technique ($\sim 10\text{-}20\text{\AA}$ of the top surface), oxidation states of the elements could be determined by the binding energy of the elements. As the analysis involves the outermost electron energy of the element (unlike an inner shell electron as in Auger Spectroscopy), the binding energy obtained will be different for different compounds of the same element.²⁶

* Developed at Lawrence Berkeley Laboratory, Materials and Molecular Research Division.

Spectra of the different glasses, Ag, and silver compounds were obtained on the McPherson ESCA 36 electron spectrometer. Except for Ag metal all other materials were run as finely powdered samples brushed onto one side of a double stick scotch tape. In all the cases the contaminant C_{1s} line was used as a reference. This line was arbitrarily assigned a binding energy of 285.0 eV for the spectrometer.

Mg K_{α} x-rays (1253.6 eV) were used as the ionizing radiation. To get these x-rays electron currents of 35mA accelerated by 9kV voltage were used to bombard a Mg target. Binding energies were determined by finding the center of the peak at half width in the spectra obtained. Comparison of the intensities (normalized) was made to obtain semi-quantitative results on the concentration of each element in the glass surface study.

b. Surface area measurements: Surface areas of the glass particles in different size fractions were measured using a Quantasorb meter, (made by Quantachrome Co.) using the BET, Nitrogen adsorption method.

c. Sessile drop measurements: To study the LBS glass/alumina interfaces, sessile drop studies of glass on alumina substrate (96 w/o) and on sapphire were conducted in an air atmosphere using an open tube Lindberg Heviduty furnace. The contact angles were measured at 700°C using a tele-goniometer after the drop attained an equilibrium angle. Then the samples were sectioned, mounted and polished for microscopic observation, using the standard specimen preparation techniques.

RESULTS AND DISCUSSION

The new process developed to obtain a proper microstructure in glass-metal thick film systems is outlined in Fig. 4. In the new microstructure a continuous electrical path is provided by the metallic film coated around the glass particles instead of by the conventional bulk metallic particles. It is important to have a strong adherence of the metal film to glass to maintain continuity of the metal phase, even after the final firing step, to obtain a good conductor. Earlier work²² has indicated that the surface characteristics of the glass phase are very important in achieving this goal. With acid etching (later termed surface activation) of the glass particles, thick film conductors with as low a metal (Ag) content as 20 w/o were obtained (Table 3). To understand the development of the microstructure in these thick films, a detailed analysis of the material characteristics and the different steps of the new process are carried out in this section.

A. Materials

Lead borosilicate glasses (LBS glasses) were chosen as the standard glasses in this study for the following reasons. The softening temperature of these glasses are comparatively low at high lead contents (~400-450°C) and the thermal expansion coefficient can be varied by varying the composition. Additionally, the system is well studied.

Measured thermal expansion coefficients of the glasses in this system are given in Tables 4 and 5. Table 4 gives the results of the present work and Table 5 gives the results from the study by Vest and co-workers.²⁷ As thermal expansion for glasses can be expressed as an

additive property based on experimentally determined oxide coefficients,²⁸
the expression for the expansion coefficient (α_{glass}) is given as

$$\alpha_{\text{glass}} = W_{\text{PbO}} \alpha_{\text{PbO}} + W_{\text{B}_2\text{O}_3} \alpha_{\text{B}_2\text{O}_3} + W_{\text{SiO}_2} \alpha_{\text{SiO}_2}$$

where α 's are the thermal expansion coefficients and W's are the weight fractions of the different components in the glass. By measuring the α_{glass} for different compositions of SiO_2 , B_2O_3 and PbO (minimum of three different compositions) and by knowing the weight percentages, a set of simultaneous equations are obtained and solved for α_{PbO} , $\alpha_{\text{B}_2\text{O}_3}$ and α_{SiO_2} (contributions to the expansion coefficient by the component oxides) to obtain concurring results (Table 4 and Table 5).

For the glasses of the present study, contributions by the component oxides were found to be

$$\alpha_{\text{PbO}} = 1.33 \times 10^{-7} \text{ in/in}^\circ\text{C}$$

$$\alpha_{\text{B}_2\text{O}_3} = -.357 \times 10^{-7} \text{ in/in}^\circ\text{C}$$

$$\alpha_{\text{SiO}_2} = -.277 \times 10^{-7} \text{ in/in}^\circ\text{C}$$

Both B_2O_3 and SiO_2 give a negative contribution to the expansion coefficient. For the glass compositions studied by Vest et al., the contributions were calculated to be

$$\alpha_{\text{PbO}} = 1.199 \times 10^{-7} \text{ in/in}^\circ\text{C}$$

$$\alpha_{\text{B}_2\text{O}_3} = -.321 \times 10^{-7} \text{ in/in}^\circ\text{C}$$

$$\alpha_{\text{SiO}_2} = -.287 \times 10^{-7} \text{ in/in}^\circ\text{C}.$$

When the respective contributions were used to calculate the expansion coefficient of the glass, good correlations between the calculated and measured values were obtained in both cases. For a constant PbO content, an increase in the B_2O_3 content (and hence a decrease in the SiO_2 content) slightly lowers the expansion coefficient. This is due to B_2O_3 having a more negative contribution than SiO_2 . The above contributions vary sharply from the values given by English and Turner²⁹ for these oxides:

$$\begin{aligned}\alpha_{PbO} &= 1.06 \times 10^{-7} \text{ in/in } ^\circ\text{C} \\ \alpha_{SiO_2} &= .05 \times 10^{-7} \text{ in/in } ^\circ\text{C} \\ \alpha_{B_2O_3} &= -.66 \times 10^{-7} \text{ in/in } ^\circ\text{C}.\end{aligned}$$

These linear contributions were calculated based on the assumption that silica carried the expansion of fused quartz into the glass. The factors calculated in the present study are different from the other published results as well (Table 6).^{30,31} All of these published results arose from a study of different systems of glasses. The particular system of glasses as well as the composition regions are, however, very important in determining the effect of each additional component oxide on the thermal expansion coefficient of a glass. The factors determined in this study hold good for the high lead content (~70 w/o PbO) lead borosilicate glass system. The softening points of these different compositions are less than 450°C. From the expansion curve the transformation temperature range was found to be around 410°C-465°C for the different compositions.

The particular glass chosen for this study had the composition 70 PbO, 20 B_2O_3 , 10 SiO_2 (by weight) whose measured expansion coefficient

was 7.9×10^{-6} in/in $^{\circ}$ C (Fig. 9). The substrate used was 96% alumina which had an expansion coefficient of 8×10^{-6} in/in $^{\circ}$ C over a temperature range of 0-1000 $^{\circ}$ C.³² As the expansion coefficient of glass is less than that of the alumina substrate, the glass film on the substrate tends to be in compression after firing, which is a desirable factor.

B. Glass-Alumina Interface

The surface of the alumina substrate as seen from SEM is shown in Fig. 10, which indicates the presence of some surface porosity. From the EDAX analysis the impurities detected on the surface were magnesium and silicon (Fig. 11). There is a considerable amount of silica in these 96% Al₂O₃ substrates. Conventional conductor films have lead borosilicate glass as a flux which bonds the metal to the substrate. Hence, it is important to understand the nature of interfacial bonding between lead borosilicate glass and alumina (96%). Contact angle measurements of the glass drop on alumina and sapphire substrates indicated good wetting of these substrates by glass. In an air atmosphere contact angles of 6-8 $^{\circ}$ were obtained at 600 $^{\circ}$ C on both alumina and sapphire substrates. Strong adherence was observed and the edges of the drop were irregular. Cross-sectional analysis of the interface using SEM-EDAX was done and Fig. 12 shows the micrograph of the interface of alumina and glass. From the x-ray line mappings, there is a qualitative indication that (i) dissolution of alumina in glass and (ii) reaction of silica phase (present in Al₂O₃ with glass) must be responsible for the strong bonding observed. The peaks and drops observed in the x-ray line mappings of Al, in the Al₂O₃ region are due to the topographical changes on the surface. At the interface x-ray line intensity of both Pb and Al

do not vary sharply, reaching zero level in a $\sim 5\mu\text{m}$ distance across the interface. There is also a step observed in the x-ray line intensity of Al at the interface. The micrograph also indicates the possibility of the presence of a different phase (see P in Fig. 12) at the interface. Kim et al.,²⁰ studying the mechanism of adhesion of thick films to the Al_2O_3 substrates, could not identify any reaction and hence concluded that there is no chemical bonding between the glass and the substrate. But, with the strong adherence obtained and the above observations, there is a strong indication that a chemical reaction initiated by a drive towards chemical equilibrium is contributing to the development of chemical bonds across the interface. For a quantitative analysis, however, more detailed study of the interface is necessary.

C. Surface Activation

In the new thick film conductors developed, precious metal coated glass particles are used instead of the conventional metal particles, thereby reducing the total volume of the metal in the system. In such systems, it is then necessary to have strong bonding between the metal film and the glass particle. To obtain a good conducting film with the least amount of silver metal, treatment of glass particles by dilute HCl was found to be a critical step.²² Table 3 gives the sheet resistivity of some of these conducting films. Without the acid treatment, even though the metal content was not changed, insulating films were obtained.

The surface of the high lead content glass is activated when treated with diluted HCl . HCl treatment is crucial in getting strong adherence between the glass and the metal film. High lead content glasses essentially exhibit a two phase structure,³³ wherein a microdispersed phase

is embedded in a silica rich phase. Dilute hydrochloric acid would dissolve the microdispersed lead rich phase leaving micropores on the surface of the glass (Fig. 13). In addition, the activity of the surface is enhanced by a chemical reaction. The H^+ ions in the acid and Pb^{2+} ions in the remaining glass take part in an ion exchange reaction which is given as



These H^+ ions make the glass surface active as they are capable of entering into further reactions in the later steps of the process, aiding in the development of strong bonds between metal and glass.

To understand the effect of acid treatment on glass surface in greater detail, the glass surface and the crystals obtained from the acid filtrate (after etching) were analyzed.

When the filtrate (obtained after filtering the glass particle - acid mixture) was held in a pyrex glass container for 2-3 weeks, needle shaped crystals precipitated out of the solution. Figure 14 shows these crystals as observed in the scanning electron microscope. EDAX analysis marked the presence of Pb, Cl and Si in these crystals and analysis was not possible. The x-ray diffraction pattern obtained for these crystals is shown in Fig. 15; however, it was not possible to identify the exact crystal composition. It is possible that this is a complex structure with Pb, Cl, Si (and possibly B also) having a nonstoichiometric composition hitherto unknown. However, this result indicates that silica and possibly a little B_2O_3 are also leached out along with lead oxide. X-ray photoelectron spectroscopy study of the glass surface before and after etching

provides more conclusive proof for this observation.

The photoelectron spectra obtained for etched and unetched glass powders are given in Figs. 16 and 17. The binding energies (B.E.) obtained for Pb, B and Si peaks (given in Table 7) were calibrated using the containment C_{1s} line with an assigned binding energy of 285.0 eV. The relative intensities for these peaks were measured by counting the number of divisions (spectra being plotted on the same scale) and multiplying that number by the number of scans, time of scan and sensitivity, which is characteristic for each element.

The lead borosilicate glass was etched with .01N HCl for 45 secs. To measure the effect of acid leaching on the composition at the surface, intensity ratios of Pb/Si, B/Si and Pb/B in both etched and unetched samples were calculated.

These values are tabulated in Table 8. Both Pb/Si ratios decrease considerably after etching, whereas, the ratio Pb/B increases only slightly. The intensities of the spectra (proportional to number of photoelectrons/sec) depend on the molar concentration of the elements. As the initial composition of the glass is already known (70 PbO 10 SiO₂ 20 B₂O₃ Wt%), it is quite possible to calculate the weight ratios of Pb, Si and B after acid treatment using the above intensity ratios. The weight ratios of these elements before and after acid treatment are given in Table 9. The Pb/Si ratio decreases from 7 to 5.264 and the B/Si ratio decreases from 2 to 1.364 after acid treatment. This is a strong indication of the leaching of B in addition to Pb. In fact, the Pb/B ratio increases slightly (3.5 to 3.858), indicating a higher percentage of B leached in comparison with Pb. Thus the acid treatment changes the surface

composition of the glass drastically. The surface of the glass is now rich in silica as Pb and B get leached out by the acid. However, a very small amount of SiO_2 is also leached as indicated from the study of crystals obtained from the etching solution. By acid treatment, principally Pb and B are leached in large amounts and this results in a silica rich shell (with a higher softening point) around the glass particles in addition to an activated glass surface.

D. Precious Metal Coating on Glass

Scanning electron micrographs of the etched glass particles coated with silver are shown in Fig. 18. The silver film coating is formed by thermal decomposition (at 250°C) in an air atmosphere of an organometallic compound of silver (in this case silver resinate) dissolved in an organic solvent (xylene). Xylene evaporates off at 140°C (boiling point of xylene) and silver resinate decomposes at 210°C (from TGA experiments) to give metallic silver. Silver content in the composite particles shown in the figure is ~25 w/o. Average size of the glass particles is $\sim 25\mu\text{m}$ and the thickness of the silver film is calculated to be $\sim .25\mu\text{m}$ from measuring the surface area of the glass particles to be covered by the precious metal. The silver film has a spongy structure and is quite uniform in thickness. The uniformity in the thickness of the film is due to the spreading of the resinate solution on the etched glass surface.

Wetting experiments conducted on bulk glasses - both etched and unetched, indicated (i) an acute contact angle with the unetched glass and (ii) spreading (0° contact angle) of the resinate solution on the etched glass surface. However, a minimum etching time (20 mins with .01N HCl, 5 mins with .1N HCl) was necessary to develop good bonding

between glass and silver after decomposition in air (at 250°C). The etching also develops a surface roughness. Spreading of the resinate solution on the etched glass is aided by both the H⁺ implantation and the surface roughness generated by the acid treatment. It is difficult to separate these effects from one another as the roughness is created by dissolving the lead rich phase with simultaneous implantation of the H⁺ ions at the glass surface. The spreading of the resinate solution is also related possibly to the development of bonding between silver and the glass after the decomposition of the silver resinate.

With unetched bulk glasses, the adherence of the silver film was poor and the film flaked off easily on gentle scratching. Strong adherence, however, was obtained with an unetched glass when decomposition of the resinate was done at temperatures >480°C in an air atmosphere. After such a deposit, if the silver film is heated to high temperatures beyond the melting point of silver (holding the glass in an alumina container at 1100°C), it remains as a film on the glass surface. There is strong bonding and also an indication of reduction in the volume of metal with time. However, no quantitative studies on the adhesion energy or solubility of silver in glass was done.

In the fired thick films using unetched glass powders, resistivities higher than $10^{12} \Omega/\square$ were obtained due to the absence of a continuous metallic phase (Fig. 19). If extreme care is taken to prevent flaking of the silver film (after decomposition at 250°C) from the unetched glass particles during mixing, it is possible to get lower sheet resistivities. In some runs, sheet resistivities as low as $1\Omega/\square$ were obtained using unetched glass particles (with 30 w/o Ag). Strong bonding between

glass particles and the metal film is preferred at all times. Decomposing the resinate at temperatures $>480^{\circ}\text{C}$, which results in good bonding of the metal to the glass without etching of the glass, is impractical as the glass particles would soften and sinter together. The particles then are not small enough for screen printing. Etching provides good bonding between silver and glass at favorably low temperatures (as low as 210°C). Sheet resistivities of thick film conductors obtained with etched glass particles, which were strongly bonded to silver, were as low as $75\text{m}\Omega/\square$ with 30 w/o of silver. Figure 20 shows an optical transmission micrograph of a conducting thick film developed by this process. If the decomposition of silver resinate is done in N_2 (at 250°C), silver to glass adherence is poor even with the etched glass particles. The film flakes off easily on gentle scratching indicating weak bonding at the interface of metal and glass. Adherence does not develop even when the specimen is heated beyond the transformation temperature range of the glass system ($\sim 480^{\circ}\text{C}$) if N_2 atmosphere is used. When the thick films were fired in N_2 with no prior decomposition of the resinate in air, they were found to be insulating even with 30 w/o of Ag. Figure 21 shows the scanning micrograph of a thick film (25 w/o Ag) using acid etched glass particles which were fired in N_2 at 980°C for 30 mins. Silver phase agglomerates to spheres indicating no wetting of the silver by glass in the presence of nitrogen.

E. Reaction Mechanisms

According to earlier understanding $^{22}\text{H}^+$ ions implanted during acid treatment took part in an ion exchange reaction with Ag^+ from the silver resinate solution. X-ray fluorescence spectra of etched and unetched

glass particles - treated with silver resinate solution at 80° and then thoroughly washed with xylene - had indicated such a reaction. A silver peak was obtained for the etched glass particles and no trace of Ag was observed for unetched particles. However, x-ray fluorescence cannot indicate the valence state of silver present on the surface of these glass particles. To understand the reaction at this step of the process, x-ray photoelectron spectroscopy (XPS) studies were done on these particles.

The bonding energies obtained for Ag 3d5/2 electron peaks in the x-ray photoelectron spectra of different specimens studied are given in Table 10a. A typical spectrum obtained for pure silver metal is shown in Fig. 22. Again, the C_{1s} contaminant line (with an assigned binding energy of 285.0 e.V.) was used for calibration. For comparison, Table 10b gives the B.E. values obtained for silver and some silver compounds by other researchers. These studies have shown that most of the silver compounds show a shift (generally an increase) in the electron binding energy compared to that of pure metal, which is quite consistent with the present results. The binding energy obtained in the case of Ag metal is 368.1 e.V. and for AgNO₃ it is 368.45 e.V. For etched glass powders which are treated with silver resinate solution (at 80°C) and then washed thoroughly, the binding energy obtained for Ag 3d5/2 electron is 368.4 e.V. which is the same as obtained for silver resinate. This result conclusively indicates that the silver peak obtained with the glass powders is due to small quantities of silver resinate trapped in the pores at the glass surface and not to of any ion exchange between the etched glass particle and silver resinate as thought earlier. This deduction is also supported by the fact that silver resinate in xylene is a nonconducting

solution. However, when photoelectron spectrum is obtained after the silver resinate treated etched particles are heated to 250°C (whereby whatever silver resinate is trapped in the pores decomposes to give pure silver), the silver peak obtained has a binding energy of 368.2 e.V. which differs by 0.1 e.V. from the value obtained for silver metal. This increased value is most probably due to the following reasons. After the resinate is decomposed to silver, it oxidizes in the presence of O_2 and H^+ (on the glass surface, implanted by acid treatment) and then the silver ions diffuse into the glass. The binding energy of Ag electrons are then different as Ag^+ ions are embedded in the glass structure providing a different environment and bonding structure than in the pure metal. These Ag^+ ions share the oxygen atoms existing in the glass network, and the binding energy obtained could be expected to be closer to that of Ag_2O . From the results of Dickinson et al.³⁴ the difference $(B.E.)_{Ag_2O} - (B.E.)_{Ag} = 0.1$ e.V. which is the same as the B.E. difference of Ag peak obtained for the silver diffused glass particles under study (etched, treated with silver resinate, washed with xylene and then decomposed) and silver metal. These observations lead to the conclusion that strong chemical bonding develops between silver and glass after the silver resinate is decomposed (at temperatures $>210^\circ C$) in the presence of oxygen and H^+ ions.

This strong bonding between the etched glass and silver is due to chemical bonding when there is saturation of metal oxide at the interface. In other words, we have a continuity in the electronic structure which is made possible by oxidation of silver to Ag^+ and its subsequent diffusion into glass. The most probable reaction for this effect occurs in the

presence of H^+ ions and oxygen:

| | <u>E° Volts</u> |
|--|-----------------|
| $O_2 + 4H^+ + 4e^- \rightarrow 2H_2O$ | 1.229 |
| $4(Ag^+ + e^- \rightarrow Ag)$ | .800 |
| <hr/> | |
| $O_2 + 4H^+ + 4Ag \rightarrow 2H_2O + 4Ag^+$ | .429 |

Oxidation of silver in the presence of H^+ and oxygen is thermodynamically very favorable with $\Delta G = -165.6$ KCal/mole, so oxidation will take place after the decomposition of silver resinate into silver. This reaction explains the lack of bonding when the decomposition of the resinate is done in a N_2 atmosphere, or when the surface of the glass is not acid treated. The presence of both H^+ and O_2 are equally important. Lack of bonding in the N_2 atmosphere indicates that the surface roughness gives only a small contribution to the bonding of the metal to glass and the major contribution to the bonding is chemical in nature which is achieved by the oxidation of silver in the presence of oxygen at the interface as explained by the above reaction.

Strong bonding observed in unetched glasses (i.e. in the absence of H^+ ions) in air atmosphere at high temperatures ($\sim 480^\circ C$, above the softening point of the glass) is due to surface oxidation of Ag at these temperatures and subsequent solution of this interfacial oxide layer. When the silver films on these glasses are heated to $1100^\circ C$ and held there for sufficient times ($\sim 1/2$ hr), solution continues and considerable reduction in the volume of silver results, supporting the earlier observation. More detailed depth profile studies using Auger or photoelectron spectroscopy need to be done in the future.

F. Firing Effects

Firing is the very important final step in the making of a thick film conductor. During firing the printed thick film goes through a series of changes. First, the organic vehicle burns out (around 450-500°C) leaving a very porous film. Subsequent changes during firing were monitored in the hot stage SEM as well as using conventional sample preparation techniques for high temperature microstructure observation. Even though the vacuum conditions of the SEM hot stage affect the microstructure development (due to increased degassing in the glass phase and lack of oxygen in that atmosphere), hot stage SEM study gives valuable information regarding the behavior of glass and metal phases during firing. Glass particles used in these thick films appeared to soften and flow only above 600°C. Above this temperature, the sharp edges of the particles started becoming rounded and glass flow was observed at the edges of the thick film (Fig.23). Even though the lead borosilicate glass has a softening point of 450°C, the etched glass particles have a silica rich shell and the metal film around them. These layers prevent the flow of the glass until 600°C, after which they could no longer protect the inner core of glass from flowing.

At temperatures around 500°C ($\sim 0.5 T_{m.p.}$ for silver), silver to silver sintered contacts are formed and at temperatures beyond 600°C, due to glass flow, rearrangement of these coated particles takes place. Also, glass wets the alumina substrate by flowing out of the coating and develops strong bonding at the substrate - thick film interface. Even though the final resistivity of the thick film can be affected by choosing different firing times and temperatures, in the present system

very little change in the sheet resistivity value was observed when the films were fired at temperatures ranging from 500°C to 750°C and times of 0 to 30 mins. Transmission optical micrographs in Fig. 24 show the microstructure of the films fired at different temperatures. The film fired at 500°C shows the porosity existing between the silver coated glass particles after all the organics were burnt out, but before any glass flow has occurred. However, silver to silver sintered contacts are made (sheet resistivity is quite low, $R_s \approx 160\text{ms}/\square$ with 25 w/o Ag) at this temperature. At 600°C, all the pores are closed but not much displacement of the metal film is observed. As the firing temperature increases, glass flow increases and with it the tendency of the silver film to agglomerate into chains. Micrograph of the film fired at 700°C shows big islands of glass, surrounding which is the silver phase which has been transformed from a film structure to agglomerated chain configuration due to glass flow at these temperatures. Films fired at 800°C show no conduction indicating discontinuity in the metal phase. The bonding between glass and silver is strong and solubility of silver increases at higher temperatures. Due to increased diffusion of Ag^+ from the interface into the bulk of the glass at these temperatures, the links in the chain structure of silver became thinner and thinner, finally leading to a discontinuous metal phase (and hence an insulating film). Thus there is a limit to the highest possible firing temperature (with 20-44 μm glass particles it was $\sim 750^\circ\text{C}$). When smaller size particles were used (with an average size 2.5 μm), glass began to flow at much lower temperatures. The highest possible firing temperature was also reduced to 700°C. This reduction is due to a much thinner silica shell and thinner metal coating

around these smaller particles. The surface area varies inversely as the size of the particle. Smaller particles will have a larger surface area to be etched and coated. With a constant amount of acid (for etching) and metal (for coating), the smaller glass particles would therefore have thinner silica shells and metal films around them. Micrographs shown in Fig. 25 show larger glass islands as a result of early glass flow (i.e. at lower temperatures) in these thick films with smaller glass particles. Sheet resistivity is also higher in these films (Table 11) which is a result of the thinner metal coating. This dependence will be explained in detail in the next section.

The firing range could be increased by using matrix particles that do not flow and thus maintain the intended microstructure at higher temperatures (up to 950°C). Also, as solderability is an important criterion for thick film conductors, a solderable matrix material should be used. A nickel/silver composite thick film system (with a little addition of glass as flux) was conceived to achieve these improvements. This system is discussed in detail at a later stage.

G. Dependence of Sheet Resistivity on Metal Content and Matrix Particle Size

For the type of microstructure that is developed in this study it is quite possible to predict the final sheet resistivity knowing the metal content and the average glass particle diameter. In the ideal case, a uniformly thick conducting metal film exists around the matrix particles. If we have spherical matrix (glass) particles of uniform diameter D , then the thickness of the metal film F_m can be calculated for various metal contents (V_m). The thickness of the film will depend on the size of the matrix particles. Let V_g be the volume content of the matrix (glass in this case) phase.

Total surface area (S) of the glass particles to be covered by the metal is given by

$$S = \pi D^2 n \quad (1)$$

where n is the number of glass particles in the volume V_g . The volume of each spherical matrix particle, v , is given by

$$v = 4/3 \pi (D/2)^3 \quad (2)$$

The number of particles n , in the volume V_g is then given by

$$n = V_g / v = V_g / 4/3 \pi (D/2)^3 \quad (3)$$

Substituting equation (3) in the expression (1) for the surface area and simplifying,

$$S = 6V_g / D \quad (4)$$

If V_m (Cm^3) is the available metal volume to cover an area S (Cm^2), the thickness of the metal film will be

$$t_m = V_m / S = V_m / V_g \cdot D/6 \text{ cms.} \quad (5)$$

Further, if there are only two phases and V's are expressed as volume percents

$$t_m = \left[\frac{V_m}{(100-V_m)} \right] \cdot D/6. \quad (6)$$

The variation of the metal thickness with the matrix particle diameter for various metal to matrix phase volume ratios has been plotted in Fig. 26. For a constant volume ratio, the thickness of the coated film decreases with the size of the matrix particle as there will be a larger surface area to cover. The variation of the film thickness with different metal contents for different matrix particles sizes is shown in Fig. 27. For a constant particle diameter, thickness varies slowly until the metal content is 50 volume % and then increases very sharply. For the glass particle diameter of $1\mu\text{m}$ the thickness variation of the film with metal content becomes very prominent after 70 Vol.% of the metal.

The thickness of the metal film is important in determining the sheet resistance of the thick film conductor with the type of microstructure developed in this study. The glass phase is essentially an insulator ($10^{14} \frac{\Omega}{\square}$) and does not contribute to conduction. Thus, conduction occurs when there is continuity of the metal phase; otherwise, the thick film is essentially an insulator. Once there is good continuity, the sheet resistivity of the thick film will depend mainly on the thickness of the conducting film around the glass matrix phase. It is important that the metal to metal contacts are well sintered since the

sheet resistivity depends on the number of metal to metal contacts.

This dependence is significantly altered for firings at higher temperatures and also for films which are printed thin (thickness <0.6 mil).

It was also noted that the thick films have a higher sheet resistivity when the thickness is significantly less than 1 mil. For a .5 mil thick film with 25 w/o Ag sheet resistivities (R_s) ~500 m Ω /□ were obtained. To reduce the number of variables for the system, thick films of 1 mil thickness were used as a standard for all the measurements.

Sheet resistance for the thick films (R_s) in the present study can be calculated as follows. It is known that sheet resistance for a single phase conductor film is defined as $R_s = \rho/t$ where ρ is the bulk resistivity of the conducting material and t is its thickness. The sheet resistance of the thick films is a function of the thickness of the coated metal film. It can be written as

$$R_s = \rho / (K \cdot t_m) \quad (7)$$

where K is a proportionality constant, for a constant thickness of the thick film. On combining Eq. 5 and Eq. 7

$$R_s = \frac{6\rho}{KD} (V_g/V_m) \quad (8)$$

where ρ is the resistivity of silver, D is the glass particle diameter and V_g/V_m is the glass to metal volume ratio. K is the proportionality factor which is a constant for a given thickness of a thick film and also a given particle size range. It is also important that firings of the films be in the optimum range so as to achieve the required

microstructure. K was experimentally determined for a set of thick films (25 w/o* Ag, thickness, 1 mil) which were fired at 600°C for different times by measuring their sheet resistivities. The value of K determined in this manner is equal to 0.1 for film thicknesses of 1 mil and this value could be used to determine the R_s for thick films with different metal contents and particle diameters. However, it is important that the fired films have thicknesses close to 1 mil and the firings are done between 500-750°C for times varying from 5 to 30 mins.

The close correlation between the theoretically calculated and the experimentally measured sheet resistivities for varying metal contents is seen in Fig. 28. These films (thickness 1 mil) used acid etched glass particles of size range 20-44 μ m and firings were done between 500-700°C for times between 8 and 20 mins. The value of $K = 0.1$, however, indicates a large deviation from the ideal microstructure. When the particle size is varied, thickness of the metal film and hence, the sheet resistivity, changes. Figure 29 compares the data obtained using different glass particle size ranges - <10 μ m, 10-20 μ m, 20-30 μ m. Theoretical curves were obtained using an average diameter for each range, in the sheet resistivity calculations. Good correlation between calculated and measured values of R_s seen here supports the model discussed above.

The sheet resistivity would also depend on factors like the degree of sintering of the contacts, number of metal to metal contacts (which would depend on the printing and the firing steps of the process). Also, the nonsphericity of the glass particles leads to a large deviation from

* See Appendix for w/o \leftrightarrow V/o.

the ideal microstructure. All of these factors make the introduction of the proportionality constant necessary. For an ideal microstructure the value of K will be unity. In the glass-silver thick film system, however, the deviations from the ideal microstructure cannot be eliminated because of the nonsphericity of the glass particles and because of the flow behavior of glass matrix during the firing, which would move silver film into new configurations, while maintaining the continuity. Even if we measure the surface area of glass particles and then calculate the thickness of the metal film for a constant volume of metal, (which would eliminate the nonsphericity deviation), there still will be a fudge factor necessary to correlate the experimental results to the model. This is due to the firing effects which are prominent in this system as there are large amounts of glass present.

As we will see later, in nickel/silver systems with spherical nickel matrix particles and with a glass content of 5w/o, the value of K is equal to 1, indicating that the microstructure is close to ideal.

H. Nickel-Silver System

The flow diagram for processing of a nickel/silver glass conductor is shown in Fig. 5. In this system nickel particles form the matrix and silver is coated on these particles by slow thermal decomposition of silver resinate in the presence of air flow and constant stirring. Uniform coatings of silver on nickel particles are achieved (Fig. 30) with sufficient adherence. These coated particles are mixed with glass frit (<10 w/o) and an organic vehicle and printed on an alumina substrate. The firing is done in an air atmosphere instead of the conventional inert atmosphere used for base metal thick films. Sheet resistivities of the fired films are given in Table 12. With as low a silver content as 20 w/o, low sheet resistivities ($10-15\text{m}\Omega/\square$) are obtained. These values are lower than conventional precious metal thick films containing 80-90 w/o Ag, which have sheet resistivities of the order of $25-50\text{m}\Omega/\square$. The resistivities of the nickel-containing films are also lower than the values obtained with glass - silver thick film conductors (with 20 w/o Ag, R_s is $\sim 230\text{m}\Omega/\square$). There is, however, some scatter in the values with films fired at higher temperatures due to higher glass content. With 5 w/o glass conducting films ($R_s = 25\text{m}\Omega/\square$) are obtained with firing temperatures as high as 950°C (with glass-silver system highest firing temperature was $<800^\circ\text{C}$). However, the maximum firing temperature is restricted by the melting temperature of silver for reasons discussed later. Figure 31 shows the microstructure of a nickel-silver thick film conductor (25 w/o Ag, fired in air at 605°C for 15 mins) as seen in an SEM. The granular structure of silver films around nickel particles is noticeable. (Silver to nickel bonding, both in inert and air atmospheres, will be discussed

in detail in Part II).

The sheet resistivity of the film which contains about 5 w/o of glass is $15\text{m}\Omega/\square$. The silver coating, even though uniform, does not prevent oxidation of the nickel completely, as determined by thermogravimetric analysis. As a result of this oxide layer, when the film is fired above 963°C (m.p. of Ag), the silver film breaks up to form globules with a 90° contact angle; the loss of silver metal continuity results in the formation of an insulator. The only phase contributing to conduction is silver because of the oxide layer (insulator) between the silver film and nickel particles.

The model developed to calculate the sheet resistivity of glass-silver thick film conductors could be used to study the effect of silver content on the sheet resistivity of nickel/silver/glass films.

Using equation (8)

$$R_s = \frac{6 \rho_{\text{Ag}}}{K D_{\text{Ni}}} V_{\text{Ni}}/V_{\text{Ag}} \quad (9)$$

where D_{Ni} is the diameter of nickel particles, $V_{\text{Ni}}/V_{\text{Ag}}$ is the nickel to silver volume ratio, ρ_{Ag} is the bulk resistivity of silver, and K is a proportionality constant. By measuring R_s for one set of fired films K was calculated to be ~ 1.0 indicating that the microstructure obtained is close to ideal. R_s was then calculated and also experimentally measured for films with varying Ag content and firing conditions (within the temperature-time range of 550°C to 950°C and 0 min to 30 min). The good correlation between theoretical and experimental data is seen in Fig. 32.

These thick films have good solderability with commercial Pb-Sn solders unlike the glass-silver thick films. This behavior is due to the fact that the matrix particles are also wettable by the solder.

Thus the new base/precious metal composite conductor system, which has only about 25 w/o of precious metal, is a definite improvement on the existing thick film conductor systems because it can be fired in air and is solderable. In order to obtain lower sheet resistivities, oxidation of the nickel metal would have to be prevented by firing in inert atmospheres. The base metal then would not only provide matrix particles, but would also contribute to conduction. In the air-fired conductors, however, since the actual conducting phase is only a thin film ($\sim 0.25\mu\text{m}$) some of the property advantages (like low noise level and loss factor) that the conventional thin films have over thick films at high frequencies, could be realized (e.g., for microwave applications).

SUMMARY AND CONCLUSIONS

Present study resulted in a new concept of microstructure for thick film conductors. By having a metal film coated around the matrix (glass) particles of the thick film, efficient use of precious metal phase could be achieved. Conductors were obtained with metal (silver) contents as low as 20 w/o. The sheet resistivities obtained with 40 wt% of silver (~45 m Ω /sq) were favorably comparable with the sheet resistivities of conventional thick films using 80 to 90 wt% of precious metals. Good adherence between lead borosilicate glass (matrix) and silver (metal coating) was achieved by dil. HCl treatment of the glass particles. H⁺ ions implanted during this treatment entered into further reaction with silver and oxygen to generate Ag⁺ ions. These silver ions went into solution with glass contributing to the formation of a chemical interface and therefore a good adherence between glass and silver. Similar microstructures can be achieved with other precious metals (Au, Pt, etc.). (Thick film conductors were obtained using Au and Pt coated glass particles. However, more detailed study is needed for the glass- Au, Pt thick film conductor systems).

An empirical model developed in this study predicts the sheet resistivities from glass particle diameter and the metal (silver) content used. As the conduction is through the metal phase, thickness of the metal film around the matrix particles is important in determining the sheet resistivity of the thick film. The model developed was verified experimentally. When the glass-silver thick films were fired at temperatures higher than 750°C, the microstructure broke down due to the glass

flow and resulted in a non-conductor. Adhesion of the thick film conductors with the substrate was excellent. However, due to the large amounts of glass used, these thick films need a solderable metal overprint over the areas which are to be soldered.

Nickel-silver composite thick films which use nickel matrix particles coated with silver (amount: as low as 20 w/o), were air fireable unlike commercial base metal thick film systems (which need to be fired in inert atmospheres). Also, these thick films were solderable (with lead-tin solders) and had a wider temperature range for firing (600-900°C) than the glass metal composite thick films. The adhesion between the thick film and the substrate was good and was achieved by the small amount of glass added (5 w/o) to the thick film paste. As nickel oxide layer developed between nickel and silver during firing (please see Part II for details), conduction in the thick film was essentially due to the silver film. So the model developed to predict sheet resistivities of glass-metal thick films was good for nickel-silver thick films also. The concept of having a precious metal film around base metal matrix particles can be extended to other base metal (Cu, Ni) - precious metal (Au, Ag, Pt) systems (preliminary experiments with Cu-Ag system were successful in obtaining good thick film conductors). This would make thick film conductors very economical.

Table 1. Sheet Resistivities of Some Conventional Thick Film Conductors.

| System | Thickness | Sheet Resistivity (milliohms/sq) | Ref. |
|-------------------|-----------|-------------------------------------|------|
| DuPont 9755 Pt/Ag | .6 mil | 50 | 11 |
| DuPont 9596 Pt/Au | .8 mil | 60 | 11 |
| DuPont 9885 Pt/Au | .7 mil | 70 | 11 |
| DuPont 9572 Pd/Au | .8 mil | 80 | 11 |
| DuPont 9843 Pd/Ag | .6 mil | 30 | 11 |
| Au-Pt (75-25 w/o) | 1 mil | 100 | 12 |
| Au-Pd (60-40 w/o) | 1 mil | 100 | 12 |
| Ag-Pd (80-20 w/o) | 1 mil | 30 | 12 |

The solids in these thick films have >90 w/o of precious metals.

Table 2. Relative Cost and Bulk Resistivity of Metals Used in Thick Film Conductors.

| Metal | Relative Cost (per unit wt.) | Bulk Resistivity, ρ ($\mu\Omega - \text{Cm}$) |
|----------|---------------------------------|---|
| Platinum | 7312 | 10.6 |
| Gold | 5849 | 2.4 |
| Silver | 263.2 | 1.6 |
| Copper | 1 | 1.7 |
| Nickel | 2.74 | 6.8 |

Table 3.

| Silver Metal Content w/o | Surface Treatment (45 sec.) | Firing Temp. °C | Time min. | Sheet Resistivity mΩ/□ |
|--------------------------------|-----------------------------------|--------------------|--------------|------------------------------|
| 40 | 0.25 N HCl | 550 | 8 | 44 |
| | " | 575 | 14 | 32 |
| 30 | 0.01 N HCl | 500 | 20 | 80 |
| | " | 500 | 30 | 120 |
| | " | 600 | 8 | 85 |
| | " | 640 | 8 | 70 |
| | " | 700 | 8 | 80 |
| 25 | 0.01 N HCl | 500 | 8 | 160 |
| | " | 600 | 8 | 165 |
| | " | 700 | 8 | 160 |
| 20 | 0.01 N HCl | 500 | 30 | 230 |

Table 4. Thermal Expansion Coefficients in Lead Borosilicate Glass System. (Present study)

$$\alpha_{\text{glass}} = W_{\text{PbO}} \cdot \alpha_{\text{PbO}} + W_{\text{B}_2\text{O}_3} \cdot \alpha_{\text{B}_2\text{O}_3} + W_{\text{SiO}_2} \cdot \alpha_{\text{SiO}_2}$$

| Composition (wt%) | | | Expansion Coefficient (in units of 10^{-6} in/in/°C) | | |
|-------------------|------------------|-------------------------------|--|--|-------|
| PbO | SiO ₂ | B ₂ O ₃ | α_{measured} | $\alpha_{\text{calculated}}$ (using the contributions by the components) | |
| 1 | 70 | 30 | 0 | 8.53±.4 | 8.48 |
| 2 | 70 | 25 | 5 | 8.18±.4 | 8.43 |
| 3 | 70 | 20 | 10 | 8.57±.4 | 8.40 |
| 4 | 70 | 15 | 15 | 8.47±.4 | 8.36 |
| 5 | 70 | 10 | 20 | 7.9 ±.4 | 8.29 |
| 6 | 75 | 15 | 10 | 9.5 ±.4 | 9.2 |
| 7 | 80 | 15 | 5 | 10.0 ±.4 | 10.04 |
| 8 | 80 | 5 | 15 | 9.8 ±.4 | 9.96 |

Calculated contributions for the component oxides:

$$\alpha_{\text{PbO}} = 1.33 \times 10^{-7} \text{ in/in/°C}$$

$$\alpha_{\text{B}_2\text{O}_3} = -0.357 \times 10^{-7} \text{ in/in/°C}$$

$$\alpha_{\text{SiO}_2} = -0.277 \times 10^{-7} \text{ in/in/°C}$$

Table 5. Thermal Expansion Coefficients in Lead Borosilicate Glass System. (Ref. (27))

| | Composition (wt%) | | | Expansion Coefficient (in units of 10^{-6} in/in/°C) | |
|---|-------------------|------------------|-------------------------------|--|--|
| | PbO | SiO ₂ | B ₂ O ₃ | α_{measured} (Ref.27) | $\alpha_{\text{calculated}}$ (present study) |
| 1 | 50 | 40 | 10 | 4.52 | 4.522 |
| 2 | 55 | 35 | 10 | 4.72 | 5.265 |
| 3 | 60 | 30 | 10 | 5.53 | 6.009 |
| 4 | 63 | 25 | 12 | 6.45 | 6.448 |
| 5 | 71 | 19 | 10 | 7.23 | 7.644 |
| 6 | 71 | 4 | 25 | 7.50 | 7.595 |
| 7 | 76 | 14 | 10 | 8.40 | 8.388 |
| 8 | 81 | 9 | 10 | 9.55 | 9.132 |

Calculated contributions for the component oxides:

$$\alpha_{\text{PbO}} = 1.199 \times 10^{-7} \text{ in/in/°C}$$

$$\alpha_{\text{B}_2\text{O}_3} = -0.321 \times 10^{-7} \text{ in/in/°C}$$

$$\alpha_{\text{SiO}_2} = -0.288 \times 10^{-7} \text{ in/in/°C}$$

Table 6. Component Oxide Contribution to Thermal Expansion of LBS Glass (Ref. 29, 30, 31)

| Oxide | Contribution to Linear Expansion (in 10^{-7} in/in °C) | | |
|-------------------------------|---|---------------------|---------------------------|
| | English & Turner | Mayer & Havas | Winkelmann & Schott |
| PbO | 1.06 | 1.4 | 1.00 |
| SiO ₂ | 0.05 | 0.27 | 0.27 |
| B ₂ O ₃ | 0.66 | 0.033 | 0.033 |

Table 7. Binding Energies of Pb, Si, B Photoelectrons

| Element/electron | | B.E. (eV) |
|------------------|---------|-----------|
| Pb | 4 f 7/2 | 139.2 |
| B | 1 S | 192.57 |
| Si | 2 P | 102.55 |

Table 8. XPS of Lead Borosilicate Glass — Peak Intensity Ratios.

| Elements | Peak Intensity Ratios | |
|----------|-----------------------|--------|
| | Unetched | Etched |
| Pb/Si | 4.076 | 2.774 |
| Pb/B | 4.24 | 4.526 |
| B/Si | 0.9615 | 0.61 |

Table 9. XPS of Lead Borosilicate Glass - Relative Surface Concentration *

| Elements | Relative Wt. Ratios at the Surface | |
|----------|------------------------------------|---------------|
| | Initial | After Etching |
| Pb/Si | 7/1 | 5.264/1 |
| Pb/B | 3.5/1 | 3.858/1 |
| B/Si | 2/1 | 1.364/1 |

* Peak intensities of the spectra obtained depend on the molar concentration of elements at the surface.

Table 10a. Binding Energies of Ag $3d_{5/2}$ Electrons (Present Study).

| Specimen | B.E (e.V.) |
|--|------------|
| (i) Silver metal | 368.1 |
| (ii) Silver nitrate | 368.45 |
| (iii) Silver resinate | 368.4 |
| (iv) Glass powder, treated with silver resinate and washed with xylene | 368.4 |
| (v) Glass powder with treatment of (iv) and decomposed at 250°C. | 368.2 |

Table 10b. Binding Energies of Silver $3d_{5/2}$ Electron in Different Compounds. (Ref. (34))

| Compound | Binding Energy (eV) |
|---------------------|---------------------|
| Silver fluoride (a) | 368.4 |
| Silver bromide (a) | 368.0 |
| Silver chloride (a) | 368.1 |
| Silver oxide (b) | 368.4 |
| Silver nitrate | 368.4 |
| Silver bromate | 369.0 |
| Silver acetate | 368.7 |
| Silver metal | 368.3* 368.2 |

(a) Co-ordination number of silver ion is six.

(b) Co-ordination number of silver ion is two.

* Reference: G. Johansson, et al., J. Electron Spec. Rel. Phen. 2, p. 295, (1973).

Table 11. Sheet Resistivities of Thick Films with Different Glass Particle Sizes.

| Average Glass Particle Size | Metal (Ag) Content (wt %) | Rs (Ω /square) |
|-----------------------------|---------------------------|------------------------|
| 2.5 μ m | 20 | 2.6 |
| | 25 | 1.8 |
| | 30 | 0.8 |
| | 40 | 0.6 |
| 15 μ m | 20 | 0.435 |
| | 25 | 0.300 |
| | 30 | 0.130 |
| | 40 | 0.085 |
| 25 μ m | 20 | 0.25 |
| | 25 | 0.175 |
| | 30 | 0.075 |
| | 40 | 0.050 |

Table 12. Sheet Resistivities of Ni-Ag Thick Film Conductors.

| Glass Content wt% | Wt% AG | Firing | | R _s (Milliohms/sq.) |
|----------------------|--------|----------|------------|-----------------------------------|
| | | Temp(°C) | Time(Min.) | |
| 10 | 20 | 600 | 10 | 15 |
| | | 600 | 30 | 15 |
| | | 600 | 12 | 12 |
| | | 650 | 6 | 25 |
| | | 700 | peak | 30 |
| | | 710 | 5 | x |
| | 900 | peak | x | |
| | 30 | 600 | 10 | 12 |
| | | 700 | 10 | 25 |
| | | 800 | 10 | 35 |
| | | 900 | peak | 40 |
| | 20 | 600 | 10 | 20 |
| 700 | | 10 | 22 | |
| 800 | | 10 | 20 | |
| 900 | | peak | 25 | |
| 25 | 605 | 12 | 15 | |
| | 600 | 10 | 15 | |
| | 600 | 6 | 12.5 | |
| | 605 | 15 | 15 | |
| | 700 | 10 | 12 | |
| | 800 | 16 | 15 | |
| 5 | 30 | 605 | 10 | 12 |
| | | 600 | 10 | 10 |
| | | 700 | 12 | 10 |
| | | 800 | 10 | 12 |
| 35 | 600 | 10 | 8 | |
| | 605 | 12 | 8 | |
| | 700 | 10 | 8 | |
| | 750 | 10 | 10 | |
| | 800 | 10 | 12 | |
| 40 | 600 | 10 | 6 | |
| | 605 | 10 | 8 | |
| | 700 | 5 | 8 | |
| | 805 | 5 | 10 | |
| | 915 | peak | 25 | |

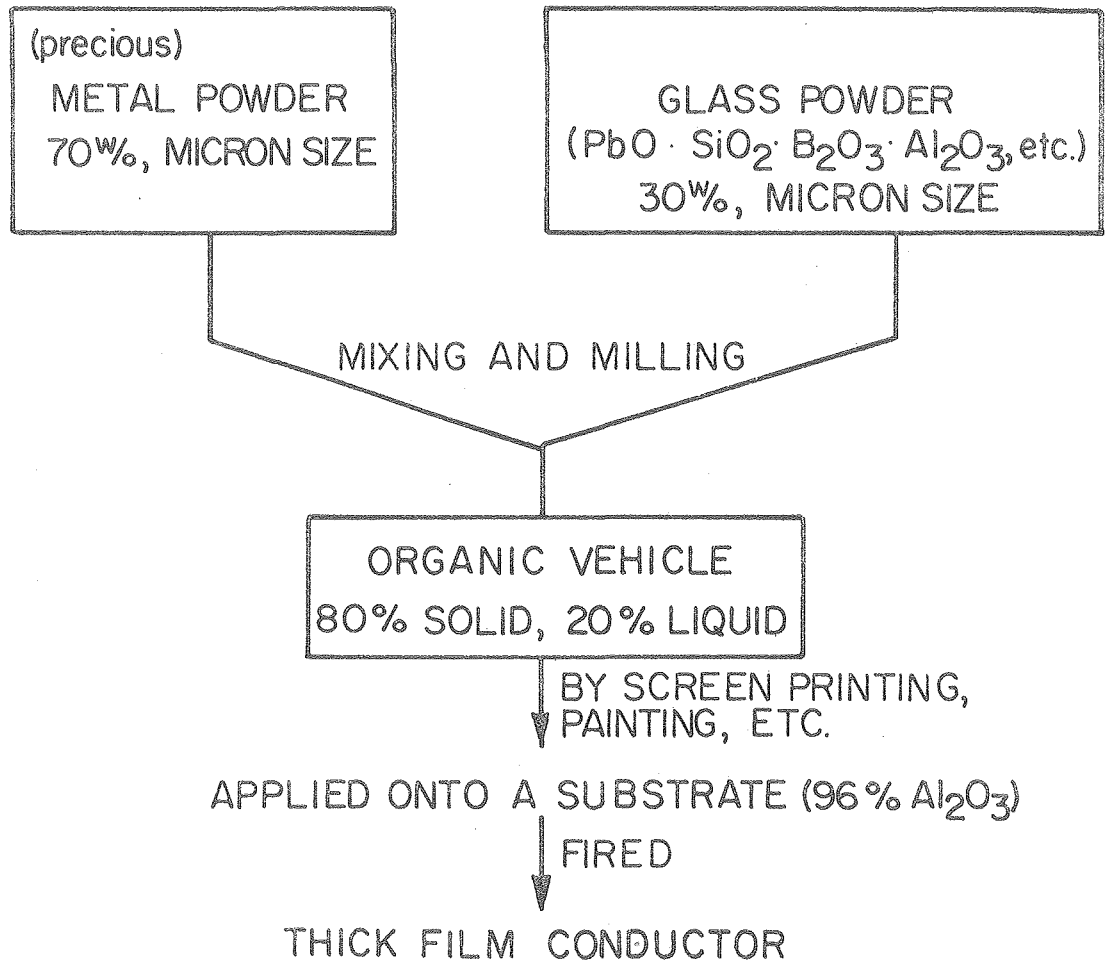
FIGURE CAPTIONS

1. Flow diagram for the processing of conventional thick film conductors.
2. Schematic diagram showing the conventional microstructure for conducting thick films.
3. Schematic diagram showing the intended microstructure for a new system of thick film conductors.
4. Flow diagram of the new process for glass-metal thick film conductors.
5. Flow diagram for the processing of nickel-silver thick film conductors.
6. Weight loss characteristics of the lead borosilicate glass particles (20-44 μ m) treated with .01N HCl for varying times.
7. Circuit diagram for the sheet resistivity measurements.
8. Voltage-current characteristics of the conductive thick film.
9. Linear expansion curve for the lead borosilicate glass.
10. Scanning electron micrograph of the surface of the 96% Al₂O₃ substrate used in the study.
11. Energy dispersive analysis of the x-rays from the surface of the above alumina substrate. Mg, Si are present as impurities.
12. Alumina-glass interface as observed in SEM. Region 'P' is possibly a different phase. X-ray line mappings of Pb and Al across the interface are also shown.
13. Surface of the HCl treated lead borosilicate glass as seen in an SEM.
14. Scanning electron micrograph of the crystals obtained from the etchant HCl solution after etching the lead borosilicate glass.

15. X-ray diffraction pattern of the crystals seen in Fig. 14.
16. X-ray photoelectron spectra of etched glass.
17. X-ray photoelectron spectra of unetched glass.
18. Acid treated lead borosilicate glass particles coated with silver.
19. Non-conducting thick film obtained using surface passive (unetched) glass particles. (20-44 μ m).
20. Conducting thick film obtained using etched glass particles (20-44 μ m).
21. Scanning electron micrograph of the thick film (25 w/o Ag) fired in N₂ (980°C, 10 min). Even though acid treated glass particles are used, film is non-conducting as silver agglomerates.
22. X-ray photoelectron spectrum of silver metal.
23. Hot stage scanning electron micrograph of the thick film at 640°C (25 w/o Ag).
24. Optical transmission micrographs of thick films (25 w/o Ag) fired at different temperatures.
25. Optical transmission micrograph using smaller glass particles (<10 microns) which were acid treated (.01N HCl, 2 1/2 min).
26. Variation of metal coating thickness (T_m) with glass particle size (D_g) for different metal/glass volume ratio.
27. Variation of metal thickness with metal volume for different glass particle diameters.
28. Dependence of sheet resistivity on the metal content for the thick film conductor system developed in this study.
29. Variation of sheet resistivity with metal content for different glass particle sizes. (Size range indicated within parenthesis).

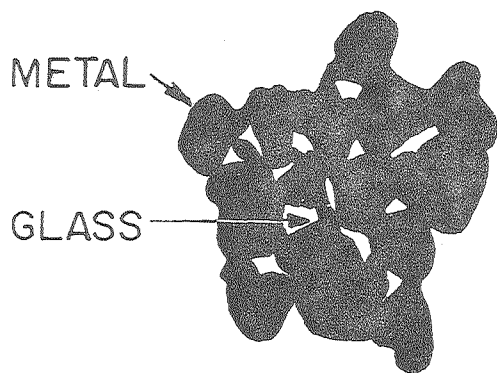
30. Silver coated nickel particle as seen in an SEM.
31. Scanning electron micrograph of a nickel-silver thick film conductor (25 w/o silver, 5 w/o glass, fired in air at 605°C for 15 mins).
Grain structure of the silver film around the nickel particles can be seen.
32. Variation of sheet resistivity with silver content in nickel-silver thick film conductors. Good correlation between theoretical and measured values can be seen.

PROCESSING OF CONVENTIONAL THICK FILM CONDUCTORS



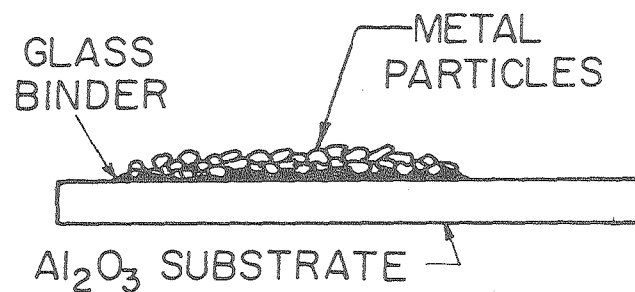
XBL 759-7372

Fig. 1



CONVENTIONAL MICROSTRUCTURE

METAL PARTICLES IN CONTACT WITH EACH OTHER. GLASSY PHASE BOUND IN BETWEEN.



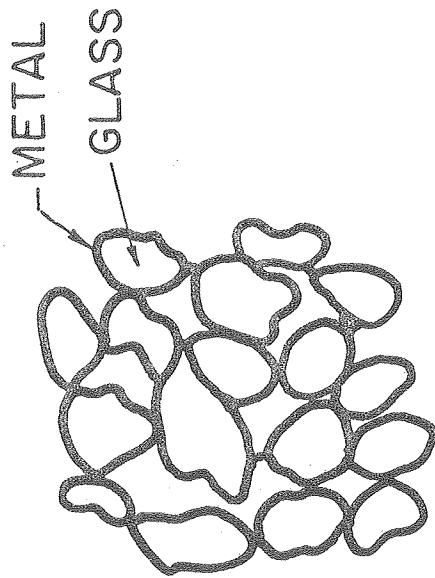
CROSS SECTIONAL VIEW

GLASSY PHASE BINDS THE METAL PARTICLES IN CONTACT WITH ONE ANOTHER TO THE SUBSTRATE.

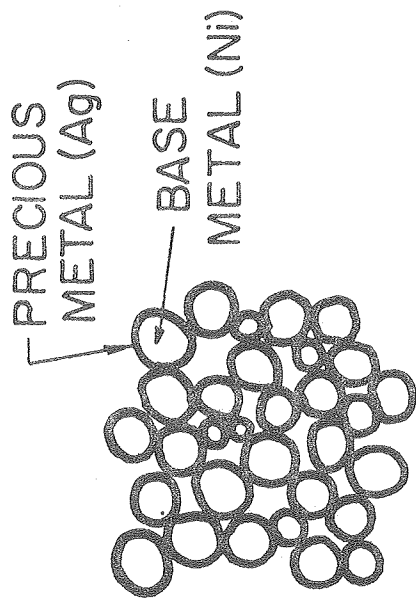
XBL 7910-7268

Fig. 2

INTENDED MICROSTRUCTURE

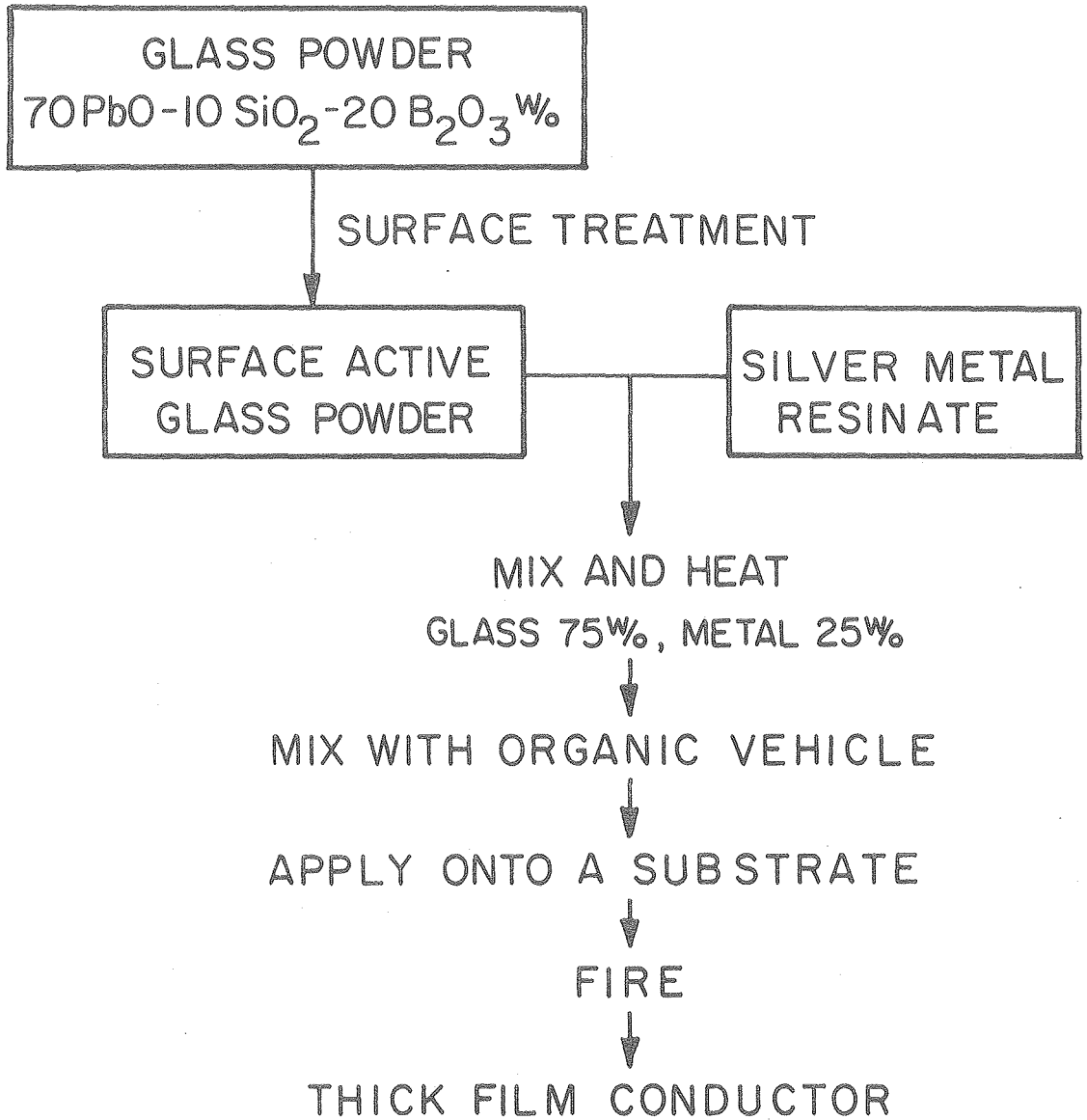


GLASS PARTICLES
WITH A METALLIC COAT
IN CONTACT WITH EACH
OTHER



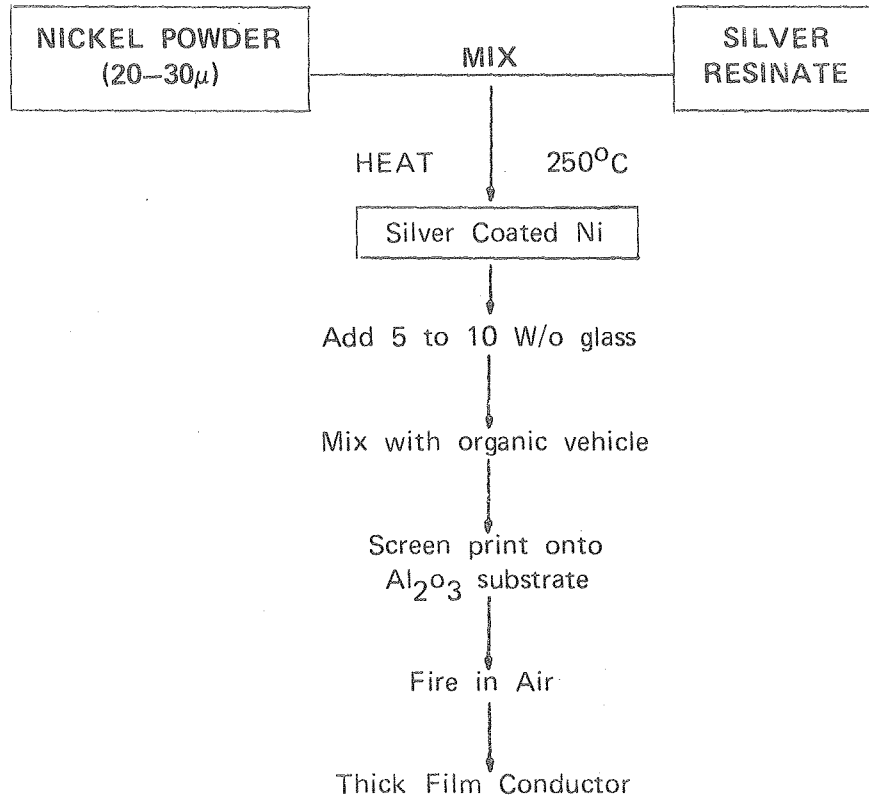
SPHERICAL METAL (Ni)
PARTICLES COATED
WITH PRECIOUS METAL

NEW PROCESS FOR INTENDED MICROSTRUCTURE



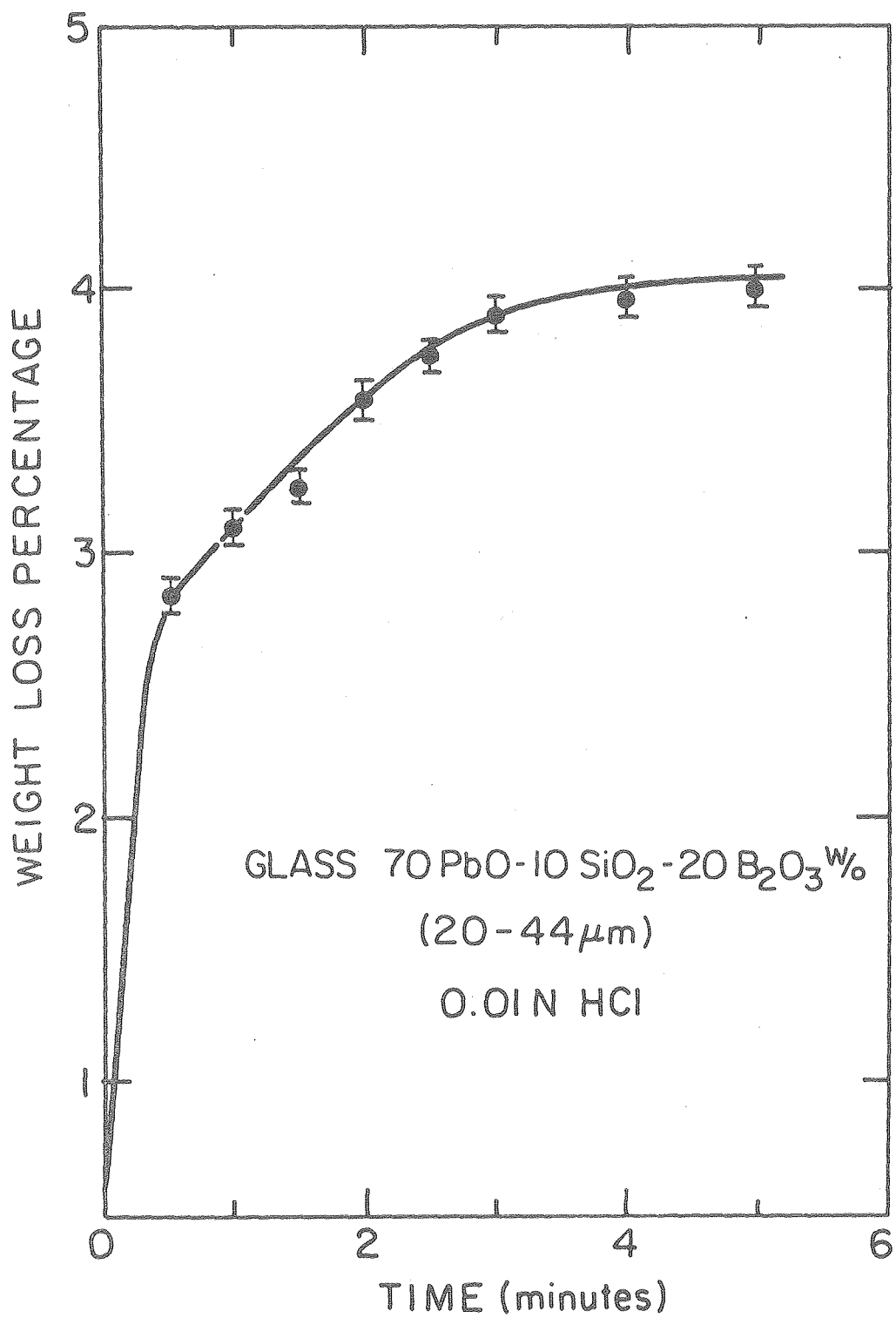
XBL 759-7 369

Fig. 4



XBL 799-12052

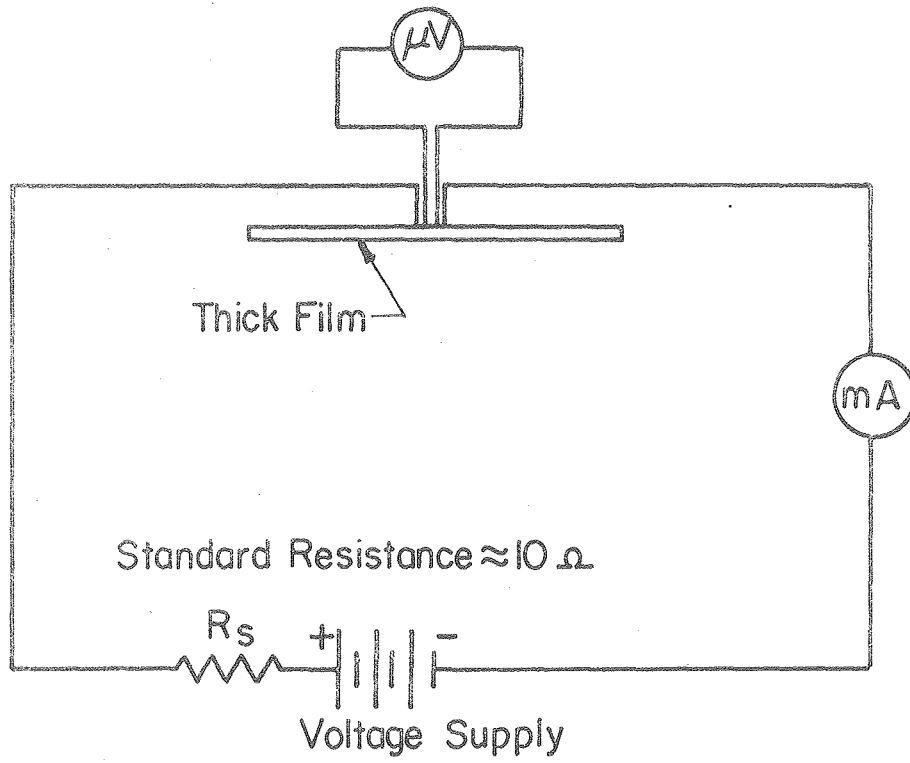
Fig. 5



XBL 759 -7367

Fig. 6

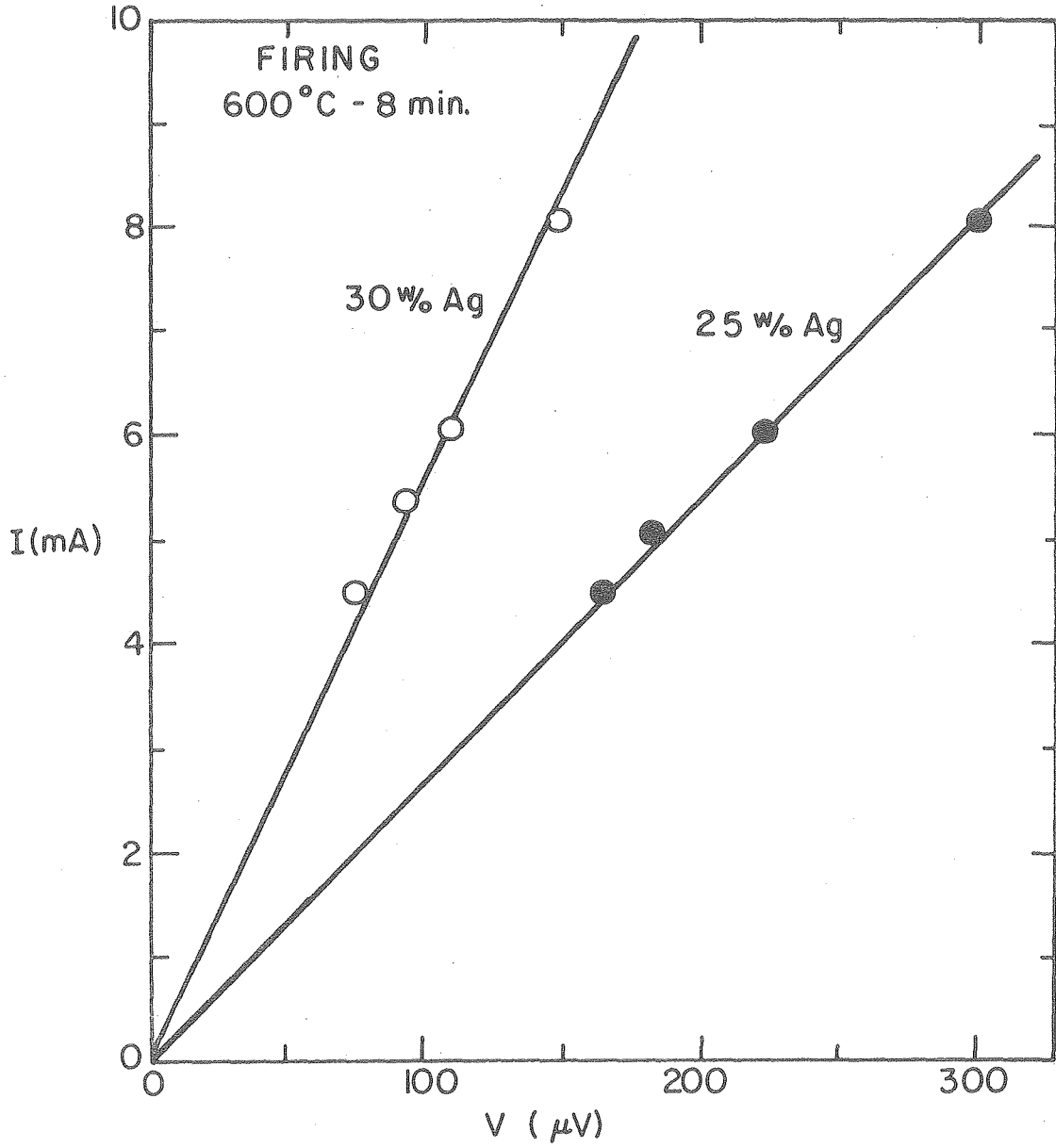
CIRCUIT DIAGRAM



XBL 7512-10,014

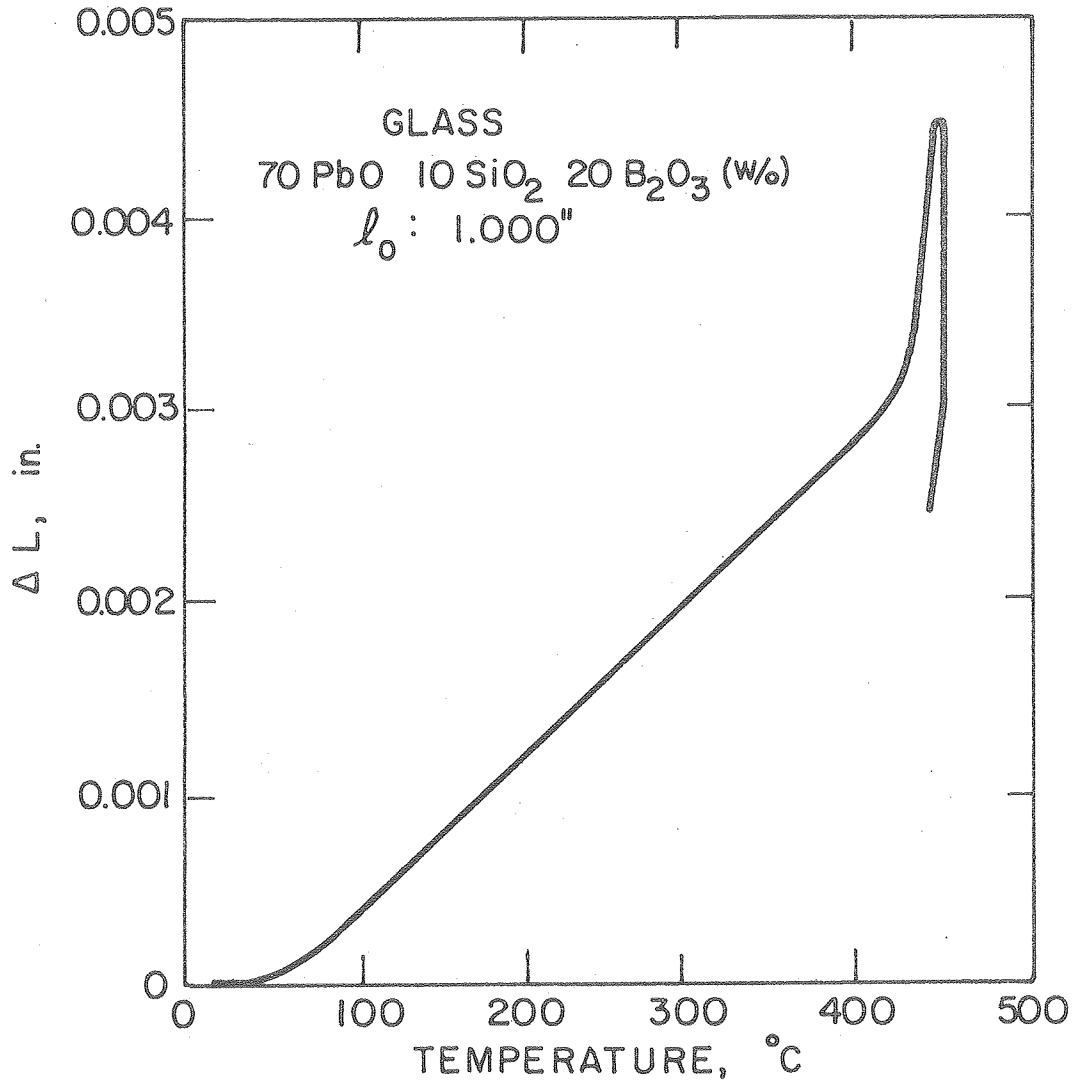
Fig. 7

V-I CHARACTERISTICS OF CONDUCTIVE THICK FILM



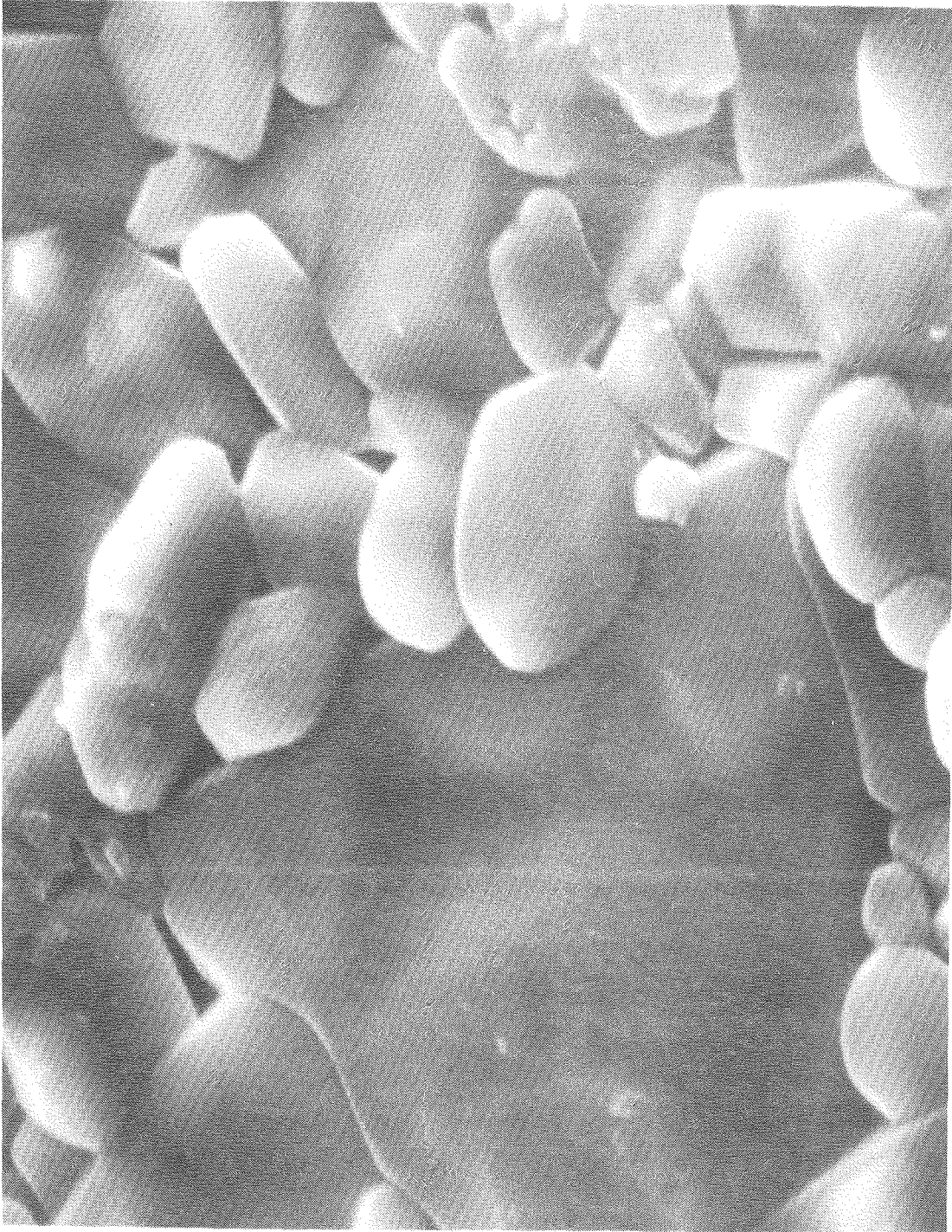
XBL 765-6866

Fig. 8



XBL7910-7270

Fig. 9

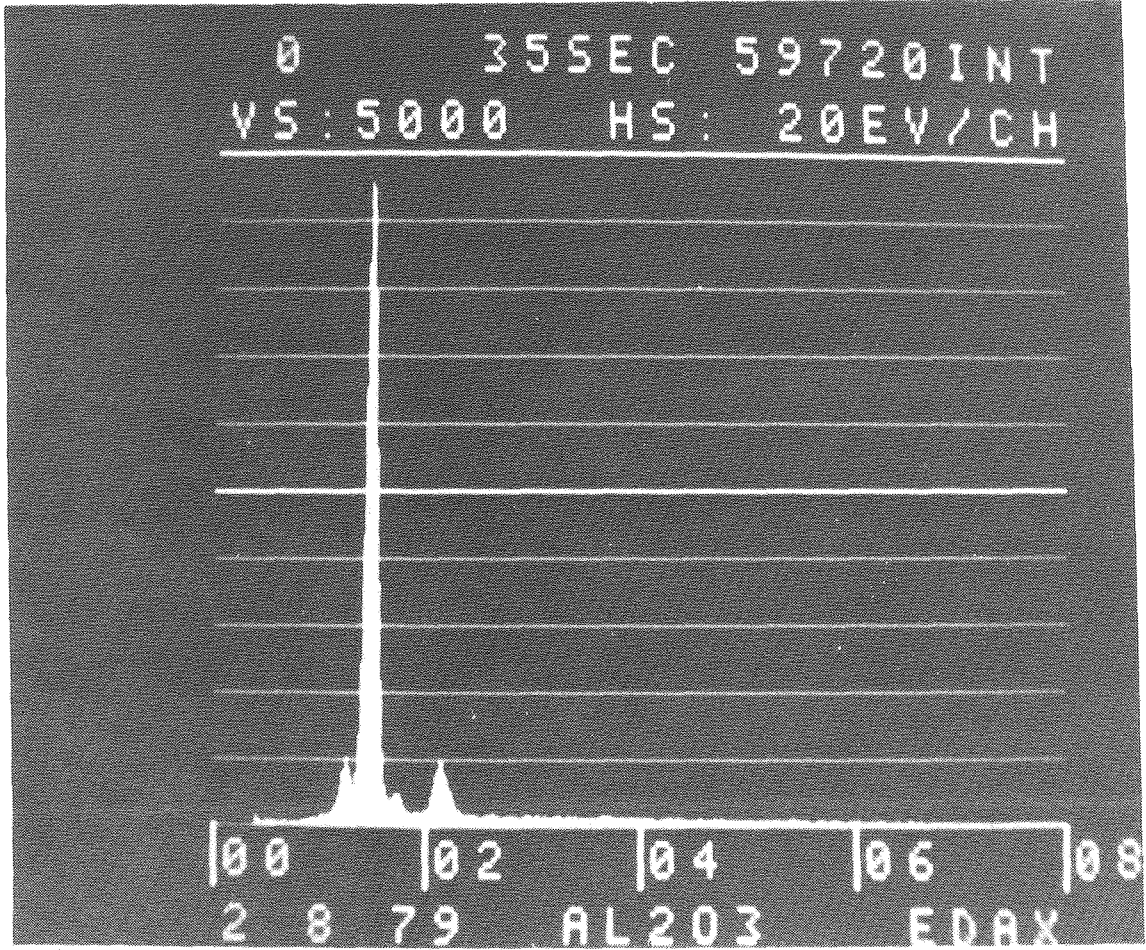


2 μ m
└────────┘

XBB 790-16052

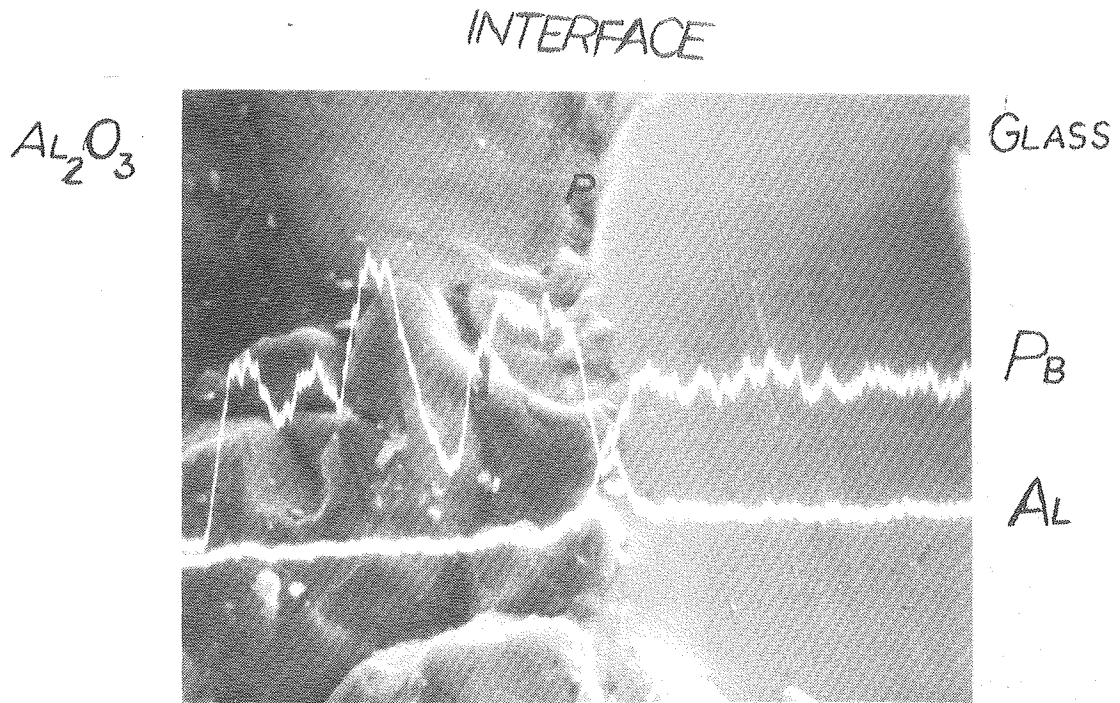
Fig. 10

Mg Al Si Au
| | / /



XBB 790-16053

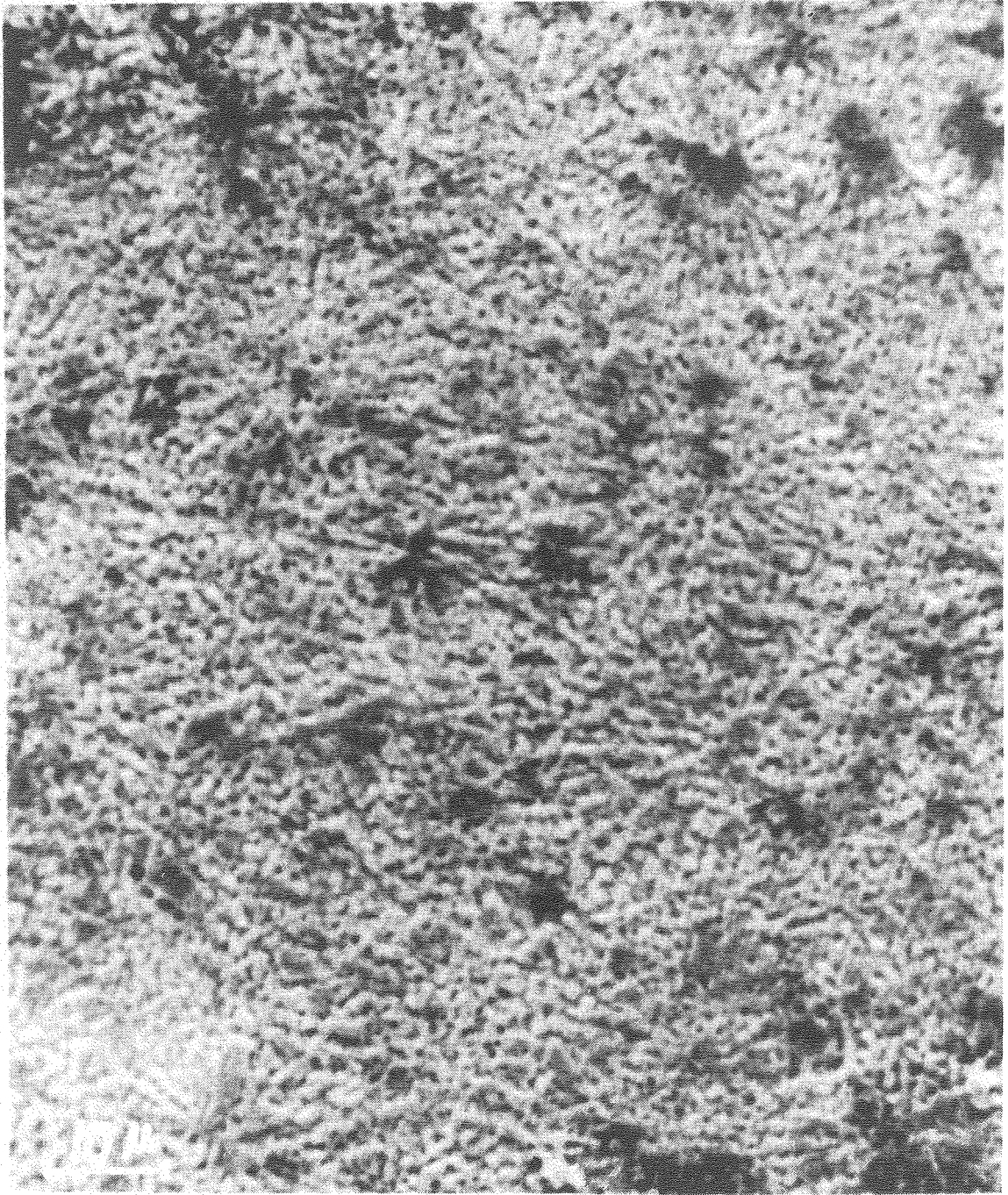
Fig. 11



5μ

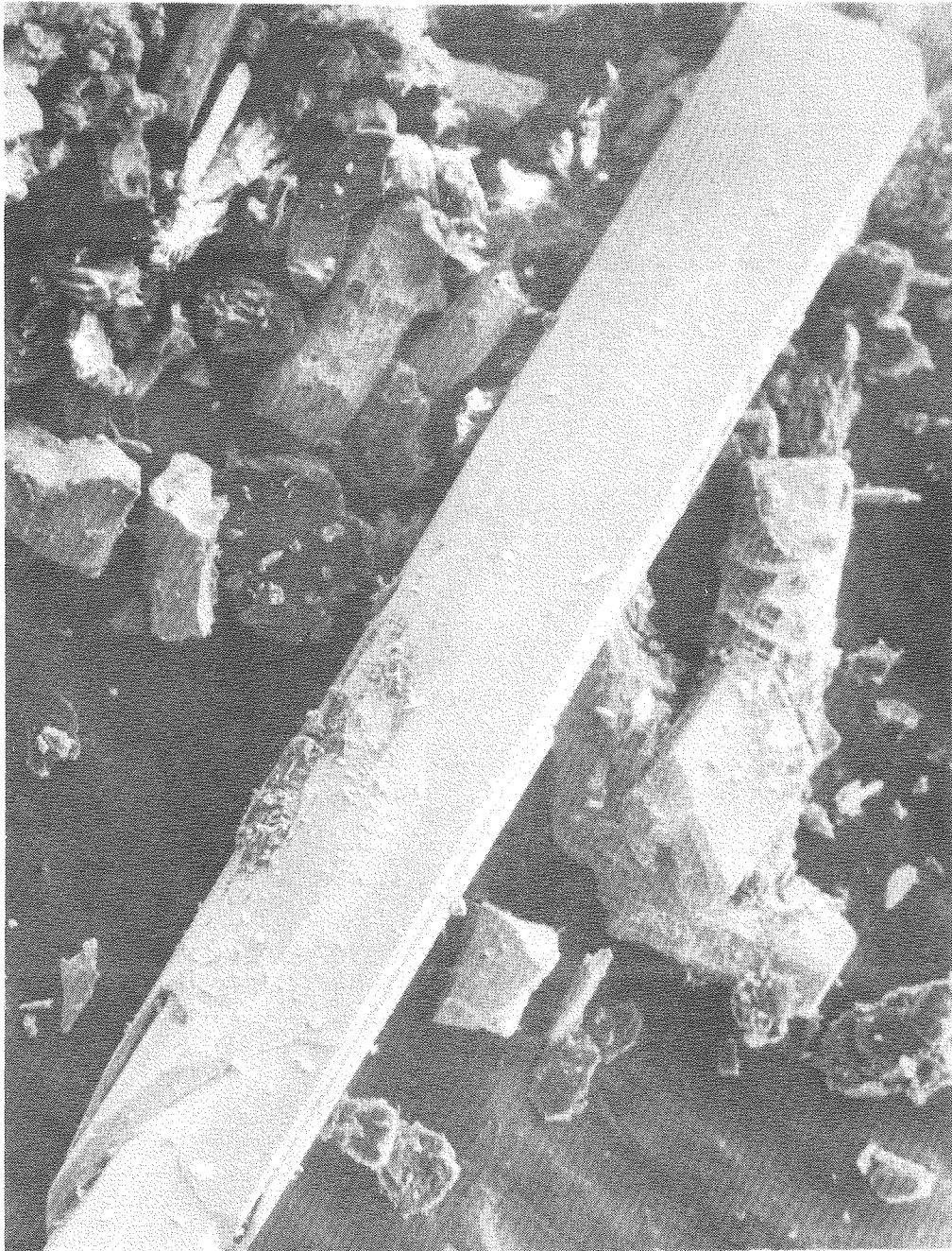
XBB 790-16054

Fig. 12



XBB 765-4532

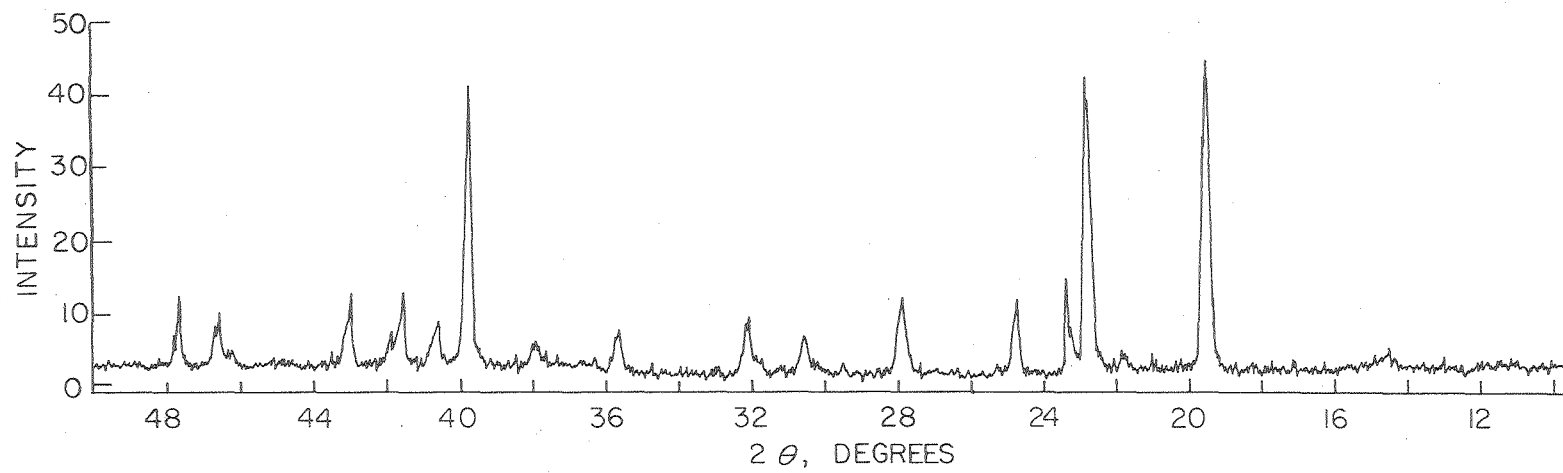
Fig. 13



XBB 799-12809

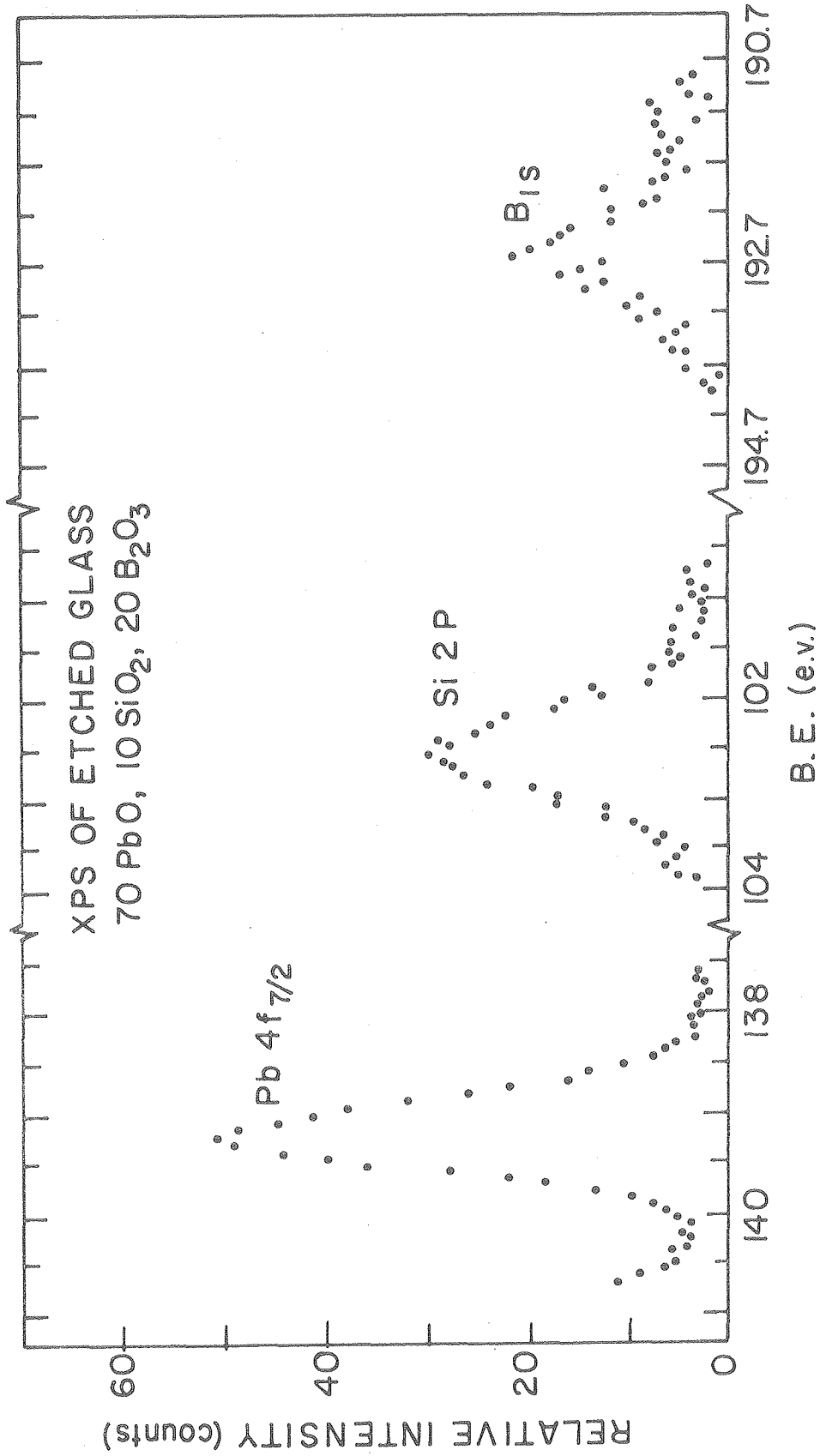
5 μ m

Fig. 14



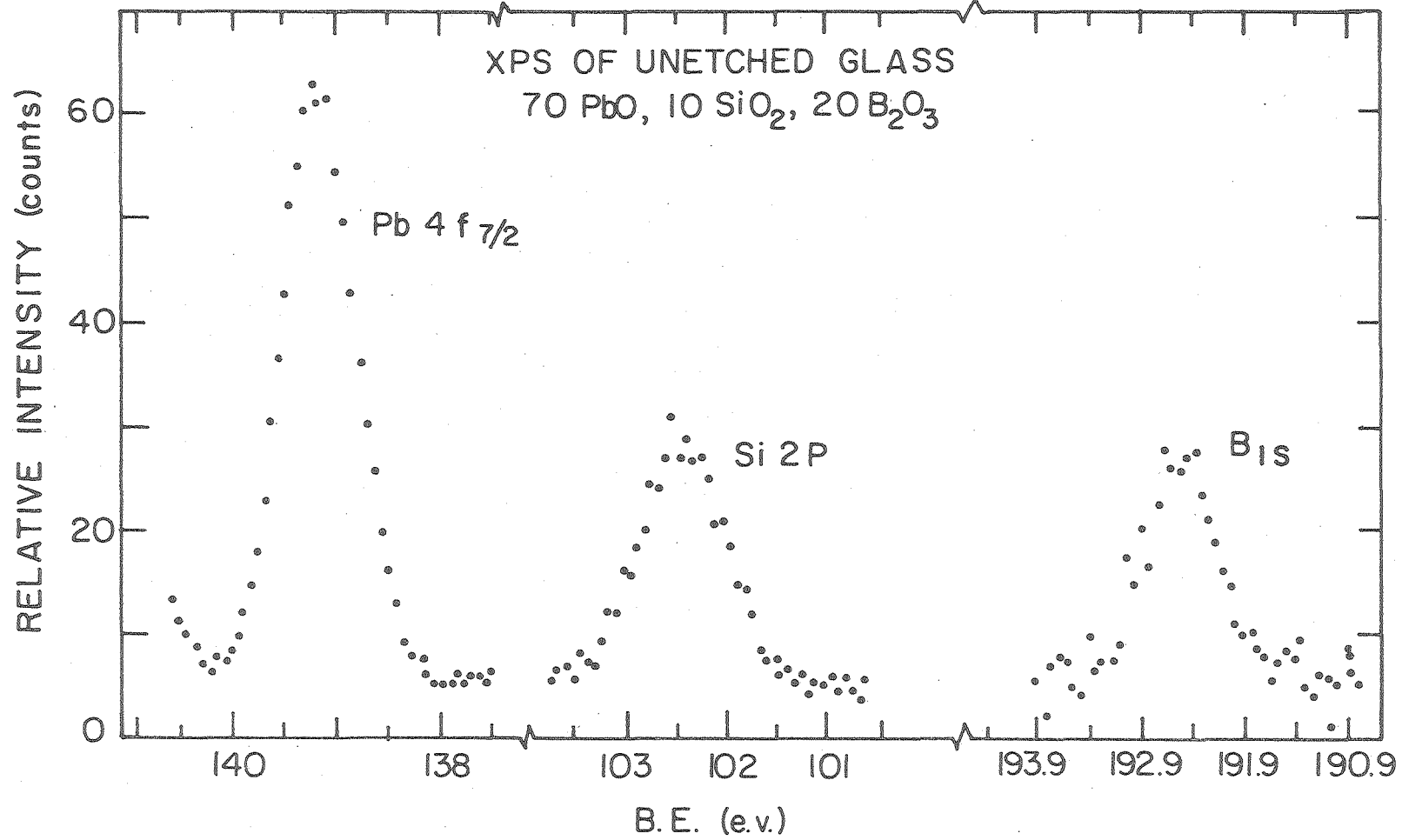
XBL 7910-7271

Fig. 15



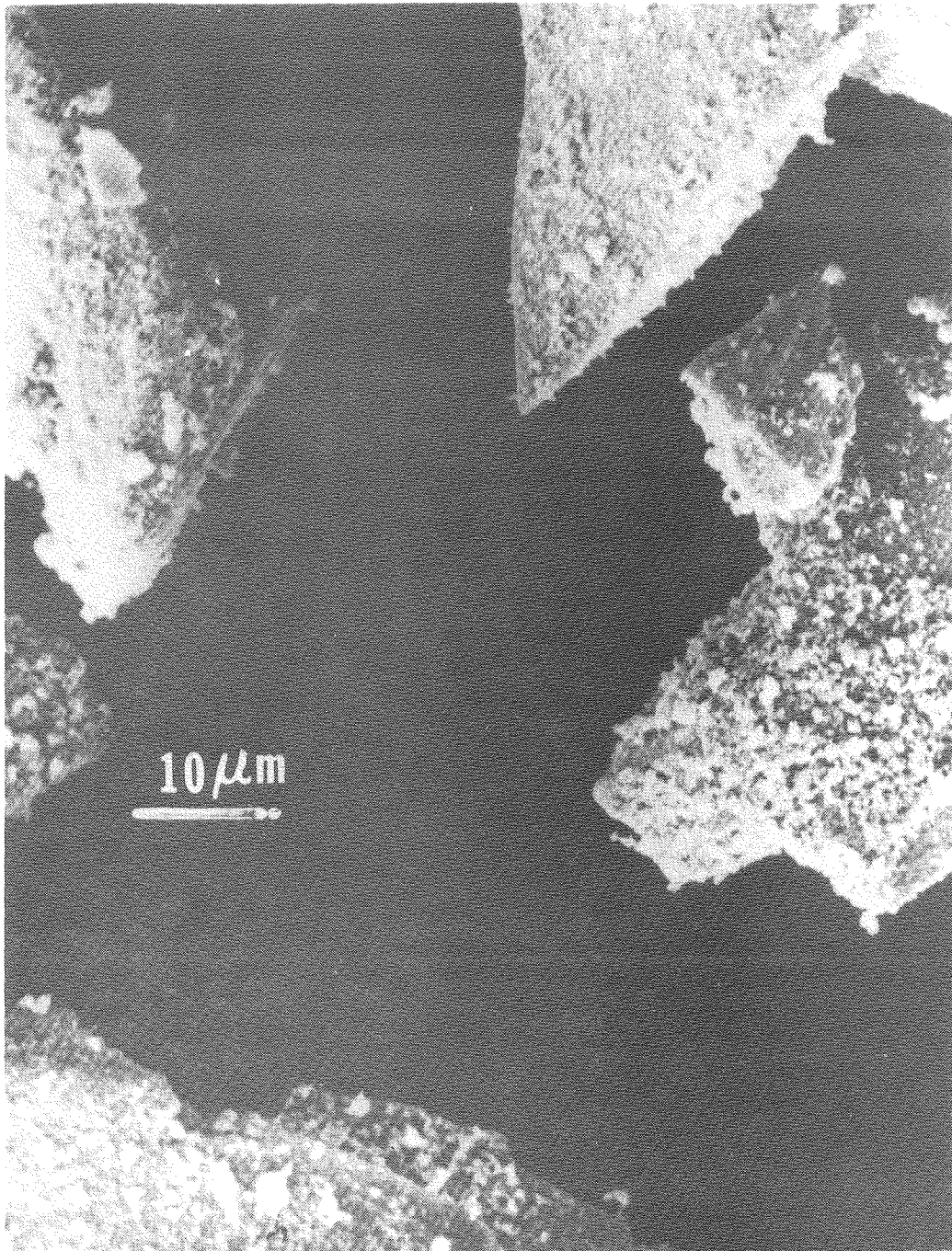
XBL 7911-14535

Fig. 16



XBL 7911-14533

Fig. 17

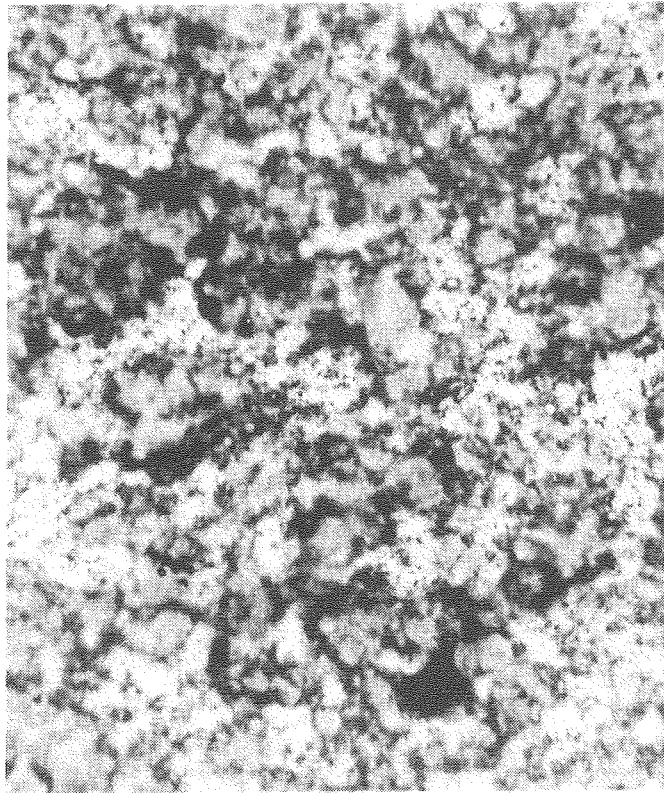


XBB 790-13852

ACID TREATED LEAD BOROSILICATE GLASS PARTICLES COATED WITH SILVER AS SEEN IN SEM.

Fig. 18

THICK FILM OPTICAL TRANSMISSION MICROGRAPH
(25^W% Ag, FIRING 600°C, 8 MIN.)



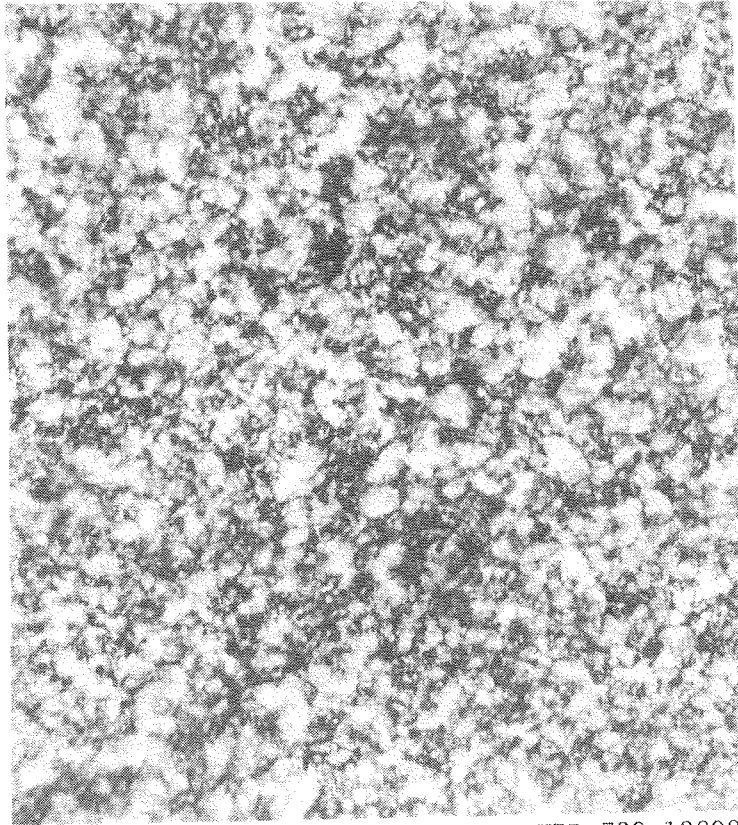
XBB 799-12810

62 μ m
┌───┐

SURFACE PASSIVE GLASS POWDER

Fig. 19

THICK FILM OPTICAL TRANSMISSION MICROGRAPHS
(25^W% Ag, FIRING 600°C, 8 MIN.)

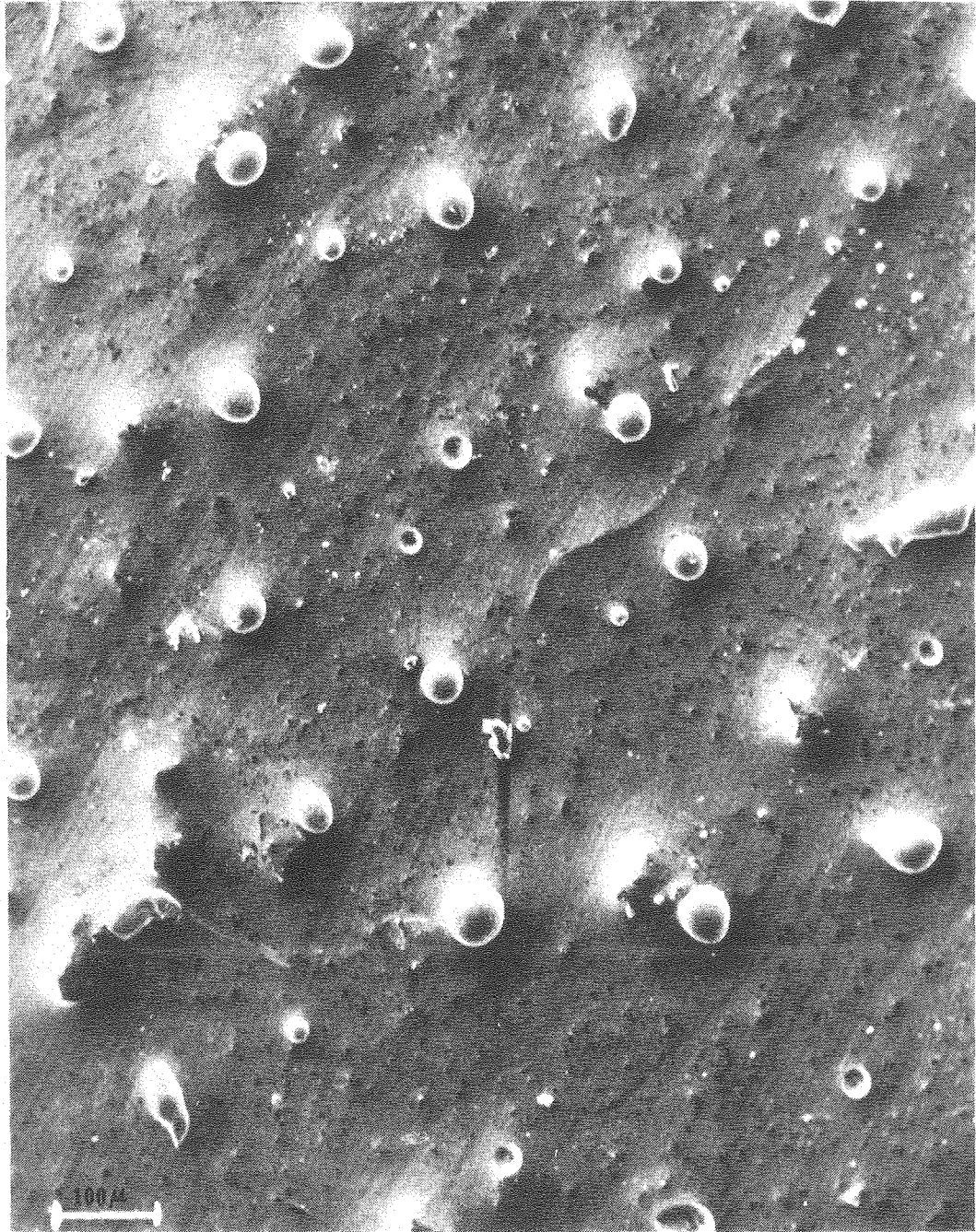


XBB 799-12808

124 μm
┌───┐

SURFACE ACTIVE GLASS POWDER

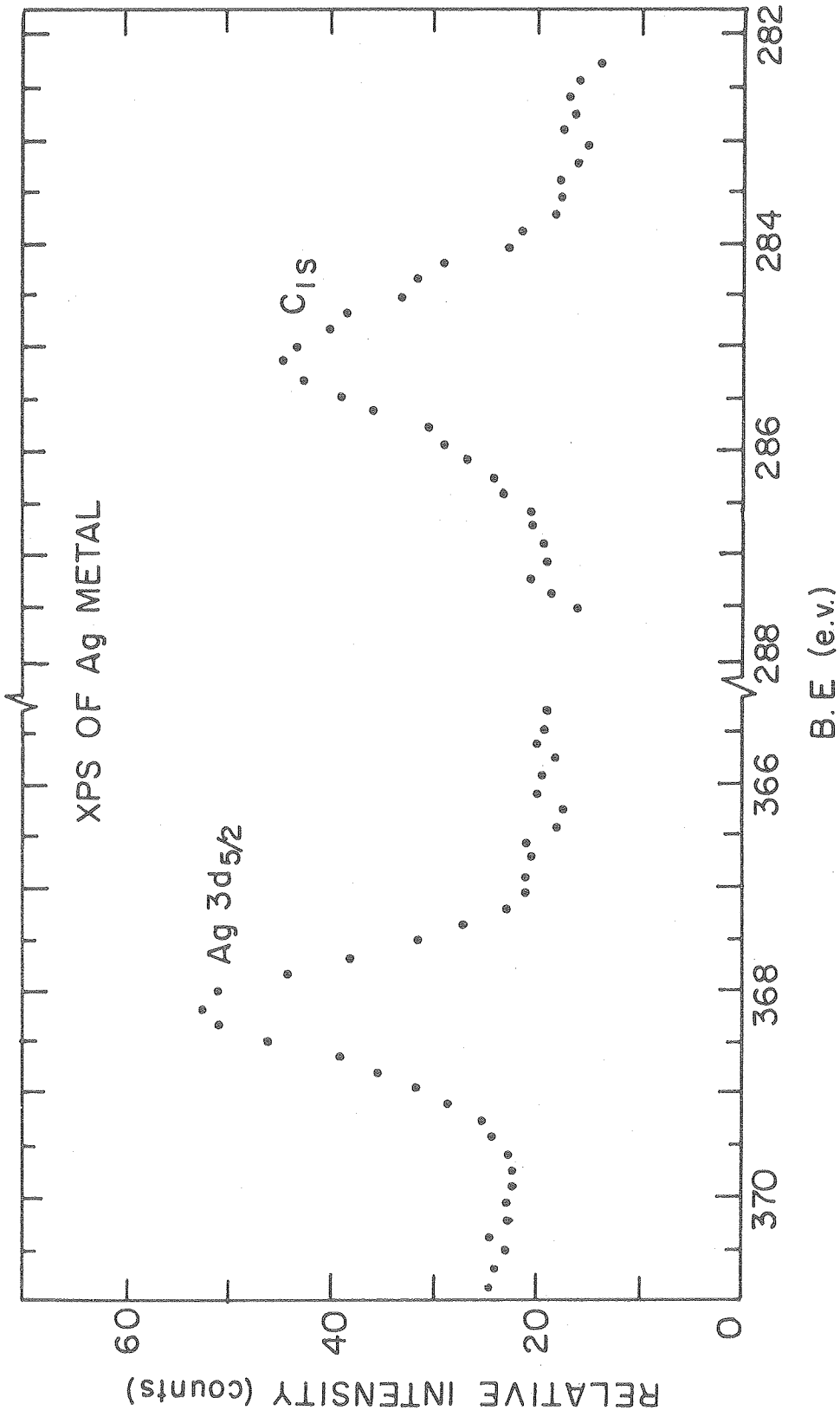
Fig. 20



XBB 790-13851

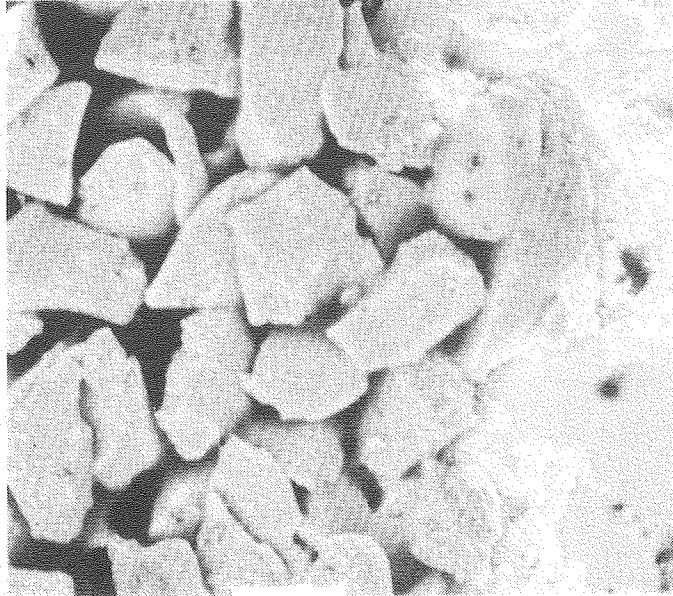
SCANNING ELECTRON MICROGRAPH OF THICK FILM FIRED IN N_2 - 980° , 10 min.
EVEN THOUGH ACID TREATED GLASS PARTICLES ARE USED, AGGLOMERATION OF
SILVER IS OBSERVED.

Fig. 21



XBL 7911-14534

Fig. 22



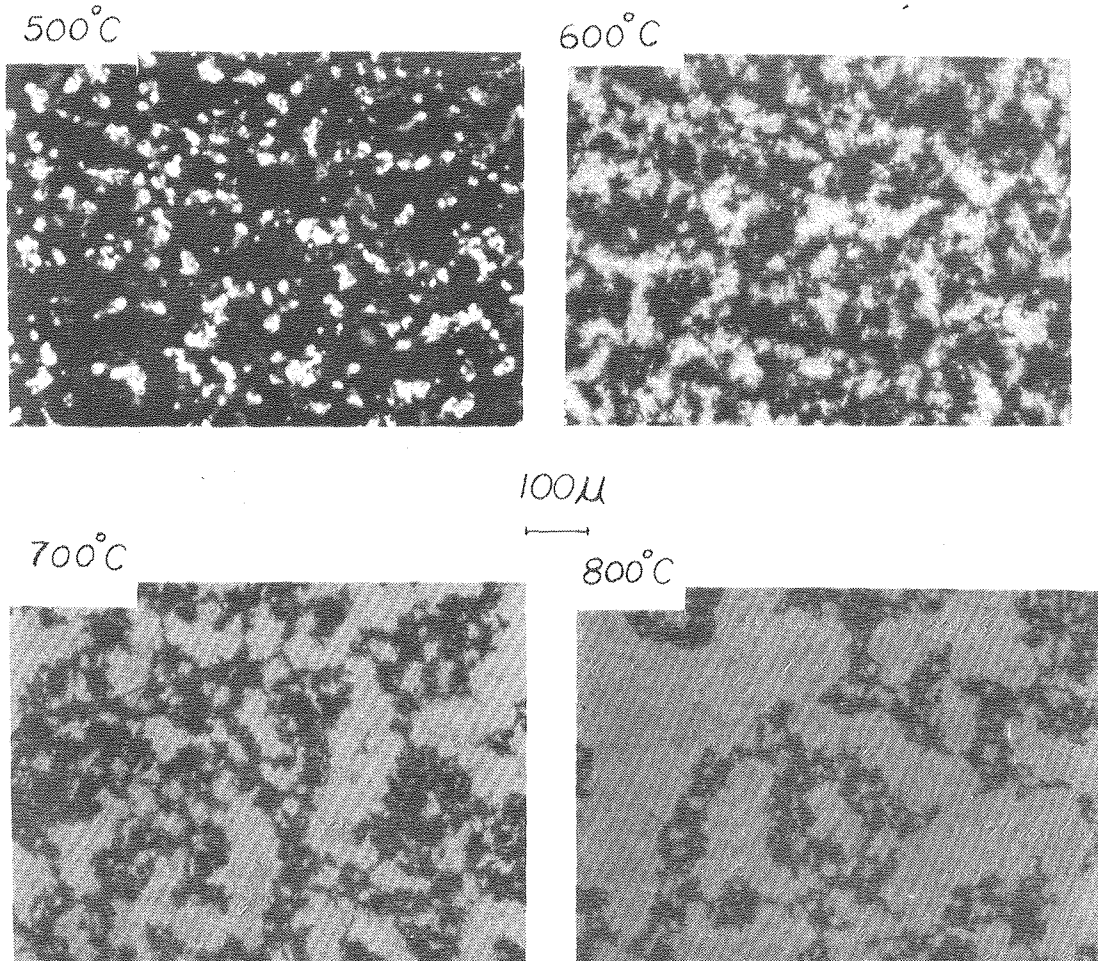
33 μ m

SCANNING HOT STAGE MICROGRAPH OF THE THICK FILM (25 W/O Ag)
AT 640°C (ARROW SHOWS THE EDGE OF THE THICK FILM)

XBB 790-14962

Fig. 23

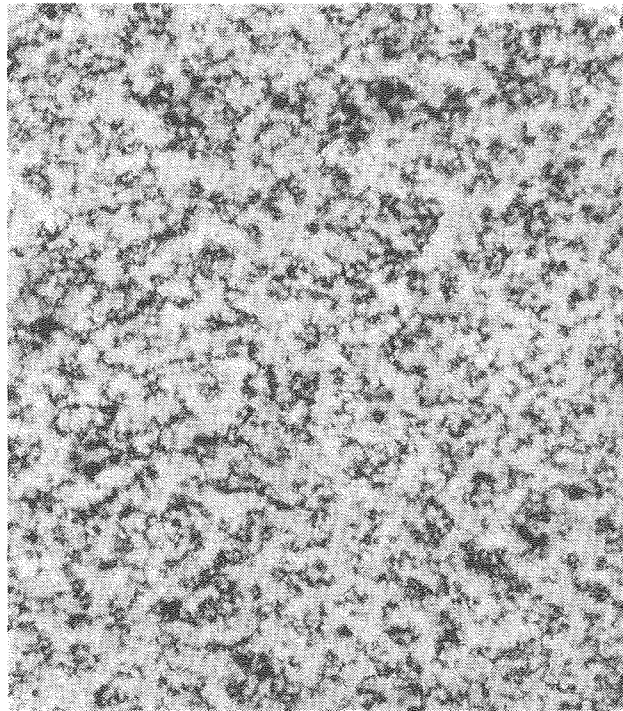
OPTICAL TRANSMISSION MICROGRAPHS OF THICK FILMS (25 W/O Ag)
FIRED AT DIFFERENT TEMPERATURES.



FIRING TIME
10 MIN.

XBB 790-14963

Fig. 24



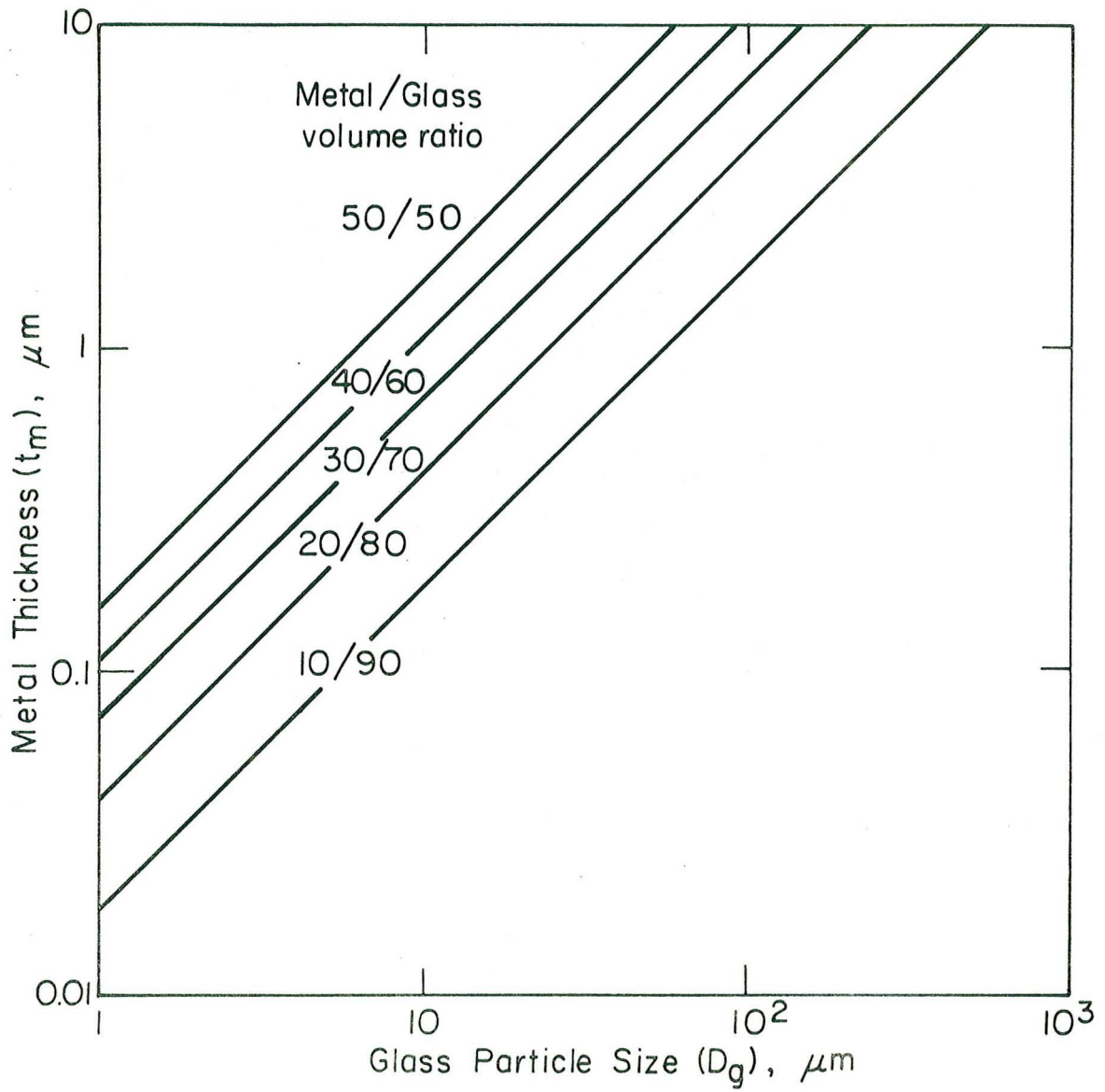
83 μ M
┌──────────┐

FIRING - 600°C 12 MIN, Ag - 25 W/O

GLASS PARTICLE SIZE < 10 MICRONS, ETCH - .01 N HCL 2 1/2 MIN

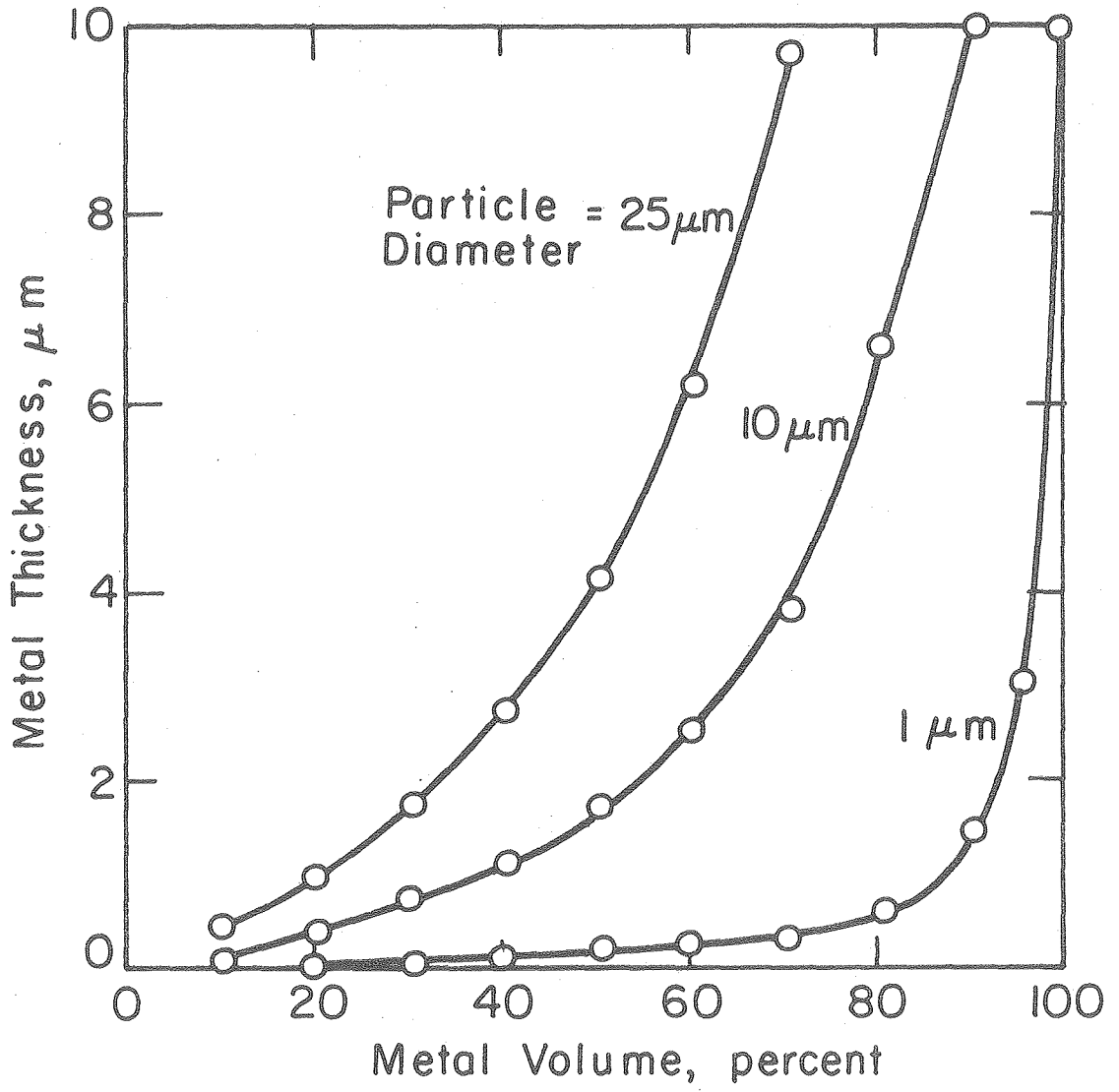
XBB 790-14961

Fig. 25



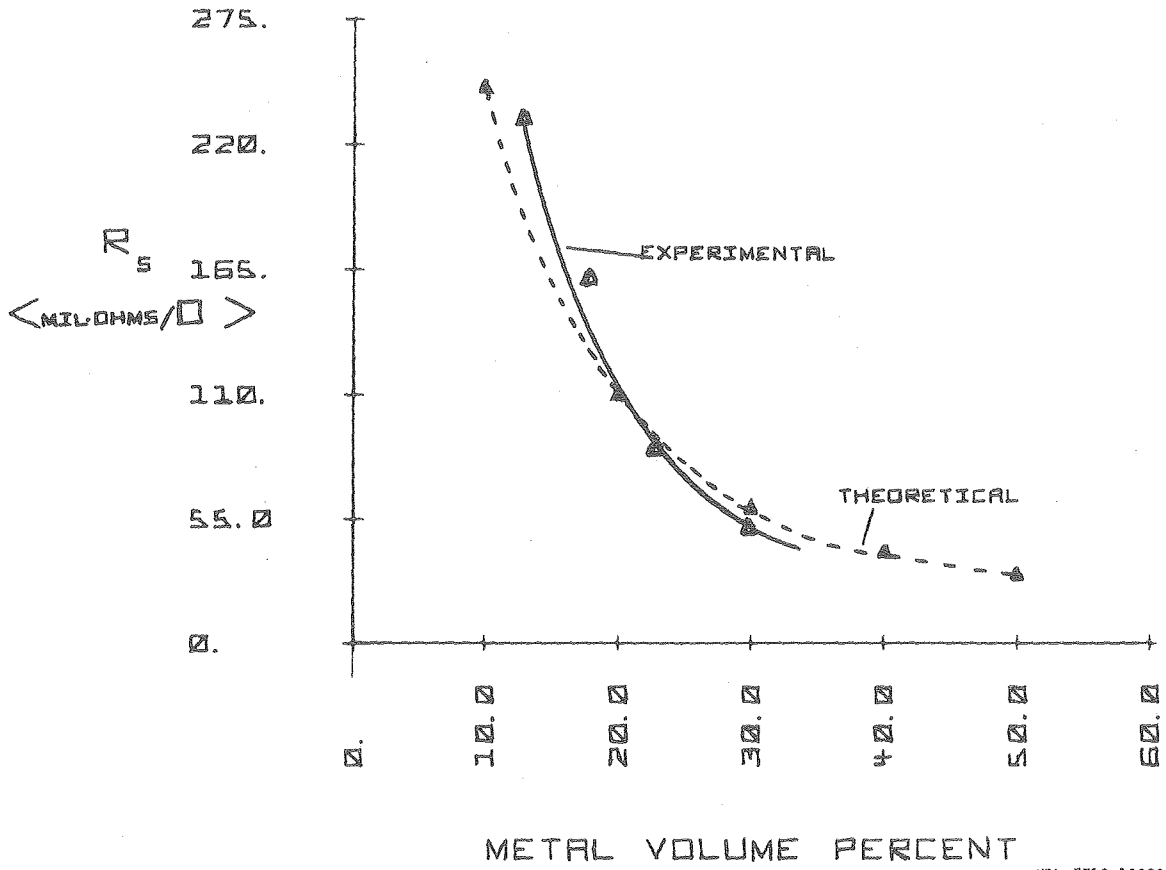
XBL 7710-6293

Fig. 26



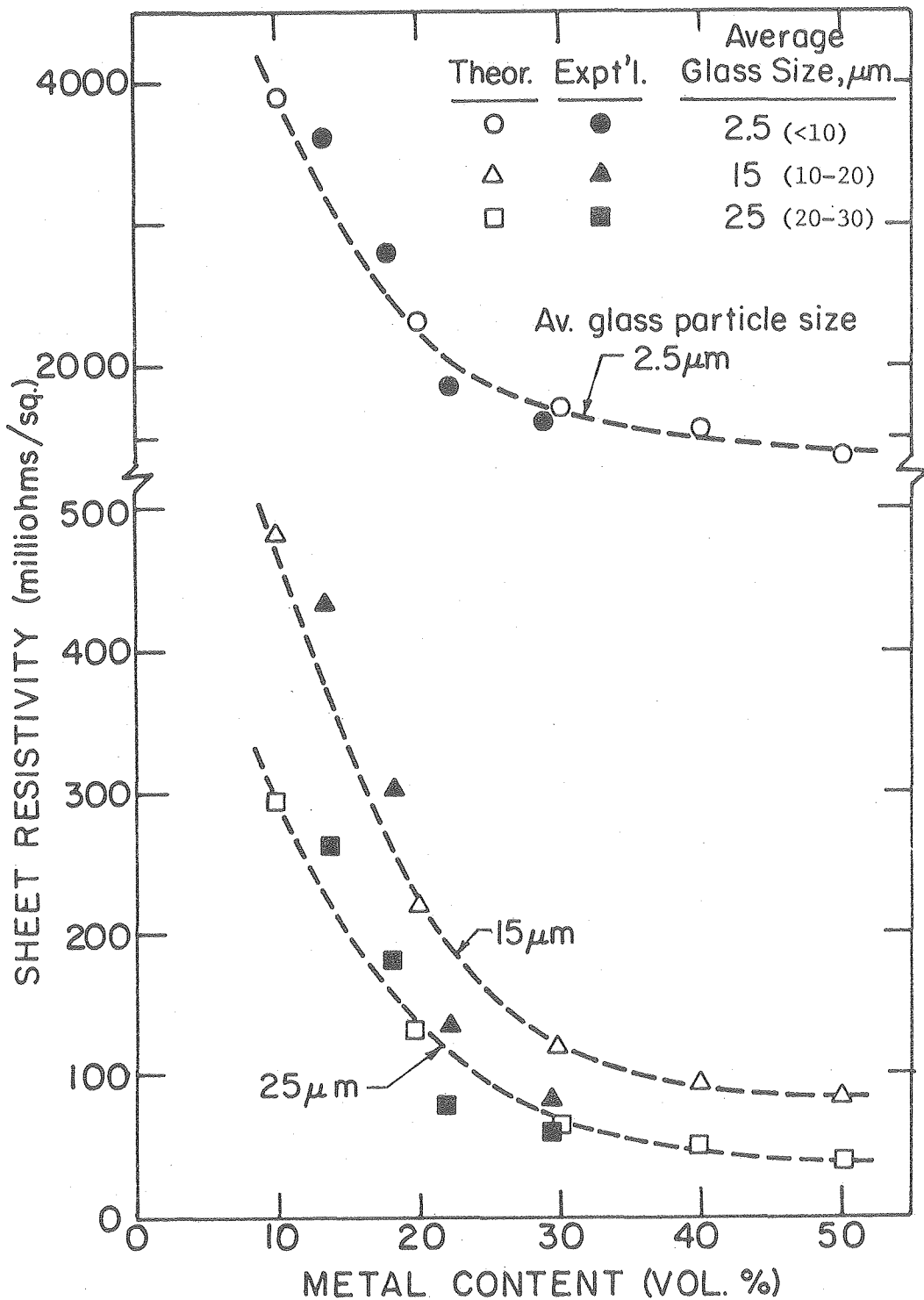
XBL7 710-6292

Fig. 27



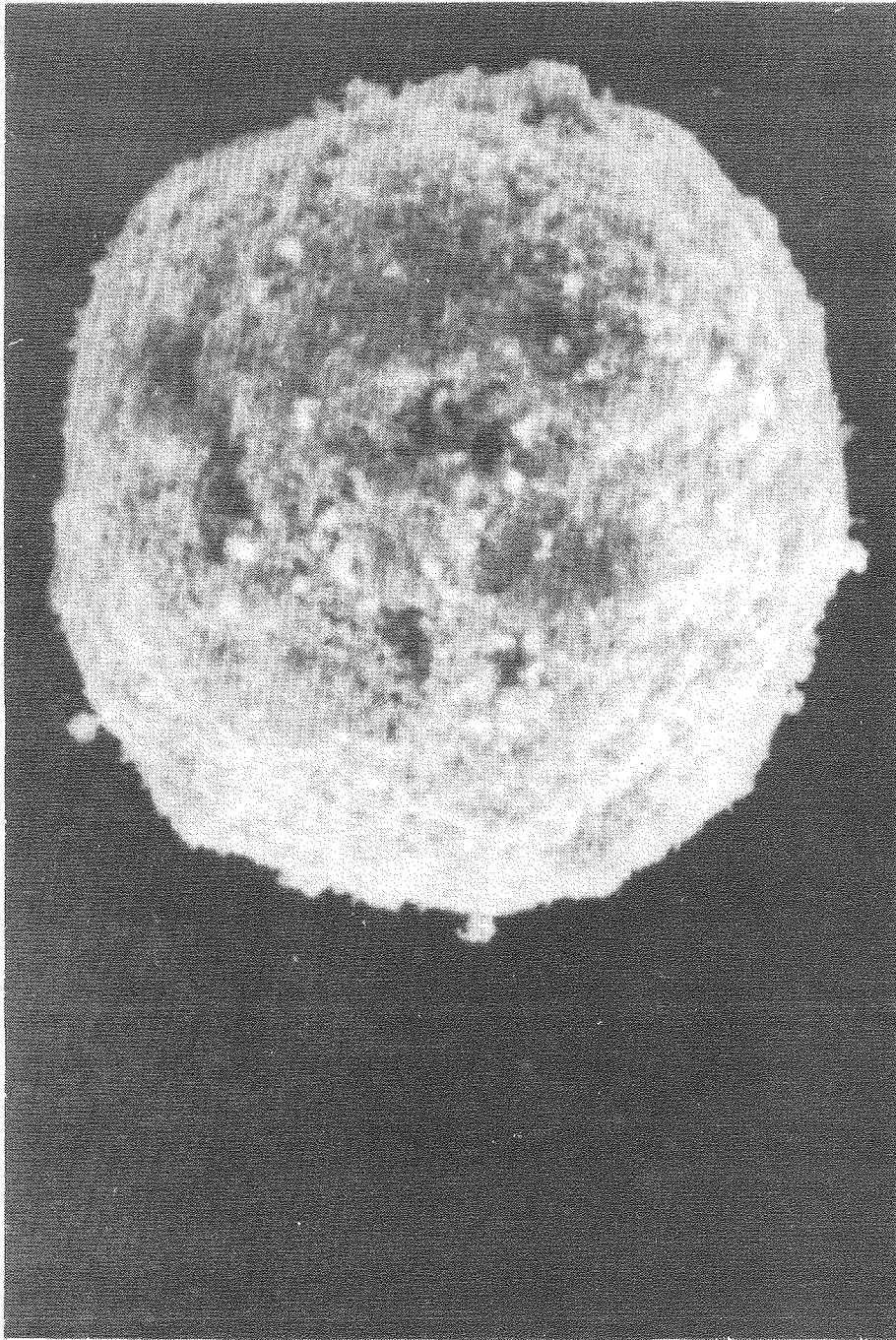
XBL 7710-10282

Fig. 28



XBL 7911-14532

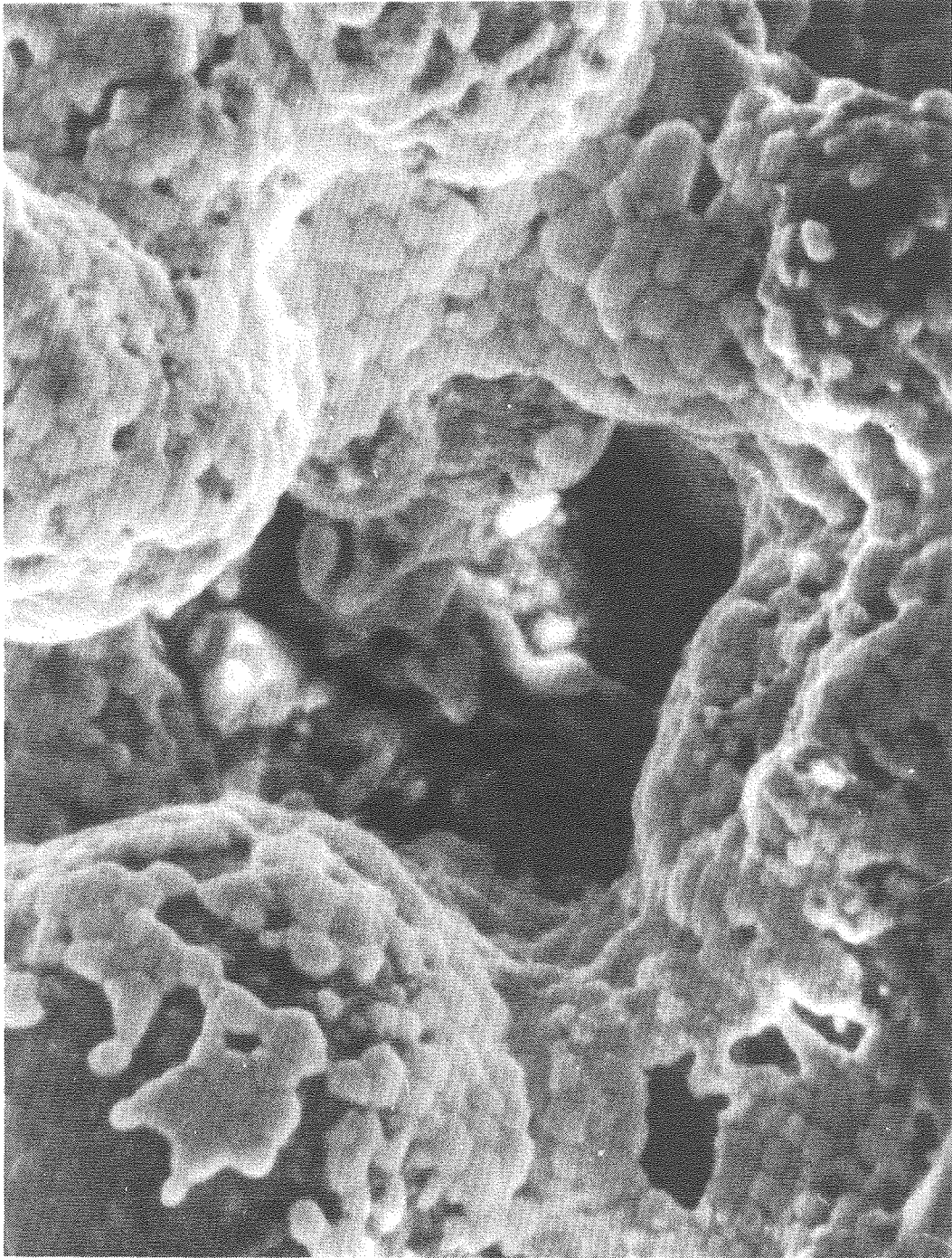
Fig. 29



10μ

XBB 790-14960

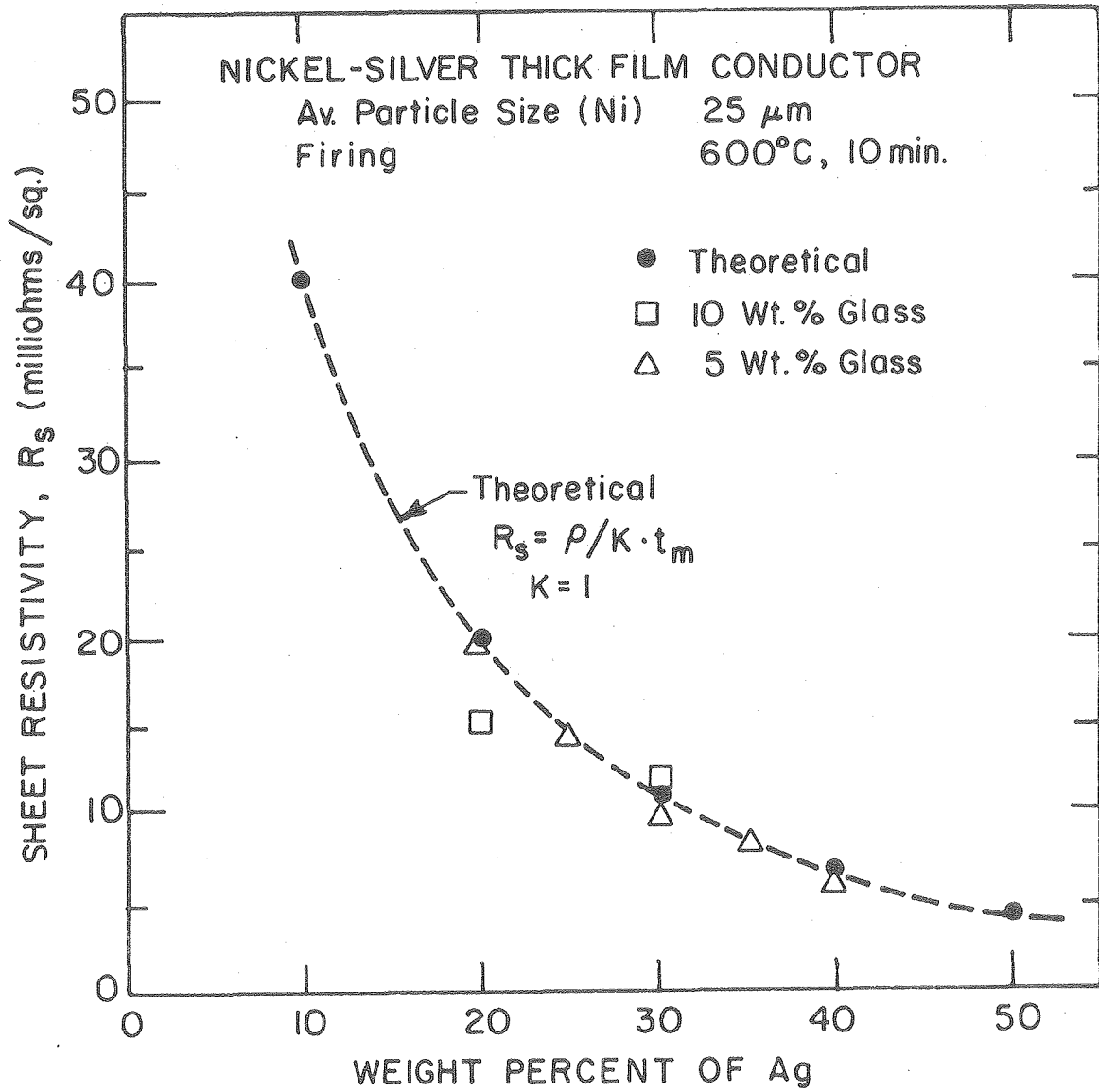
Fig. 30



14 μ

XBB 790-14959

Fig. 31



XBL7911-14531

Fig. 32

REFERENCES

1. a. A. L. Stuijts, Chap. 19, p 443, b. Bernard Jaffe, Chap. 20, p 475, in Ceramic Microstructures, Ed. R. M. Fulrath and J. A. Pask, John Wiley & Sons, 1968.
2. Kiyoshi Okazaki, in Ceramic Microstructures, '76, p. 564, Ed. R. M. Fulrath and J. A. Pask, Westview Press, Inc., CO, 1977.
3. Henry H. Nester and Thomas E. Salzer, Proceedings of First Technical Thick Film Symposium, International Society for Hybrid Microelectronics (ISHM), p. 1, 1967.
4. Karel Kurzweil and James Loughran, Solid State Technology, p. 36, May 1973.
5. Joseph P. Budd, Proceedings of International Society for Hybrid Microelectronics Symposium, p. 359, 1968.
6. Henry Fenster and P. E. McHale, Proceedings of International Society for Hybrid Microelectronics Symposium, p. 219, 1968.
7. K. S. Williams, Proceedings of International Society for Hybrid Microelectronics Symposium, p. 497, 1968.
8. James Loughran and Karl Kurzweil, IEEE Trans. on Parts, Hybrids and Packaging, V. PHP-10, No. 2, June 1974.
9. Donald W. Hamer, Proceedings of International Society for Hybrid Microelectronics Symposium, p. 6.1.1, 1970.
10. Walter H. Kohl, Chap. 15, Handbook of Materials and Techniques for Vacuum Devices, Reinhold Publishing Corp., 1967.
11. "DuPont Product Literature," E. I. DuPont De Nemours & Co., Electronic Products Division, Wilmington, DE, Feb. 1978.

12. Jon A. Van Hise, Proceedings of ISHM Symposium, p. 185, 1969.
13. Paul W. Polinski, Solid State Technology, p. 31, May, 1973.
14. Sanford S. Cole, Jr., Proceedings of 1972 ISHM Conference, p. 2-A-1-1, 1972.
15. T. Kobota and T. Shinmura, Proceedings of ISHM Symposium, p. 81, 1969.
16. T. T. Hitch, Journal of Electronic Materials, V. 3, No. 2, p. 553, 1974.
17. R. W. Vest, Technical report on 'Conduction Mechanisms in Thick Film Microcircuits', Purdue University, West Lafayette, IN, Dec., 1975.
18. S. J. Horowitz, et al., Solid State Technology, V. 22, No. 3, p. 27, March 1979.
19. M. V. Coleman and G. E. Gurnett, Solid State Technology, V. 22, No. 3, p. 45, March 1979.
20. H. G. Kim, et al., Solid State Technology, V. 22, No. 3, p. 62, March 1979.
21. Voddarahalli K. Nagesh and Richard M. Fulrath, U.S. Patent No. 4,130,671, December 1978.
22. V. K. Nagesh, M.S. Thesis, Lawrence Berkeley Laboratory, LBL-5172, June 1976.
23. David Mentley, M.S. Thesis, Lawrence Berkeley Laboratory, LBL-5176, June 1976.
24. R. W. Berry, P. M. Hall and M. T. Harris, Chap. 7, Thin Film Technology, Pub. Van Nostrand Reinhold Co., 1968.

25. Modern X-ray Analysis, III, Pub. EDAX International Inc.,
Prairie View, IL (1975).
26. J. H. Escard and D. J. Brion, J. Am. Ceram. Soc., 58, [7-8], p. 296
(1975).
27. R. W. Vest, Chap. 4, p. 76, Technical report on 'Conduction
Mechanisms in Thick Film Microcircuits,' Pub. Purdue University,
West Lafayette, IN, December 1975.
28. A. J. Andrews, Chap. 3, 2nd Edition, Porcelain Enamels, Pub.
Garrard Press, Champaign, IL.
29. English and Turner, J. Am. Ceram. Soc. 12, p. 760, (1929).
30. Mayer and Havas, Sprechsaal, 42, p. 497, (1909) and 44, pp. 188,
207, 220 (1911).
31. Winkelmann and Schott, Wiedemann's Annalen Bd., 51, p. 731, (1894).
32. W. D. Kingery, et al., Introduction to Ceramics, 2nd Edition, Chap.
12, p. 592, Pub. John Wiley & Sons, 1975.
33. W. Vogel, 'The Cellular Structure of Glass' - Structure of Glass,
V. 2, p. 17, 1960.
34. T. Dickinson, et al., J. of Solid State Chemistry, 13, p. 237 (1975).

PART II

WETTING STUDIES

I. INTRODUCTION

The study of interfaces is quite important to understand the composite systems. To develop good glass-metal, ceramic-metal and even metal-metal seals, knowledge of the interfaces is crucial. Wetting behavior studies through sessile drop experiments is one of the widely used methods to study the interfaces. Detailed studies on wetting behavior of sodium disilicate glasses on platinum, gold and iron, and of borate glasses on gold and platinum have been performed.^{1,2,3} Most of the conventional thick film systems use lead borosilicate glass as a binder between precious metals (Pt, Ag, Au) and the ceramic substrate (Al_2O_3).⁴ In order to understand the microstructure development in these thick film systems, interface studies of lead borosilicate glass and precious metal systems is important. Also, as seen in Part I, base metal (Ni)-precious metal (Ag) composite systems are potentially economic. In order to get a basic understanding of the interface relations in these composite systems, contact angle studies of lead borosilicate glass on silver, gold and platinum and of silver on nickel metal were undertaken.

CURRENT UNDERSTANDING

For a solid-liquid-vapor system in thermodynamic equilibrium the relation between the interfacial tensions (energies) and the contact angle θ of the liquid drop on the solid substrate, can be explained by Young's equation

$$\gamma_{SV} - \gamma_{SL} = \gamma_{LV} \cos \theta \quad (1)$$

where γ_{SV} , γ_{LV} , γ_{SL} are the interfacial tensions, subscripts S, L and V represent solid liquid and vapor phases (Fig. 1).⁵ This equation, which represents the balance of the horizontal components of the forces acting at the three phase contact, has been derived by many methods,⁶ all of which assume chemical equilibrium. Two equilibrium configurations of the liquid drop on a solid are shown in Fig. 1. When $\theta > 90^\circ$, the liquid does not wet the solid and when $\theta < 90^\circ$, the liquid wets the solid. When $\theta \leq 0^\circ$, the liquid spreads over the solid. Relative magnitudes of the interfacial tensions determine whether the contact angle will be acute or obtuse. The degree of wetting is increased with a decrease in the contact angle θ . Wetting occurs if the surface energy of the solid is reduced by the liquid and non-wetting occurs if it is increased by the liquid.

A liquid and solid will form an interfacial bond if the resultant interface energy will be lower than the sum of the surface energies of the two phases. The energy of adhesion is given by Dupre's equation⁷

$$F_{ad} = F_{SG} + F_{LG} - F_{SL} = \gamma_{SG} + \gamma_{LG} - \gamma_{SL} \quad (2)$$

where F is the interfacial (surface) energy and γ is the interfacial tension. In most cases, F's and γ 's are interchangeable. A modified Dupre's equation, taking into account the mechanical strain factor and the effect of any inhomogeneities present at the interface — like a void, a reaction product, atomic mismatch etc., could be written as

$$F_{ad} = K (F_{SG} + F_{LG} - F_{SL} - F_{Strain}) \quad (3)$$

where K is a proportionality constant.

Combining Young's equation (1) and Dupre's equation (2), the force of adhesion is given by

$$\gamma_{ad} = \gamma_{LG} (1 + \cos \theta) \quad (4)$$

The contact angle of the sessile drop can be an indication of the strength of adhesion. It can also be an indication of the reduction of the interfacial energy. For a given system, the smaller the contact angle, the larger will be the reduction in interfacial energy and the stronger will be the adherence. Hence, the sessile drop measurements provide valuable information regarding the interface formation and adherence in the glass-metal systems.

Earlier work on glass-metal systems has shown that good wetting and adherence depends on the formation of a strong chemical bond rather than van der Waal's bond. According to the understanding developed in this laboratory, to form chemical bonds all along the interface and thus have a continuity in the electronic structure across the interface, saturation of the glass at the interface with the low valent oxide of the metal is a prerequisite.⁸ Here the surface oxygen atoms can intercoordinate with the surface oxygen atoms of the glass. If the oxide of the metal is completely dissolved by the glass before its saturation with the oxide, glass will be exposed to fresh metal and such an interface without a reaction will lead to a weak van der Wall's bond. However, if the glass at the interface becomes saturated just as the available oxide is dissolved, strong chemical bonding will result.

The effect of atmospheric conditions and adsorbed substances on the surface energies of the solid substrates are also very important in the

analysis of the contact angle measurements. The effect of chemisorbed contaminants on the wetting behavior of sodium borate glass and sodium disilicate glass on gold and platinum has been studied in this laboratory.^{8,9} Table 1 summarizes some of these results. The presence of oxygen lowered the contact angle and also improved the adherence as compared to the values obtained in vacuum with both of these glasses. The increased driving force for wetting has been explained as being due to a greater saturation of the interface with the metal. At low partial pressures of oxygen, oxygen has been shown to adsorb strongly only on the stepped surfaces of platinum and very rarely on (111), (100), or (110) surfaces.¹⁰ Even though there are no stable bulk oxides of gold at elevated temperatures, surface oxides have been observed to be stable, changing valencies of the surface gold atoms being responsible for the stability. The chemisorption of oxygen, water vapor and selected hydrocarbons on gold and silver have been studied in detail, by many researchers using surface analytical techniques like LEED, Auger and photoelectron spectroscopy.^{11,12}

Water adsorption is shown to increase the contact angle of sodium disilicate and borate glasses on gold and platinum due to the reduction in the surface energy of the metal substrates.^{2,3,8} Carbon adsorption on platinum also causes increased contact angles of borate glasses on platinum.² In the presence of oxygen, decreased contact angles on Pt have been explained to be due to the oxidation of adsorbed carbon with an increase of γ_{SV} as opposed to any reduction of the interfacial energy. However, the effects of the absence of oxygen and adsorption of carbon impurities on the substrate have not been separately identified. Taking

these points into consideration, the study of wetting behavior of lead borosilicate glass on silver, gold and platinum were undertaken.

EXPERIMENTAL DETAILS

Sessile drop measurements of lead borosilicate glass (70 w/o PbO, 10 w/o SiO₂, 20 w/o B₂O₃) on silver, gold and platinum were conducted in different atmospheres. 99.99% pure precious metals (Ag, Au and Pt) obtained from LBL, in the form of sheets (thickness 0.010") were cut into 1 cm X 1 cm substrates. The glass prepared in the thick film studies was used to make small beads (~.5mm dia.). Also, the glass prepared by Corning Glass Works was used to obtain small chunks for sessile drop experiments.

For air atmosphere conditions a Hevi duty Lindberg tube furnace, open at both ends was used. The rate of temperature increase was ~50°C/minute and the accuracy of the temperature reading ±5°C. For vacuum and inert atmosphere conditions two contact angle furnaces were used. The first furnace (referred to as 'graphite furnace,' Fig. 2) consisted of a graphite tube resistance heating element in a vacuum chamber. Inside this tube was an alumina 'dee tube' on which the sample (glass drop on the metal substrate) was kept. The graphite tube was connected to water cooled copper electrodes using graphite holders. The vacuum chamber was connected to an oil diffusion pump (capable of providing a 10⁻⁷ torr vacuum) and to an inert gas supply. The sessile drops were viewed through the fused silica windows of the vacuum chamber.

The second furnace (referred to as 'alumina furnace,' Fig. 3) consisted of 1" diameter, 8" long, Kanthal resistant wire wound, high density alumina tube (open at both ends) inside a large vacuum chamber (10⁻⁷ torr)

which is connected to an oil diffusion pump and an inert gas supply. A sheet of tantalum was wound inside the alumina tube to reduce the partial pressure of oxygen. A leak valve on the vacuum chamber allowed inert gases to be introduced into the furnace. The pressure in both of the furnaces was measured with a cold cathode ionization gauge. A liquid nitrogen cold trap was used to condense vapors from the diffusion pump. All experiments were carried out at 2×10^{-6} torr (1.94×10^{-9} atm) at the test temperature. Under these conditions the equilibrium partial pressure of oxygen in the alumina furnace is $\sim 10^{-19}$ torr at 700°C and the equilibrium partial pressure of oxygen in the graphite furnace (calculated using the reaction $\text{C} + 1/2 \text{O}_2 \rightleftharpoons \text{CO}$) is $\sim 10^{-35}$ atm. However, due to residual leaks, outgassing of the furnace walls and other non-equilibrium conditions, P_{O_2} would be many orders of magnitude higher than these values. The graphite tube furnace was used to intentionally introduce carbon impurities into the system and study the effect of carbon adsorption on the surface energies of the precious metals by measuring the contact angles of glass drops on these metals.

The temperature in both of these furnaces was measured (accuracy $\pm 5^\circ\text{C}$) with two Pt - Pt. 10/Rh thermocouples (after calibration) which were kept close to the sample (< 8 mm above the specimen).

The contact angles were measured using a telegoniometer (made by Rame-Hart Inc., NJ) which consists of a Model 102-00-00 telescope with rotatable cross hairs moveable in x, y, z and θ directions, and a circular scale to measure the angles. The accuracy of measuring the angle with this instrument is $\pm 1^\circ$.

In the actual experimental runs, glass-metal samples were weighed before and after the experiment. Before heating to the test temperature the vacuum chamber was pumped to <10 torr (using a mechanical pump) and then pumped to $\sim 1.5 \times 10^{-6}$ torr with a cold trapped diffusion pump. The substrate and the drop were heated to the test temperature ($\sim 15^\circ\text{C}/\text{min}$. up to 400°C , $\sim 20^\circ\text{C}/\text{min}$ after that to the test temperature of 600°C , 700°C) and held until equilibrium was attained, i.e. no further change in the contact angle for 30 mins. The assembly was then furnace cooled.

The surface of the substrates at the edges of the drop were examined using optical microscopy. Some of the specimens were subjected to bending in order to separate the glass from the metal or fracture the glass (depending on the strength of bonding) to obtain qualitative data about glass-metal adherence.

The contact angle measurements of silver on nickel substrates were done in an air atmosphere and in gettered helium (alumina furnace). 99.99% pure silver shot (obtained from LBL) were used and the nickel substrates were polished before the experiment to remove any visible oxide layer and to obtain a flat surface. Contact angles were measured at 970°C after the equilibrium was established. To study the interface, the specimen (Ag drop on Ni substrate) was sectioned perpendicular to the substrate at the center of the drop using a diamond saw and then was mounted in Bakelite. Standard metallographic polishing techniques were used (final lapping with $.3\mu\text{m Al}_2\text{O}_3$) and the interfaces were examined using SEM with attached EDAX capability (see Part I for details).

RESULTS AND DISCUSSION

A. Lead Borosilicate Glass and Precious Metals

The results of the sessile drop experiments using lead borosilicate glass on silver, gold and platinum with different atmospheric conditions are tabulated in Table 2.

1.) Silver

In an air atmosphere the glass drop spread into a uniform circle (contact Angle = 0°). Spreading started at 500°C and was very fast. When the experiment was repeated with a larger amount of glass, the glass spread over the edges to the bottom side of the substrate. In both cases, crystallization was observed at the periphery. Optical micrographs in Fig. 4 show the top view of the glass-crystal transition region and crystal-silver transition region. These regions are diffused and do not have a sharp transition boundary. Figure 5 shows the crystallized edges of the glass. Spreading of glass occurred along the grain boundaries as well. A better micrograph of the grain boundaries could not be obtained because of the lack of a proper etchant and due to insufficient thermal etching at the temperatures studied. At the glass-metal interface the grain boundaries of the metal are prominently visible, indicating a stronger attack at the grain boundaries.

A finite contact angle ($\theta \sim 2^\circ$) was obtained for the glass drop on silver in vacuum (3×10^{-6} torr) in the absence of carbon contaminants at 700°C . Even though the drop attained equilibrium very quickly, the uniform and symmetric spreading obtained in air atmosphere was not observed in this case. The optical micrograph in Fig. 6A shows the edges of the drop on silver as viewed from the top. Spreading of the liquid

(glass) along the grain boundary is also noticeable. Grain boundaries below the glass layer are clearly visible. The edges of the glass drop is irregular but there is no indication of crystallization.

In the presence of gettered helium the equilibrium contact angle was acute (48°). The edge of the glass drop as seen from the top is shown in the optical micrograph (Fig. 6B). The edge of the drop has a sharp boundary with no spreading of the glass along the grain boundary.

Very strong adherence of the drop to the substrate was obtained for air atmosphere conditions. It was very difficult to remove the glass film by scratching or bending of the substrate. In vacuum conditions, the adherence was good. On bending the substrate, the glass was broken into slivers. But, in gettered He atmosphere, adherence was poor. The whole drop came off the substrate and the interfacing surfaces were clean.

An equilibrium contact angle is obtained when a balance of the horizontal components of surface tensions is reached as described by Young's equation. The sharp edge of the glass drop and its poor adherence to silver in the presence of He indicates lack of reaction between the glass and silver, and the existence of van der Waals' bonding. It is known that the surface tension of Ag measured in a helium atmosphere is the true surface tension as helium is insoluble in silver, does not chemisorb and will not be physically adsorbed at high temperatures.¹³ A surface energy of $\sim 1160 \text{ ergs/cm}^2$ at 932°C is reported for a He atmosphere. Due to the high vapor pressure of silver, some erratic values have been reported for vacuum conditions. Surface energy of silver is very sensitive to the presence of oxygen and is about 1000 ergs/cm^2 at an oxygen partial pressure of 10^{-4} torr and becomes considerably less as the

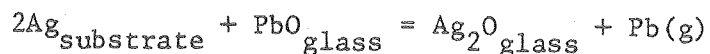
partial pressure of oxygen increases.¹⁴

A higher surface energy for silver alone would cause a decrease in the contact angle as realized from Young's Equation. Adsorption of any gases would reduce the solid surface energy and hence would have a tendency to increase the contact angle. However, the glass drop has been observed to spread in the presence of oxygen leading to good adherence. Spreading almost always is due to a reaction occurring at the interface whose free energy of reaction contributes to a reduction of interfacial energy.¹⁵ Increased wetting or the decrease of contact angle has also been attributed to interfacial reactions by many investigators.¹⁶ The presence of an oxide on the surface of silver has an important effect on the interfacial energy between glass and silver. Saturation of the interface with the oxide lowers the internal energy of glass at the interface. A sharing of the oxygens at the interface results in a continuity of electronic structure across the interface causing a reduction in the interfacial energy and strong adherence. In other words, the molten glass dissolves the surface oxide layer and as the dissolution continues the interfacial energy will be continuously reduced. The type of spreading observed in the presence of oxygen and the appearance of a compound around the periphery of the drop indicate that either the surface oxide layer formed is of significant thickness or oxygen moves through the metal to the glass-metal interface or along the interface from the edge continuously during the exposure.

The adherence is strong both at the center and at the edges of the drop. This indicates the saturation of the glass with the metal oxide along the entire interface. Oxygen adsorption on the silver metal is

quite appreciable¹⁴ and is responsible for the surface oxide needed for strong adherence all along the interface and especially at the center of the drop. However, oxygen diffusing through the interface from the edges provides oxygen to form more metal oxide to replace the dissolved oxide. At the temperature of study (700°C) glass has a very low viscosity and diffusion of Ag^+ away from the interface into the glass occurs quite readily. As more and more metal oxide goes into solution with glass, the glass composition will be considerably altered. The largest change would occur at the periphery as (i) the edge of the advancing drop gathers more and more oxide as the glass flows, which is concurrent with the understanding that reaction of the metal oxide with glass is the driving force for spreading; or (ii) the edges have an easy access to oxygen in the atmosphere. The increased reaction around the periphery is indicated by the presence of a precipitated phase.

Adherence between glass and metal was good in the case of sessile drop measurements conducted at 700°C in a vacuum (2×10^{-6} torr) with a partial pressure of oxygen of $\sim 10^{-19}$ torr. Adherence was better at the edges than at the center. The color of the glass had slightly changed to milky white, but no crystals were observed as in the case with air firing. These factors indicate the possibility of a redox reaction between silver and lead oxide in the glass. The possible reaction taking place under the conditions of the experiment is



This type of reaction is similar to the ones predicted by Brennan and Pask¹⁷ in studies on sodium disilicate glass-base metal systems. The free energy for the reaction, ΔF is given by

$$\Delta F = \Delta F^\circ + RT \ln \frac{a_{\text{Ag}_2\text{O}}(\text{glass}) \cdot P_{\text{Pb}}}{a_{\text{PbO}}(\text{glass})}$$

ΔF° , the standard free energy for the reaction is positive, since the oxidation potential of the substrate (Ag) is lower than that of Pb, which would be the cation to be reduced. (Standard oxidation potentials at 25°C are, $\text{Ag} \rightarrow \text{Ag}^+ -0.800\text{V}$, $\text{Pb} \rightarrow \text{Pb}^{2+} + 0.126\text{V}$).

The reaction therefore will be feasible if the equilibrium constant for the reaction at the interface is sufficiently <1 to get a negative ΔF . Reaction could be achieved if lead is formed in the vapor state and is immediately removed from the reaction site. At 700°C, the vapor pressure of Pb is $\sim 10^{-3}$ torr ($\sim 10^{-5}$ atm) which is quite high compared to the total ambient pressure of 2×10^{-6} torr in the furnace. This insures that the lead formed could be easily removed to maintain P_{Pb} at the interface low enough for the redox reaction to continue. Ag^+ ions resulting from this reaction can thus go into the glass, giving a chemical continuity of silver oxide at the interface and hence good adherence. It will be easier for $\text{Pb}(\text{g})$ formed at the interface to escape from the edges of the drop than from the center. Hence, there is a greater driving force at the edges, for the reaction to take place. This explains the better adherence obtained at the edges in the vacuum conditions. The irregular edges of the drop seen in Fig. 6a further support the presence of a reaction between the glass and the substrate metal. The grain

boundaries appear to be attacked more strongly as would be expected.

In the presence of gettered helium at 1 atmosphere, the adherence was poor. The whole drop could be readily removed from the surface of the metal without leaving any traces. With the high ambient atmosphere pressure it is not possible to get Pb as a vapor phase in the redox reaction. Under these conditions ΔF would be positive and hence no redox reaction can take place. This is reflected in the absence of adherence and the presence of a high contact angle (48°). This contact angle could be used to calculate the glass-metal interfacial energy (γ_{SL}) without the effect of any interfacial reaction, and this could further be used to determine the reduction of the interfacial energy due to the redox reaction at the interface under vacuum conditions. Assuming $\gamma_{SV}(\text{Ag})$ to be 1160 ergs/cm^2 ¹³ in both cases, $\gamma_{LV}(\text{glass})$ 180 ergs/cm^2 ,¹⁸ one can calculate $\gamma_{SL}(\text{He})$ 1039 ergs/cm^2 , and $\gamma_{SL}(\text{val.})$ 980 ergs/cm^2 , from these values it can be calculated that the interfacial energy is reduced by $\sim 59 \text{ ergs/cm}^2$ while the redox reaction is in progress.

2.) Gold

The LBS glass drop on gold has a finite acute contact angle in both an air atmosphere ($\theta = 18^\circ$) and vacuum ($\theta = 6.5^\circ$) at 700°C . However, the adherence obtained in vacuum conditions was poor, even though the contact angle was lower than in the air atmosphere. On bending the substrate, the whole drop came off the metal without leaving a trace. In air firing good adherence was observed. When the substrate was bent, the glass drop was broken into slivers still adhering to the substrate. On strong scratching with a sharp instrument, the center of the drop could be eroded. Adherence was stronger at the edges than the center.

The periphery of the drops as observed in the optical microscope is shown in Fig. 7. In the presence of oxygen, the edges of the drop are irregular and indicate spreading along the grain boundaries. However, in vacuum the edge of the drop is sharp and no spreading of the liquid is observed.

The absence of spreading and poor adherence obtained in vacuum conditions indicate the absence of any reaction between glass and the gold substrate. In the presence of oxygen, better adherence is due to the introduction of oxide into the interface introducing electronic continuity between the glass and the metal. Solution of the surface gold oxide also reduces the interfacial energy. Thus, stronger adherence results. The difference in adherence between the center and the edges is due (i) to the better access that the interface at the edge has to oxygen, and (ii) to the possibility of the edge of the glass dissolving more surface oxide as it moves along the surface. Since the contact angle remains constant, the edge of the drop is saturated with gold oxide. If the edge was undersaturated, the drop would continue to spread as long as the glass on the periphery was not saturated with the oxide.

The higher contact angle in air (18°) as compared with the contact angle in vacuum ($6^\circ.5$) can be explained on the basis of Young's equation. The γ_{LV} of the glass can be assumed to be constant ($\sim 180 \text{ ergs/cm}^2$). A change in the surface energy of gold due to oxygen adsorption has been observed by Udin et al.¹³ In helium, γ_{SV} is $\sim 1370 \text{ ergs/cm}^2 \pm 65 \text{ ergs/cm}^2$ at 1040°C , and in air it is $\sim 1210 \text{ ergs/cm}^2 \pm 60 \text{ ergs/cm}^2$. The corresponding values of γ_{SL} can then be calculated for air and vacuum conditions.

In air γ_{SL} becomes 1039 ergs/cm² and in vacuum, 1191 ergs/cm². A reduction of 152 ergs/cm² thus occurs in γ_{SL} in air which would cause a decrease in the contact angle. In the present case, however, the adsorption of oxygen on the metal decreases its γ_{SV} by 160 ergs/cm², thus overriding the effect of the decrease in γ_{SL} giving a higher contact angle in air atmosphere.

3.) Platinum

The glass drop on platinum has a finite contact angle of 2°-3° and remains clear in air atmospheric conditions at 700°C. On bending the substrate the glass is broken into slivers indicating strong adherence of the glass to the substrate. The periphery of the drop as seen in Fig. 8a is irregular.

The contact angle of the drop at 700°C in vacuum conditions (3×10^{-6} torr) with carbon contamination is 73° and without carbon contamination, 58°. The glass drop attained a dark color due to the reduction of PbO to metallic Pb, probably by carbon impurities (introduced by the graphite tube in the furnace) which caused a sufficient reduction in the partial pressure of oxygen. The adherence is poor in both cases and the whole drop breaks away from the substrate on bending. Figure 8b indicates a sharp boundary between the edge of the drop and the substrate with no penetration of glass along the grain boundaries.

The low contact angle and strong adherence of glass observed in air are due to the saturation of glass by metal oxide at the interface. Strong evidence observed for adsorption of oxygen on platinum surfaces¹⁰ suggests that the possible path for movement of oxygen to the glass/metal

interface is either through the metal or along the interface. Due to the solution of the surface oxide of platinum in glass the interfacial energy is greatly reduced resulting in the low contact angle (2° - 3°). However, in vacuum the partial pressure of oxygen is less than 10^{-19} torr resulting in the high contact angle (58°) of glass on platinum. Further, the adherence is very poor because of the absence of dissolution of surface oxide or any other interfacial reaction which could have resulted in a reduction of interfacial energy and a chemically continuous interface.

The glass-platinum interfacial energy (γ_{SL}) can be calculated using Young's equation with γ_{SV} (Pt) ≈ 2000 ergs/cm^{2*} and γ_{LV} (glass) ≈ 180 ergs/cm² at 700°C . For a contact angle of 58° , γ_{SL} is calculated to be ~ 1905 ergs/cm². In the air atmosphere both γ_{SV} (Pt) and γ_{SL} (interfacial energy) change. Due to the adsorption of oxygen, γ_{SV} decreases and would cause the contact angle θ , to increase. Presence of water vapor in the atmosphere would also have similar effects. However, the reduction of the interfacial energy γ_{SL} caused by the solution of metal oxide tends to reduce the contact angle. In this particular system, reduction of the interfacial energy is the dominant effect as seen by the lower contact angle obtained in air (2° - 3°) as compared with the value obtained in vacuum (58°).

Using Young's equation and the values of 180 ergs/cm² for γ_{LV} , 2° for θ , the difference ($\gamma_{SV} - \gamma_{SL}$) is calculated to be 179.8 ergs/cm².

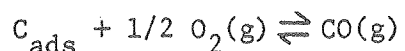
* Many different values have been reported close to this value.¹⁹

If we assume γ_{SV} (Pt) and γ_{LV} (glass) to be relatively invariant, in vacuum and air atmosphere, the reduction in the interfacial energy γ_{SL} due to reaction (dissolution of the surface oxide) can be approximated to be $\sim 84 \text{ ergs/cm}^2$. Any actual reduction of γ_{SV} in air in comparison with 2000 ergs/cm^2 in vacuum will also lead to a similar reduction of γ_{SL} .

In vacuum conditions, the presence of graphite tube introduces carbon impurities. The contact angle of glass on Pt is 73° (at 700°C) under these conditions. This is greater than the contact angle obtained without the presence of graphite tube. Surface studies have indicated strong evidence for carbon adsorption on platinum surface.²⁰ Due to this adsorption the surface energy of platinum (γ_{SV}) is reduced. Also, since the partial pressure of oxygen is very low, no change of the interfacial energy is expected as evidenced by poor adherence and a very regular periphery of the drop. The net effect would hence be a contact angle higher than the angle obtained for vacuum conditions without carbon impurities. A similar increase in contact angle due to carbon adsorption has been observed in the borate glass-platinum system.² It is possible to calculate the reduction in γ_{SV} due to adsorption of carbon impurities responsible for the increase of the contact angle from 58° to 73° . Using the values of $\gamma_{SL} = 1905 \text{ ergs/cm}^2$ obtained from contact angle measurements in vacuum (without carbon contamination) and an unchanged γ_{LV} , the reduction of γ_{SV} (platinum) is calculated to be $\sim 43 \text{ ergs/cm}^2$. Any reduction in γ_{LV} that may have occurred in the graphite furnace would result in a higher calculated reduction of γ_{SV} . This compares with the value (50 ergs/cm^2) obtained by Holmquist² in studying the carbon

contamination in borate glass-platinum system.

Using calculations similar to the ones used by Holmquist,² it is further possible to approximate the amount of carbon responsible for the reduction of γ_{SV} . From the oxidation reaction of carbon, the activity of carbon can be estimated.



$$K_{eq} = \frac{P_{CO}}{P_{O_2}^{1/2} \cdot a_c} \quad \text{where the partial pressure of}$$

oxygen and CO have replaced their activities, as at low pressures these gases could be assumed to be ideal gases. Assuming the equilibrium constant for bulk carbon oxidation to CO to be applicable

$$\text{at } 1000^\circ\text{K} \quad K_{eq} = 10^{10.459} \quad (21)$$

$$P_{O_2} \approx (.2)(3 \times 10^{-6}) \text{ torr} = 7.9 \times 10^{-10} \text{ atm}$$

$$P_{CO} \approx 2(7.9 \times 10^{-10}) \text{ atm}$$

$$a_c = 10$$

Now, using the Gibbs adsorption equation²²

$$d\gamma = \Gamma RT \ln(a_c)$$

where $d\gamma$ = change in surface energy

Γ = adsorption density, R = universal gas constant and T , the absolute temperature (1000°K)

$d\gamma$, calculated from sessile drop measurements = 48 ergs/cm² and the

amount of carbon responsible for this lowering of γ_{SV} (platinum) is calculated to be $\Gamma = 1.016 \times 10^{13}$ atoms/cm². For comparison, the (111) surface of platinum has $\sim 1.5 \times 10^{15}$ atoms/cm².

To summarize the results on platinum, absence of oxygen led to an increased contact angle caused primarily by an increased γ_{SL} due to the absence of any interfacial reaction. The presence of carbon impurities further increased the contact angle due primarily to the reduction of γ_{SV} of platinum. The effect of carbon impurities and the absence of oxygen can thus be separately understood by these sessile drop measurements conducted in vacuum with and without the presence of carbon impurities. A reduction of ~ 43 ergs/cm² occurred in the surface energy of platinum due to carbon adsorption.

B. Silver on Nickel

In air atmosphere conditions the silver sessile drop on nickel substrate had an equilibrium contact angle of 90° at 970°C. When the silver drop melted the initial contact angle was obtuse and in less than five minutes an equilibrium angle was attained. The surface of the substrate was tarnished, the drop was regular and the edge was sharp. The adherence between the drop and the substrate was good. The cross section of the interface as seen in SEM is shown in Fig. 9a. X-ray line mappings of Ag and Ni are also seen across the micrograph. Nickel oxide layer forms on the surface of nickel and exists between nickel and silver. The thickness of this layer as seen from the micrograph is $\sim 5-6\mu\text{m}$ and is fairly constant.

In gettered helium atmosphere, at 970°C an equilibrium contact angle of 9.5° was obtained (in 30 minutes time). The surface of the substrate was shiny, the drop was regular but the edges were irregular. There was very strong adherence between the drop and the substrate. The scanning electron micrograph of the cross section of the interface along with the x-ray line mappings of nickel and silver is shown in Fig. 9b. Penetration of silver into nickel can be noticed in this micrograph.

Surface energies of silver and nickel at 1000°C are given in Table 3. There is quite a good correlation between the approximated and measured surface energies (tensions) (γ_{SV}) of nickel. Surface energy (γ_{SV}) of NiO from 's value is given as 400 ergs/cm². The surface energy of solid silver is found to be very sensitive to the presence of oxygen and Fig. 10, is the reproduction of the data obtained by Buttner et al.¹⁴ In an air atmosphere the surface energy of silver(s) at 932°C will be decreased to ~450 ergs/cm² (in He atm. γ_{SV} is 1140 ergs/cm²). For liquid Ag at 970°C, however, no such data was found, but it is logical to expect γ_{LV} also to be correspondingly lower in an air atmosphere

From the 9.5° contact angle in He atmosphere γ_{Ni-Ag} could be calculated using Young's equation and the values of surface energies given above. The calculated value of γ_{Ni-Ag} is 1312 ergs/cm². In this case, $\gamma_{SV} (\gamma_{Ni}) > \gamma_{LV} (\gamma_{Ag})$ and the interfacial energy is reduced by the solution reaction (silver dissolving in nickel at the interface), resulting in very strong adherence. Both nickel and silver are f.c.c. and their atomic sizes are within 15% of each other (Table 4), but there is limited solid solution between them because of the wide difference between the internal pressures of the two elements.²³ From the phase diagram of

nickel and silver²⁴ there is a finite solubility of silver in nickel (< 2 at%) and almost zero solubility of nickel in silver. This can be qualitatively seen in the micrograph (Fig. 9b) where the intensity profile for nickel (Ni) drops to zero very quickly in the silver region, whereas silver (Ag) has a profile into the nickel region dropping to zero in < 1.5 μ m from the interface, (dark line in the micrograph indicates the scanning line).

In air atmosphere the contact angle obtained (90°) is actually the contact angle between silver and nickel oxide (thickness - 5 to 6 μ m) as evidenced from the scanning micrograph (Fig. 9a). Looking at the x-ray line scans (dark line represents the scanning line) in Fig. 9a, the concentration profile for silver (Ag) falls sharply at the silver - NiO transition boundary (in < .5 μ m into NiO region) to zero, indicating practically zero solubility of silver in NiO. However, the nickel (Ni) profile has a step in the interface layer and a comparatively slowly decreasing concentration profile into the silver region. The step observed for the nickel profile in the interface layer is due to dilution of nickel by oxygen atoms to form NiO and thus is an indirect proof that the intermediate layer is nickel oxide. Across the NiO-silver interface, the nickel intensity decreases slowly reaching zero at ~3 μ m into the silver region. This strongly indicates a probable solubility of NiO in silver even though nickel is barely soluble in silver. Good adherence of NiO-Ag supports the idea of chemical bonds existing across the interface which have resulted due to this solutioning of NiO in silver.

To explain the 90° contact angle observed in this system, which is unusual, it is necessary to understand the

thermodynamics and mechanics of wetting/spreading according to the theories developed in this laboratory by previous researchers.¹⁵

In a solid-liquid-vapor system let us consider the configuration of a small liquid sessile drop on a flat rigid solid surface existing at chemical equilibrium both in the bulk and at the interfaces.

Then a solid-liquid interface will form if the free energy change

$$\delta G = \delta \int_{SL} \gamma_{SL} dA_{SL} + \delta \int_{SV} \gamma_{SV} dA_{SV} + \delta \int_{LV} \gamma_{LV} dA_{LV} < 0 \quad (5)$$

dA = change in interfacial area, γ = interface energy.

The free energy decrease results in the driving force for the deformation of the drop.

The solid-liquid interfacial area increases and the shape of the drop changes until the minimum energy state is reached as defined by

$$\gamma_{SL} dA_{SL} + \gamma_{SV} dA_{SV} + \gamma_{LV} dA_{LV} = 0 \quad (6)$$

If the bulk volumes are non-reactive the free energy changes for the system are then associated with changes in interfacial areas. If they are reactive, the phases will react with each other through the interfaces to achieve a state of chemical equilibrium. During these non-equilibrium dynamic conditions, the interfacial tensions, hence the contact angle and the shape of the drop will be continuously changing until the system reaches a state of chemical equilibrium.

Several progressive geometric configurations of the drop and the change in the areas of the liquid-vapor and the solid-liquid interfaces vs. the contact angle (or the height of the drop h) were calculated by

Aksay et al.²⁵ and are shown in Fig. 11. The liquid-vapor interfacial area decreases from 180° to 90° and then increases as the contact angle decreases to 0°, whereas the solid-liquid interface increases continuously. As $dA_{SL} = -dA_{SV}$, equation 5 could be simplified to

$$\delta G = \delta \int_{SL} (\gamma_{SL} - \gamma_{SV}) dA_{SL} + \delta \int_{LV} \gamma_{LV} dA_{LV} \quad (7)$$

or

$$\frac{dG}{dh} = (\gamma_{SL} - \gamma_{SV}) \frac{dA_{SL}}{dh} + \gamma_{LV} \cdot \frac{dA_{LV}}{dh} \quad (8)$$

(Note: decreasing height h is considered positive).

Surface energies are assumed to be constant as chemical equilibrium is considered to be established in this system.

A net negative $\frac{dG}{dh}$ indicates that the solid-liquid interface will continue to form and the contact angle will continue to decrease; the minimum energy configuration is obtained when $\frac{dG}{dh} = 0$. This is realized when there is a balance achieved between the two terms of the equation. If $\gamma_{SV} < \gamma_{SL} < \gamma_{LV}$, then the contact angle will be obtuse. It will remain obtuse if γ_{SL} were to be constant. The significance of γ_{SL} is the following: Under chemical equilibrium conditions, the formation of a true interface could be considered analogous to the formation of a solution involving an adjustment of surface structures to form an intermediate interfacial structure (with interfacial tension between γ_{SV} and γ_{LV}). The actual magnitude of γ_{SL} , however, depends on the degree of chemical bonding or minimization of structural discontinuity across the interface developed in the system. γ_{SL} will become smaller with increased chemical bonding.

When $\gamma_{LV} > \gamma_{SV}$, as in the present case where the surface energy of liquid silver is greater than that of nickel oxide, we will have an obtuse angle to begin with. As NiO goes into solution with silver, chemical bonds are being developed. In other words, surface energy of silver γ_{LV} , is being reduced by the solid (NiO) surface energy γ_{SV} to give an interfacial energy γ_{SL} . As the reaction goes on, γ_{LV} is being continuously reduced when γ_{SL} also decreases continuously. The maximum reduction of γ_{LV} that could be achieved by the solid, however, is equal to the surface energy of the solid, γ_{SV} , i.e., $\gamma_{SL} \geq \gamma_{LV} - \gamma_{SV}$. But in any case, γ_{SL} has to be $\geq \gamma_{SV}$ as $\gamma_{LV} > \gamma_{SV}$ and if γ_{SL} is $< \gamma_{SV}$, a true interface would not be formed and the contact angle would approach 180° . With the development of chemical bonding, γ_{SL} approaches γ_{SV} and when this happens a limiting contact angle of 90° is reached according to Young's equation. Free energy Equation 8, becomes

$$\frac{dG}{dh} = \gamma_{LV} \frac{dA_{LV}}{dh} \quad (9)$$

According to this equation the minimum energy configuration is reached when the surface area of the liquid (-vapor interface) is minimum and this corresponds to a 90° contact angle from Fig. 11. In the system Ag-NiO(Ni) all the conditions specified above for a 90° contact angle are satisfied (as discussed before), and hence an obtuse angle observed initially for the silver drop reaches an equilibrium contact angle of 90° , with good adherence. This also corresponds to a spreading of the drop from obtuse to 90° . The surface energy difference between silver and NiO happens to be smaller than the surface energy of nickel. ($\gamma_{LV} - \gamma_{SV}$)

$< \gamma_{SV}$. As a result of this γ_{SL} will reach γ_{SV} before there is a complete reduction of γ_{LV} by γ_{SV} resulting in a 90° contact angle. If, however, the experiment is conducted in a helium atmosphere (Ag on NiO) an obtuse angle would be obtained as γ_{LV} of silver in helium = 960 ergs/cm^2 , $\gamma_{SV} = 400 \text{ ergs/cm}^2$ and so $\gamma_{LV} - \gamma_{SV} = 560 \text{ ergs/cm}^2$ which is $> \gamma_{SV}$. γ_{SL} will be $= \gamma_{LV} - \gamma_{SV} = 560 \text{ ergs/cm}^2 > \gamma_{SV}$. This would result in an obtuse contact angle instead of a 90° contact angle that was observed in an air atmosphere.

APPENDIX

Let us consider a solid-liquid vapor system wherein a small spherical liquid drop is placed on a flat, rigid, solid surface. Assuming negligible gravitational effects to exist, the free energy change for the system could be written as

$$\delta G = \delta \int_{SL} d(\gamma_{SL} A_{SL}) + \delta \int_{LV} d(\gamma_{SV} A_{SV}) + \delta \int_{LV} d(\gamma_{LV} A_{LV}) \quad (1)$$

As the interfacial areas would depend on the contact angle (θ) at the three phase junction point which is related to the height of the drop, h , (Fig. 11), knowledge of free energy variation with the height of the drop is desirable.

Equation 1 can be written as

$$\frac{dG}{dh} = \frac{d(\gamma_{SL} A_{SL})}{dh} + \frac{d(\gamma_{SV} A_{SV})}{dh} + \frac{d(\gamma_{LV} A_{LV})}{dh} \quad (2)$$

Let us consider the size of decreasing height to be positive.

Expanding equation 2

$$\begin{aligned} \frac{dG}{dh} = & \gamma_{SL} \cdot \frac{dA_{SL}}{dh} + A_{SL} \cdot \frac{d\gamma_{SL}}{dh} \\ & + \gamma_{SV} \cdot \frac{dA_{SV}}{dh} + A_{SV} \cdot \frac{d\gamma_{SV}}{dh} \\ & + \gamma_{LV} \cdot \frac{dA_{LV}}{dh} + A_{LV} \cdot \frac{d\gamma_{LV}}{dh} \end{aligned} \quad (3)$$

Both γ_{LV} and γ_{SV} , surface energies of liquid and solid depend on the atmosphere. As the atmosphere would remain the same throughout the

experiment and hence assuming solid, liquid to reach equilibrium with the vapor phase independently of each other, the variation of γ_{SV} and γ_{LV} would be negligible, i.e., $\frac{d\gamma_{SV}}{dh}$, $\frac{d\gamma_{LV}}{dh}$ will be zero. Equation 3 would then become,

$$\begin{aligned} \frac{dG}{dh} = & \gamma_{SL} \cdot \frac{dA_{SL}}{dh} + A_{SL} \cdot \frac{d\gamma_{SL}}{dh} \\ & + \gamma_{SV} \cdot \frac{dA_{SV}}{dh} + \gamma_{LV} \cdot \frac{dA_{LV}}{dh} \end{aligned} \quad (4)$$

If there is a reaction between solid and liquid phases, the interfacial energy will continuously change until the equilibrium is reached. Change of γ_{SL} would imply a change in the contact angle to satisfy the balance of forces and hence a change in the height of the drop, h . Further, $dA_{SL} = -dA_{SV}$ as liquid-solid interface is formed when the liquid flows over the solid-vapor interface.

$\frac{dG}{dh}$ would then become

$$\begin{aligned} = & (\gamma_{SL} - \gamma_{SV}) \frac{dA_{SL}}{dh} + \gamma_{LV} \cdot \frac{dA_{LV}}{dh} \\ & + A_{SL} \cdot \frac{d\gamma_{SL}}{dh} \end{aligned} \quad (5)$$

This would be the expression for the variation of free energy with the height of the drop for non-equilibrium conditions, where the reaction at the solid-liquid interface is still proceeding. As the reaction proceeds, h keeps decreasing (hence positive according to the sign convention) and γ_{SL} also keeps decreasing (negative). In the expression for $\frac{dG}{dh}$, the first term is positive, second and third terms being negative. A minimum

energy configuration will be obtained when $\frac{dG}{dh}$ is zero. For the case $\gamma_{LV} > \gamma_{SL} > \gamma_{SV}$, the maximum reduction of $\gamma_{LV} = \gamma_{SV}$, but in any case $\gamma_{SL} \geq \gamma_{SV}$. When this extreme condition is reached γ_{SL} would reach an equilibrium value making $\frac{d\gamma_{SL}}{dh} = 0$ and so, $\frac{dG}{dh}$ would be reduced to the expression derived by Aksay, et al.²⁵ This would lead to a limiting contact angle of 90° as observed in the silver-nickel oxide system.

SUMMARY AND CONCLUSIONS

Wetting studies of lead borosilicate glass on silver, platinum and gold were conducted in controlled atmospheres. The glass spread on silver in the presence of oxygen and good adherence developed. The driving force for spreading was provided by the reduction of interfacial energy caused by the dissolution of the surface silver oxide layer in glass. A low contact angle (of 2°) was observed for vacuum conditions. The good adherence obtained in this case was explained on the basis of a redox reaction between lead oxide and silver.

With gold, good adherence observed in the presence of oxygen was due to the dissolution of the surface oxide layer in glass at the interface (contact angle 18°). In vacuum conditions the adherence was very poor, even though the contact angle was lower (6.5°). This was explained on the basis of Young's equation.

Presence of oxygen contributed to a low contact angle ($2-3^\circ$) and good adherence between glass and platinum. In vacuum conditions carbon adsorption on platinum caused the contact angle to increase from 58° to 73° . The decrease in surface energy (γ_{SV}) of platinum due to carbon adsorption was calculated to be ~ 43 ergs/cm².

Silver wetted nickel in helium atmosphere (contact angle 9.5°). In air atmosphere, however, nickel oxide layer formed between nickel and silver, and a contact angle of 90° with good adherence was obtained. Surface energy of silver (γ_{LV}) is greater than the surface energy of NiO (γ_{SV}). As chemical interface developed between NiO and silver, γ_{LV} was continuously reduced by γ_{SV} which implied a continuous change in the interfacial energy γ_{SL} ; however the maximum reduction of γ_{LV} that could

be achieved by the solid equals γ_{SV} and in any case, $\gamma_{SL} \geq \gamma_{SV}$ for a true interface. So with the development of chemical bonding, γ_{SL} approached γ_{SV} and when this happened a limiting contact angle of 90° was reached according to Young's equation.

Table 1. Earlier Wetting Studies. (Ref. 8, 9a,b)

| Glass | Metal | Temp | CONTACT ANGLE | | | | | | Ref. |
|--|-------|--------|---------------|--|----------------|----------------|------------------|-----|------|
| | | | Vacuum | A, He, N ₂ , CO ₂ | O ₂ | H ₂ | H ₂ O | CO | |
| Na ₂ O 2SiO ₂ | Au | 1000°C | 62° | 62-65° | 35° | 65° | 65° | 65° | 8 |
| | Pt | 1000°C | 22° | 17-24° | 15° | 52° | 60°(a) | 60° | |
| 100 B ₂ O ₃ 94 B ₂ O ₃ 6Na ₂ O 69 B ₂ O ₃ 31Na ₂ O | Pt | 1000°C | 68°(b) | - | 6° | - | 0° | - | 9a |
| 6°(c) | | | | | | | | | |
| 94 B ₂ O ₃ 6Na ₂ O | Au | 900°C | 46°(b,c) | - | 6° | - | 39-60° | - | 9b |

(a) in (H₂O + N₂), 15° in (H₂O + O₂)

(b) With carbon contamination

(c) Without carbon contamination

Table 2. Sessile Drop Measurements.

| System | Atmosphere | Temp. | Contact Angle | Adherence (Qualitative) |
|-----------------|----------------|-------|---------------|-------------------------|
| LBS glass on Ag | Air | 600°C | 0° | very strong |
| | Vacuum | 700°C | 2° | good |
| | He | 700°C | 48° | poor |
| LBS glass on Au | Air | 700°C | 18° | strong |
| | Vacuum | 700°C | 6.5° | poor |
| LBS glass on Pt | Air | 700°C | 2°-3° | strong |
| | Vacuum(no C) | 700°C | 58° | poor |
| | Vacuum(with C) | 700°C | 73° | poor |
| Ag on Ni | Air | 970°C | 90° | strong |
| | He | 970°C | 9°-5 | very strong |

LBS - Lead Borosilicate glass. Vacuum - 3×10^{-6} torr.

Table 3. Surface Energies.

| Material | M.P | Temp. | Surface Energy | Ref. |
|--------------|--------|--------|---|---------------|
| Silver | 963°C | 1000°C | 920 ergs/cm ² | (i) |
| Nickel | 1453°C | 1000°C | 2280 ergs/cm ² *2160 ergs/cm ² | (ii) (iii) |
| Nickel oxide | 1957°C | 1300°C | 400 ergs/cm ² | (iv) |

References

- (i) 'Introduction to Ceramics' - W. D. Kingery, p. 183, 2nd Edition, Pub. John Wiley & Sons, NY 1976.
- (ii) 'Liquid Metals' Ed. Sylvan Z. Beer, Chap. 4(B.C. Allen) p. 198, Pub. Marcel Dekker, Inc, NY, 1972.
- (iii) 'Interfacial Phenomena in Metals and Alloys' - Lawrence E. Murr, p. 123, Addison Wesley Pub. 1975.
- (iv) 'High Temperature Inorganic Coatings' - A. A. Appen, p. 49. Published by WNT Warsaw - 1970 (translated from Russian).

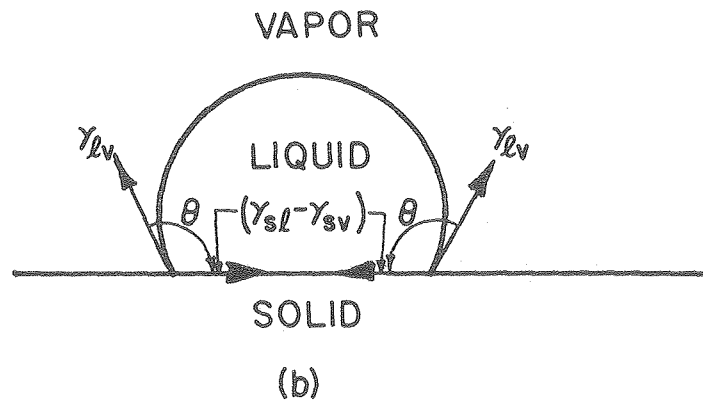
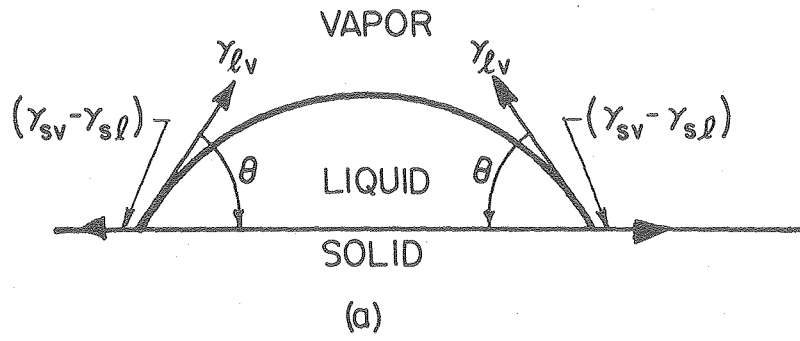
*Value approximated from liquid surface tension.

Table 4. Some Properties of Ni and Ag.

| | Ni | Ag |
|-------------------------------|--------------------------------------|---------------------------------------|
| Structure | F.C.C. | F.C.C. |
| Lattice Parameter | 3.525 A° | 4.08A° |
| Atomic Radius | 1.24 A° | 1.44A° |
| Electronic Configuration | (Ar) 3d ⁸ 4s ² | (Kr) 4d ¹⁰ 5s ¹ |
| Density | 8.9 | 10.5 gm/C.C. |
| Thermal Expansion Coefficient | 13 x 10 ⁻⁶ | 19 x 10 ⁻⁶ in/in°C |

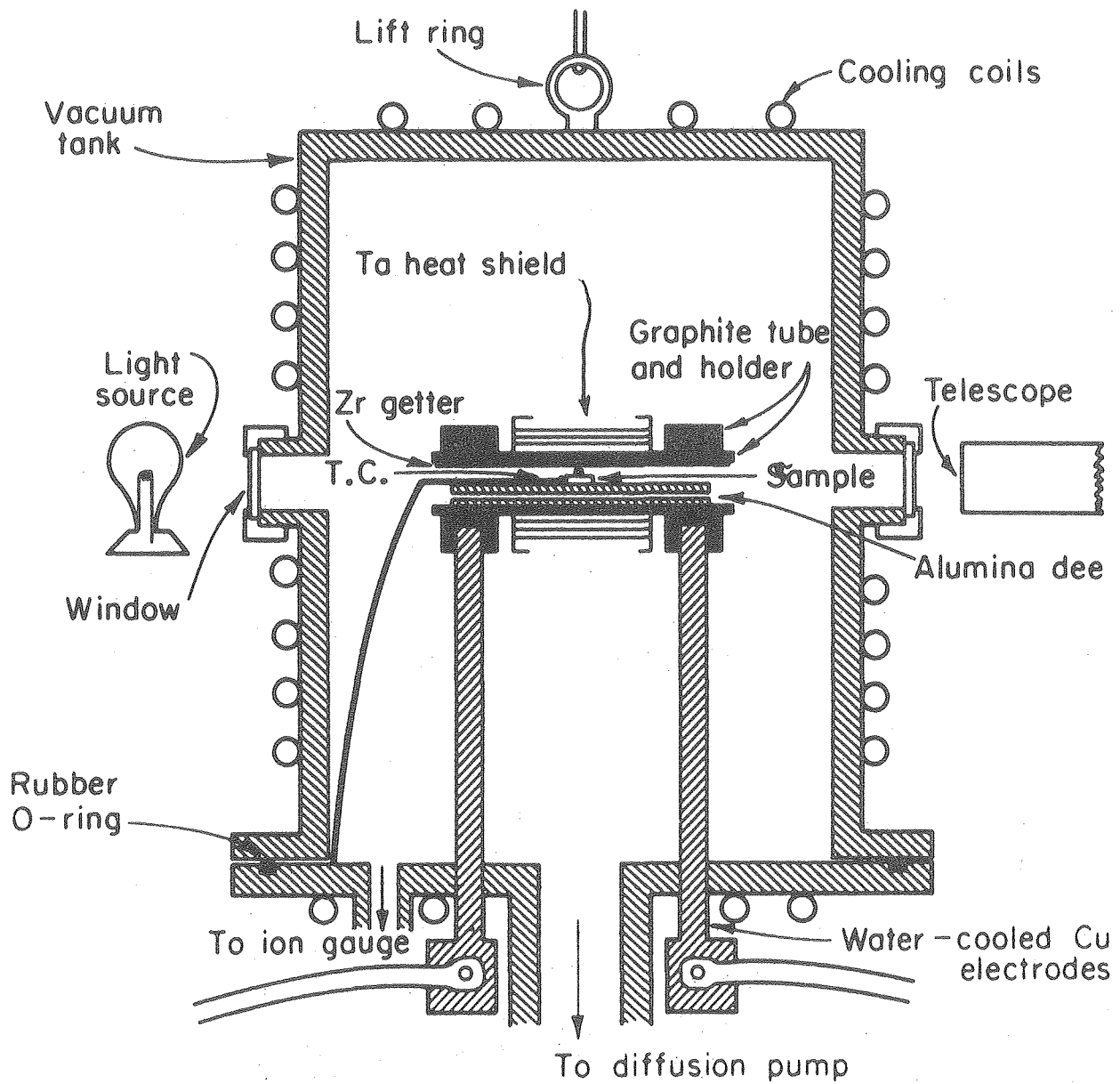
FIGURE CAPTIONS

1. Schematic of a sessile drop
 - (a) $\theta < 90^\circ$, the liquid wets the solid.
 - (b) $\theta > 90^\circ$, the liquid does not wet the solid.
2. Schematic of the 'graphite furnace' for contact angle measurements in controlled atmospheres.
3. Schematic of the 'alumina furnace'.
4. Optical micrograph of the lead borosilicate (LBS) glass drop which spread on silver substrate (at 600°C) in air atmosphere.
5. Crystallites formed at the periphery of the above glass drop.
6. Edges of the glass drop on silver substrate in (A) vacuum, (B) He. Contact angle measurements done at 700°C .
7. LBS glass drop on gold (700°C).
 - A. in vacuum
 - B. in air.
8. LBS glass drop on platinum (700°C).
 - A. in air
 - B. in vacuum.
9. Scanning electron micrograph of the nickel-silver interface. In air atmosphere NiO forms at the interface. X-ray line mappings show the variation of Ni and Ag concentration across the interface.
10. Effect of oxygen pressure on surface energy of silver (ref. 14).
11. Progressive geometric configurations of a sessile drop on a substrate and the variation of liquid-vapor and solid-liquid interface areas with contact angle θ (ref. 25).



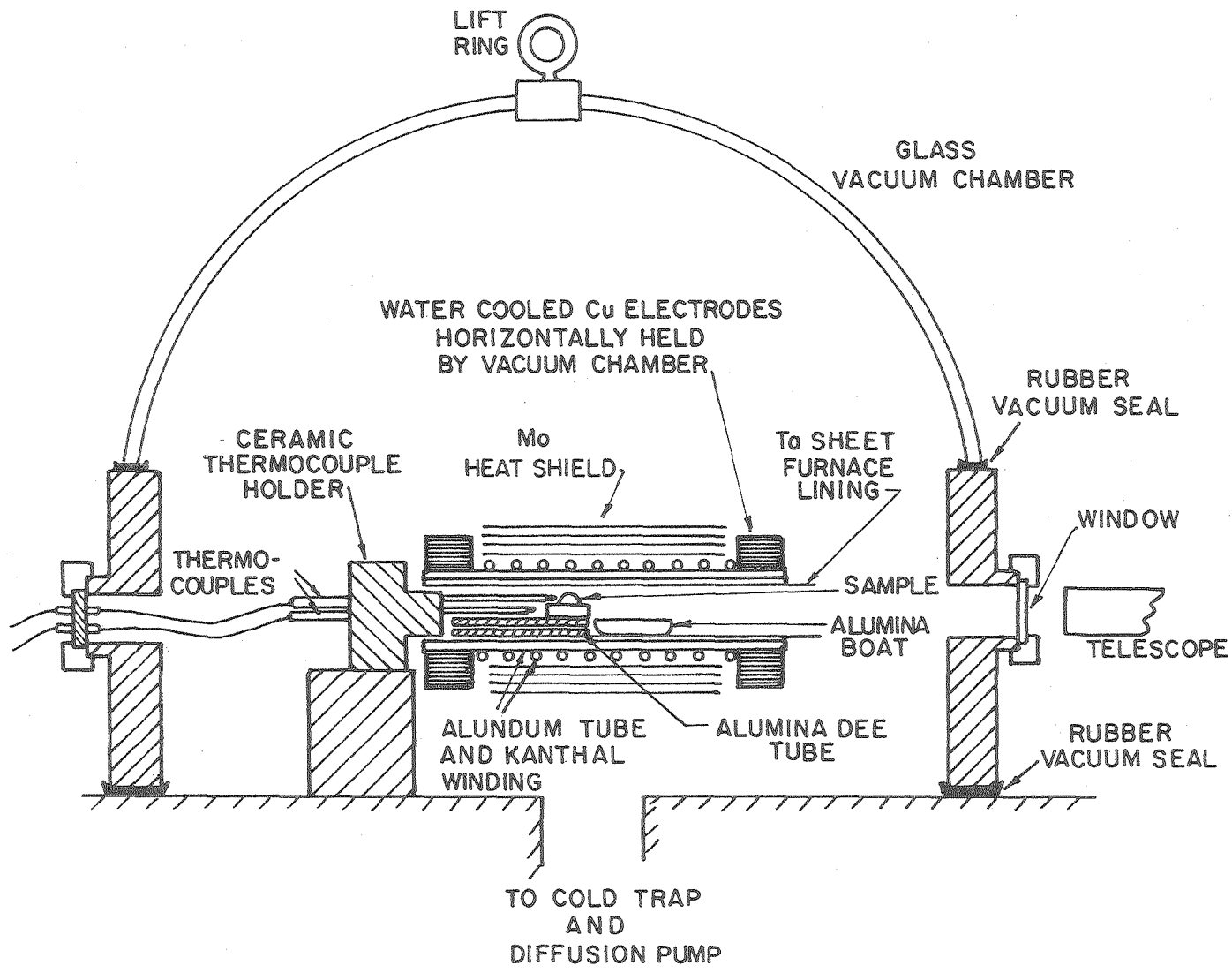
XBL 7811-6106

Fig. 1



MUB-12306

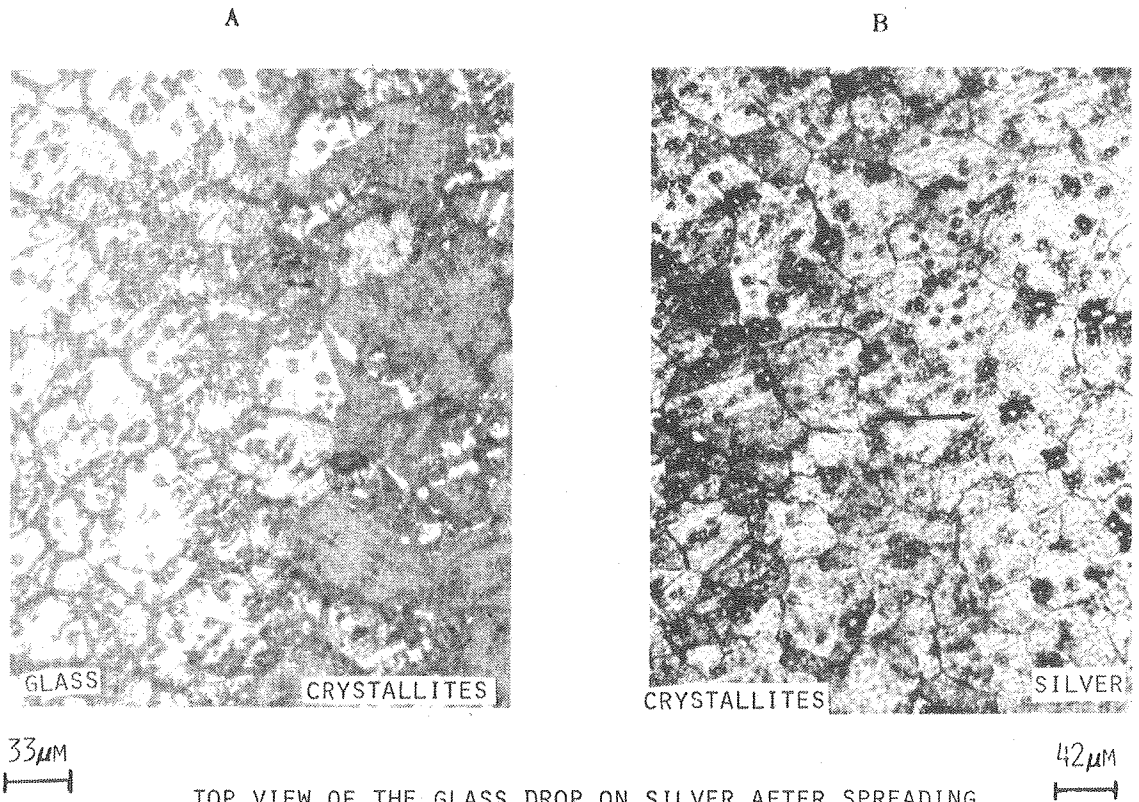
Fig. 2



-128-

XBL7811-6110

Fig. 3



TOP VIEW OF THE GLASS DROP ON SILVER AFTER SPREADING
IN AIR. ARROW INDICATES THE DIRECTION OF SPREADING.

XBB 792-2642

Fig. 4

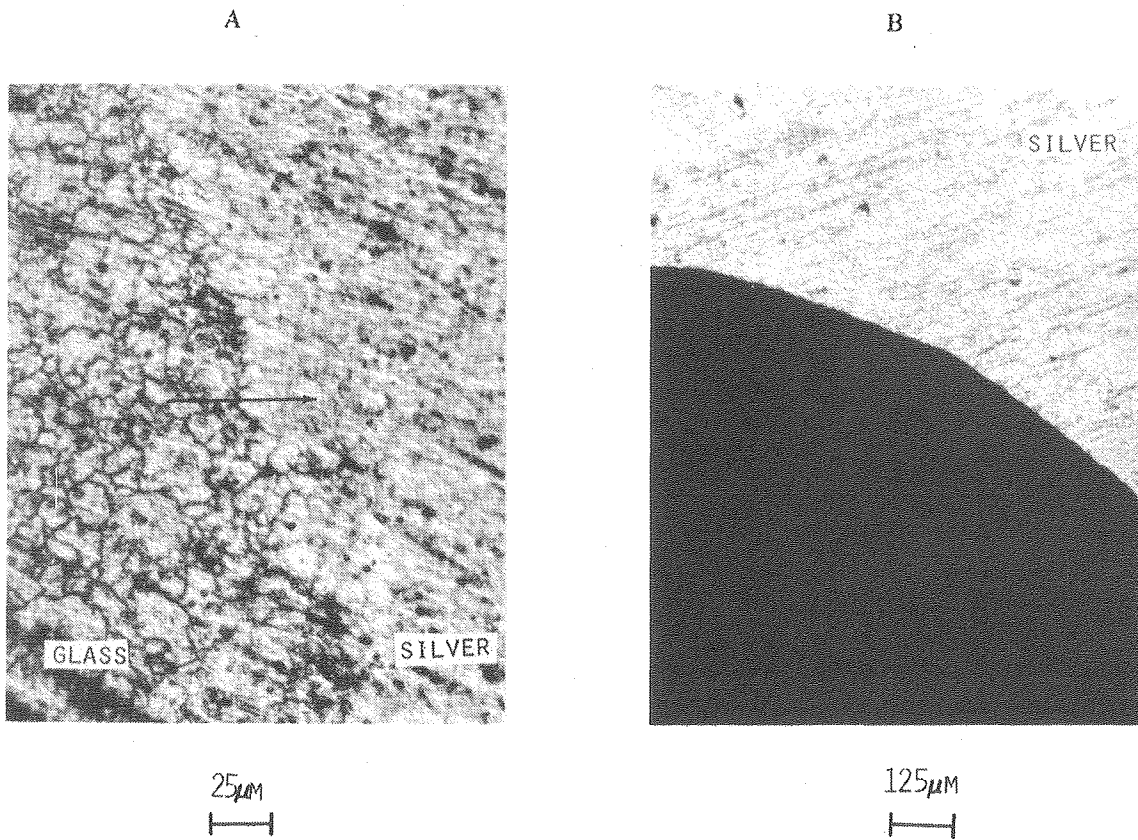


25 μ m
┌───┐

OPTICAL MICROGRAPH OF THE CRYSTALLITES FORMED AT THE PERIPHERY OF THE GLASS DROP ON SILVER AFTER COOLING.

XBB 792-2643

Fig. 5



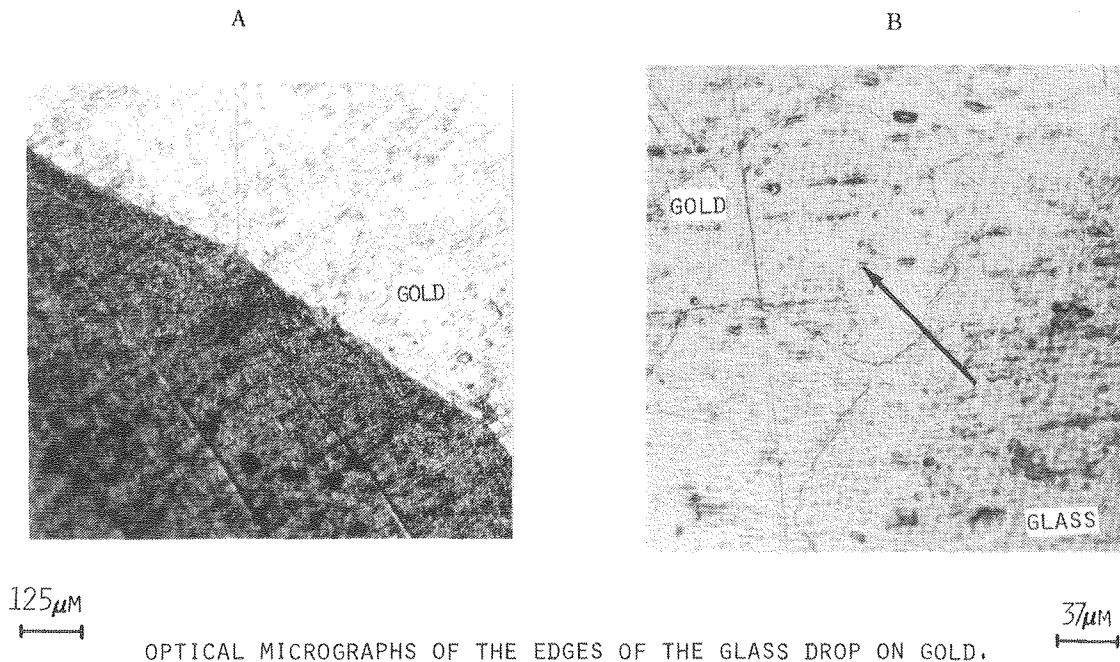
OPTICAL MICROGRAPHS OF THE EDGES OF THE GLASS DROP ON SILVER.

A. VACUUM 700°C

B. He 700°C

XBB 792-2645

Fig. 6



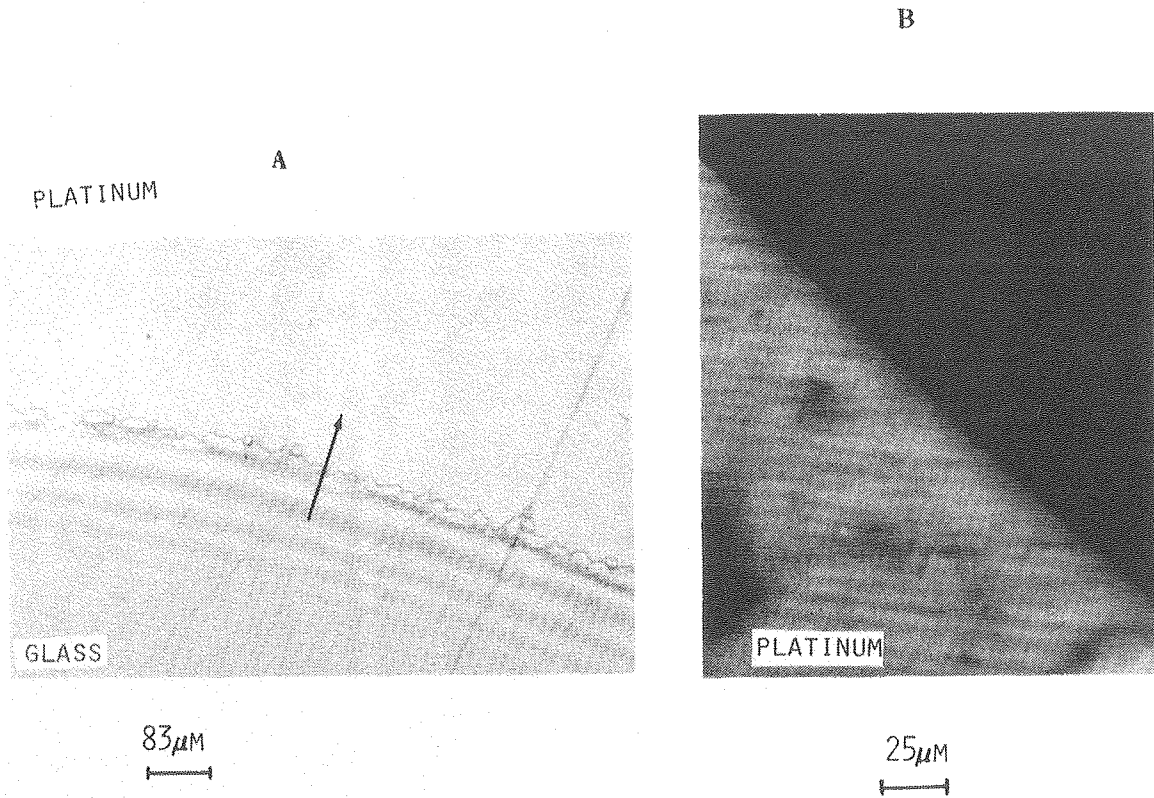
A. IN VACUUM 700°C

B. IN AIR 700°C

ARROW INDICATES THE DIRECTION OF GLASS FLOW.

XBB 792-2646

Fig. 7



OPTICAL MICROGRAPHS OF THE GLASS DROP ON PLATINUM.

A. IN AIR 700°C

B. IN VACUUM

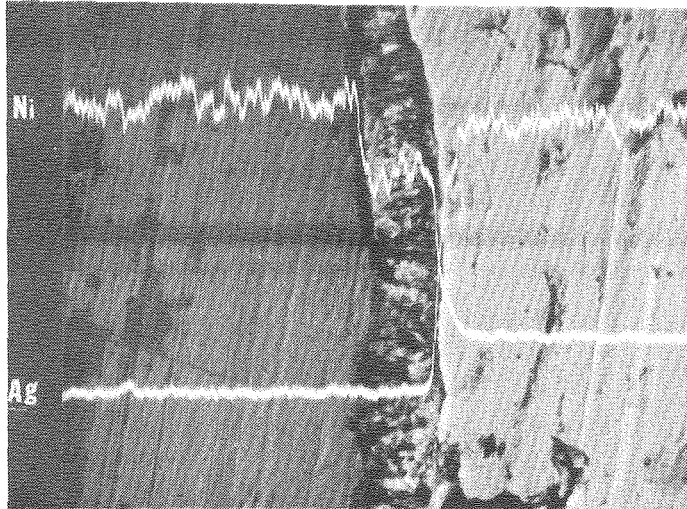
ARROW INDICATES THE DIRECTION OF GLASS FLOW.

XBB 792-2644

Fig. 8

SILVER - NICKEL INTERFACE

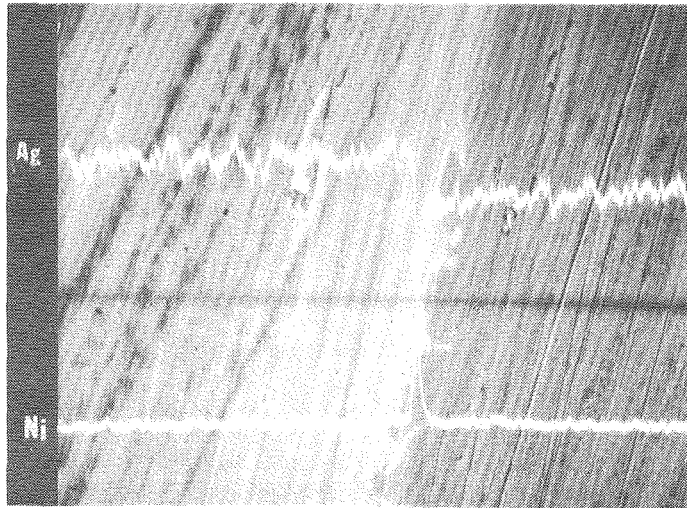
A



TEMPERATURE: 970°C ATMOSPHERE: AIR
CONTACT ANGLE (θ): 90°

5 μ

B

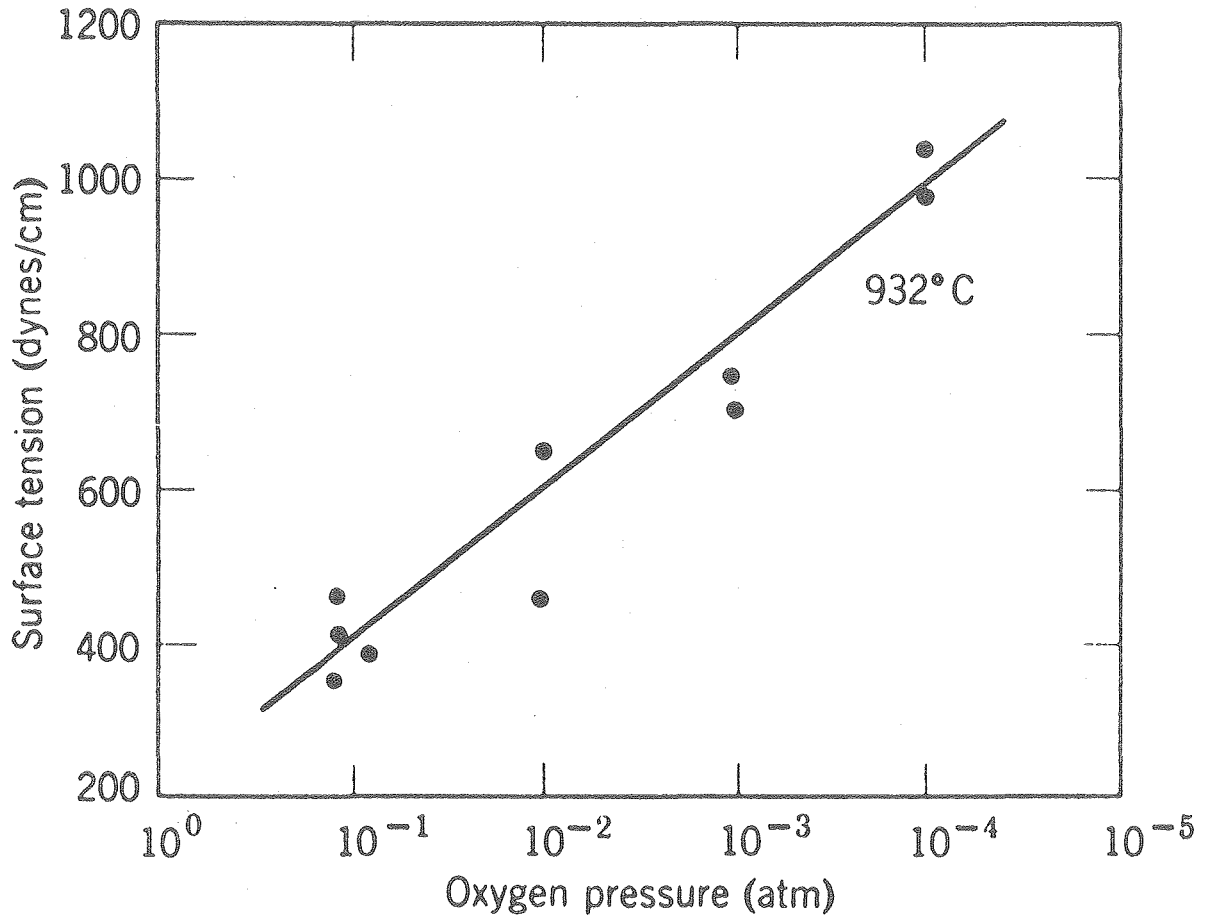


TEMPERATURE 970°C ATMOSPHERE: He
CONTACT ANGLE (θ) 90°

XBB 780-13348

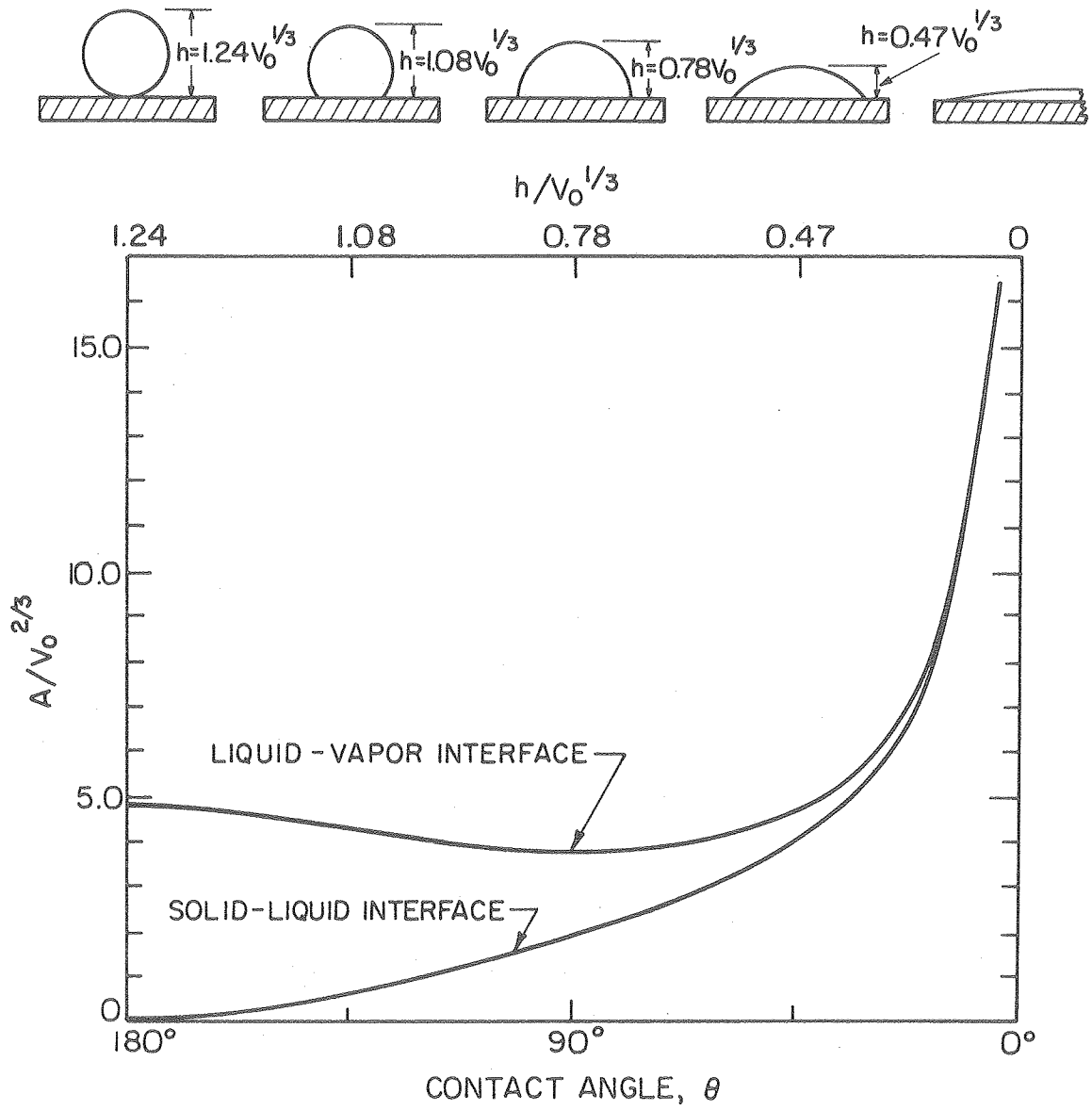
Fig. 9

Effect of oxygen pressure on surface energy of solid silver.



XBL 7912-13538

Fig. 10



XBL 738-1701

Fig. 11

REFERENCES

1. R. M. Fulrath, S. P. Mitoff and J. A. Pask, *J. Am. Ceram. Soc.*, Vol. 40, No. 8, p. 269, (Aug. 1957).
2. Glenn A. Holmquist, M.S. Thesis, Lawrence Berkeley Laboratory, LBL-3905, (May 1975).
3. Stephen T. Tso, M.S. Thesis, Lawrence Berkeley Laboratory, LBL-5776, (Dec. 1976).
4. Henry H. Hester and Thomas E. Salzer, *Proceedings of First Technical Thick Film Symposium, ISHM*, p. 1, (1967).
5. T. Young, *Phil. Trans. Roy. Soc., London*, 95, p. 65 (1805).
6. (a) J. W. Gibbs, *The Collected Works of J. Willard Gibbs - V. I.*, Pub. Longmans, Green and Co., p. 314 (1931).
(b) R. E. Johnson, *J. Phys. Chem.*, 63, [10], p. 1655 (1959).
7. A. Dupre, *Theorie Mecanique de la Chaleur*, Paris, p. 368 (1869).
8. J. A. Pask and R. M. Fulrath, *J. Am. Ceram. Soc.*, V. 45, No. 12, p. 592, (Dec. 1962).
9. (a) Glenn A. Holmquist and J. A. Pask, *J. Am. Ceram. Soc.*, V. 59, Nos. 9-10, p. 384 (Sept.-Oct. 1976).
(b) Stephen T. Tso and J. A. Pask, (to be published) Lawrence Berkeley Laboratory, LBL-8496 (Jan. 1979).
10. (a) G. A. Somorjai, *Catalysis Rev.* 7, 87 (1972).
(b) A. E. Morgan and G. A. Somorjai, *Sur. Sc.*, 12, p. 405 (1968).
11. M. A. Chesters and G. A. Somorjai, *Sur. Sc.*, 52, pp. 21-28 (1975).
12. S. Evans, *Faraday Discussion, Chem. Soc.*, 58, pp. 97-105 (1975).
13. H. Udin in 'Metal Interfaces' - A Seminar, p. 114, American Soc. of Metals, Cleveland, OH (1951).

14. F. H. Buttner, E. R. Funk and H. Udin, J. Phys. Chem. 56, p. 657 (1952).
15. A. Aksay, C. E. Hoge and J. A. Pask, J. Phys. Chem., 78 [12] p. 1181 (1974).
16. (a) M. Humenik, Jr., and W. D. Kingery, J. Am. Ceram. Soc., 37 [1] p. 18 (1954).
(b) A. C. Chaklader, et al., J. Am. Ceram. Soc., 51 [11] p. 630 (1968).
17. John J. Brennan and J. A. Pask, J. Am. Ceram. Soc., 56 [2] p. 58 (1973).
18. R. W. Vest, Technical report on 'Conduction Mechanisms in Thick Film Microcircuits,' Chap. 4, p. 81, Purdue University, West Lafayette, IN (Dec. 1975).
19. M. McLean and E. D. Hondros, J. Mat. Sci. 6, p. 19 (1971).
20. H. B. Lyon and G. A. Somorjai, J. Chem. Phys., 46, p. 2539 (1967).
21. "JANAF Thermochemical Tables," 1971 National Bureau of Standards, Washington, DC, (1971).
22. (a) J. W. Gibbs, The Collected Works of J. W. Gibbs, Longmans, Green, NY, V. 1, p. 219 (1931).
(b) E. A. Guggenheim and N. K. Adam, Proc. Roy. Soc. (London), A139, p. 218, (1933).
23. L. Brewer, Chap. 2, High Strength Materials, Ed. Victor F. Zackay, Pub. John Wiley & Sons, Inc, NY (1965).
24. M. Hansen, Constitution of Binary Alloys, Pub. McGraw Hill Book Co., NY (1958).
25. I. A. Aksay, C. E. Hoge and J. A. Pask, Lawrence Berkeley Laboratory LBL-1870, (July 1973).

This report was done with support from the Department of Energy. Any conclusions or opinions expressed in this report represent solely those of the author(s) and not necessarily those of The Regents of the University of California, the Lawrence Berkeley Laboratory or the Department of Energy.

Reference to a company or product name does not imply approval or recommendation of the product by the University of California or the U.S. Department of Energy to the exclusion of others that may be suitable.

TECHNICAL INFORMATION DEPARTMENT
LAWRENCE BERKELEY LABORATORY
UNIVERSITY OF CALIFORNIA
BERKELEY, CALIFORNIA 94720

ACKNOWLEDGMENT

I wish to express my sincere appreciation to Professor Joseph A. Pask for his continued guidance and encouragement during the course of this work. I would also like to thank Professors Alan W. Searcy and Chenming Hu for their time and effort in critically reading and commenting on the thesis.

Thanks are due to Gay Brazil for her unfailing help in manuscript preparation, Rich Lindberg (SEM assistance), Gloria Pelatowski (technical drawings) and the support staff of the Materials and Molecular Research Division, Lawrence Berkeley Laboratory.

Special thanks are due to Tony Tomsia, Paul Sharps and Dan Miller for their assistance and friendship during the course of this work. My hearty thanks are extended to Ingrid for her patient and constant encouragement during the writing of this manuscript.

I am very grateful to my parent, sisters and brother for their support, encouragement and understanding.

Finally, I would like to thank the late Richard M. Fulrath under whose guidance this work was started. He was a great teacher and a good friend. As his students, we called him 'Chief,' as he looked very fierce and forceful. But inside his heart, he was softer than a flower. Such is the nature of the virtuous. It is a great honor to have had him as a part of our experience, knowledge and outlook.

This work was supported by the Division of Materials Sciences, Office of Basic Energy Sciences, U.S. Department of Energy under contract No. W-7405-Eng-48.